UNIVERSITY OF CALIFORNIA
SANTA CRUZ

Protein kinases at the intersection of cell growth and cell division in

Saccharomyces cerevisiae

A dissertation submitted in partial satisfaction
of the requirements for the degree of

DOCTOR OF PHILOSOPHY

in

MOLECULAR, CELL AND DEVELOPMENTAL BIOLOGY

by

Akshi Atul Jasani

December 2019

The Dissertation of Akshi Atul Jasani
is approved:

Professor Douglas Kellogg, chair

Professor Seth Rubin

Professor Carrie Partch

Quentin Williams
Acting Vice Provost and Dean of Graduate Studies

TABLE OF CONTENTS

LIST OF FIGURES

LIST OF TABLES

ABSTRACT

Protein kinases at the intersection of cell growth and cell division in *Saccharomyces cerevisiae*

Akshi Atul Jasani

All cells big and small possess the ability to grow. Despite this, cells in a given population have very similar sizes, suggesting that they must possess inherent mechanisms that determine how much they grow and when to stop growing. Growth homeostasis is especially important at the time of cell division to ensure that daughter cells are the same size as their mother. Coordination of cell growth with cell division is a universal phenomenon in all orders of life; however, the mechanisms that measure cell growth have remained elusive. Moreover, it is not clear what cells "measure" as a readout of cell growth. In the following chapters, I will provide evidence that protein kinases measure signaling lipids deposited at sites of growth to gauge the extent of cell growth in *Saccharomyces cerevisiae* and then relay growth-dependent signals to relevant cell cycle control proteins to link cell cycle progression to cell growth.

In chapters 2 and 3, I present evidence that suggests that Gin4 and Hsl1 kinases are essential for coordination of cell cycle progression with cell growth. Inactivation of these kinases causes cells to behave as if they cannot detect that growth has occurred, which results in strong growth defects. Moreover, the activation of Gin4/Hsl1 is dependent on and proportional to growth. The data further suggest that activation of Gin4 by signaling lipids is the basis of measuring cell growth.

In chapter 4, I focus on the kinase Pkc1 (protein kinase C) and its role as a growth sensor for polar bud growth. Pkc1 is maximally active at G2 and is well-positioned to detect bud growth. It is activated by Rho1 and together they interact with the phosphatase $PP2A^{Cdc55}$ to link mitotic entry to polar cell growth.

ACKNOWLEDGEMENTS

As I approach closer to the end of my graduate studies, I cannot help but thank all the people who have been vital to my success. I would like to thank my mom and dad- Heena and Atul Jasani- first and foremost. Mom and dad, you have sacrificed a lot to ensure that I got the best education possible and provided me with a nurturing home environment. Mom, you were my first teacher, and I still remember how you would help me finish my homework even when you were sick.

I also want to acknowledge my high school biology teacher, Mrs. Monita Dash for being the amazing teacher that she is. I always liked biology, but her enthusiasm for the subject is what made me love it too. Under her guidance, I carried out my first ever research project using fruit flies, bananas and some old glass bottles, but it prepared me for the challenges that lay ahead of me.

I would next like to thank my husband- Swair Mehta. Swair, you have known me for more than half of my life and I couldn't have gone through grad school without your love and laughter. Every time I have felt down and depressed, you have cracked your silly jokes and made me laugh. You could never understand why I would become excited about some protein band on a blot. To you, they just looked like black "blobs". But you still rejoiced with me, while secretly rolling your eyes. You would proudly tell anyone who listened that your wife studied mold. Even though that is not accurate, it still boosted my confidence. I would also like to thank my other family- my in-laws: Rupa, Sunil and Vishesh Mehta for their love and continued support.

I want to give my sincere thanks to my advisor- Dr. Douglas Kellogg for being an amazing mentor. Doug has been everything I was looking for in a mentor. His approachability and on-hands training have been vital to my growth as a scientist. The way he likes tackling big questions in a simplified way is something that I strive for and

slowly getting better at. He has amassed such a wonderful group of people that make the Kellogg lab. A big thank you to all the Kelloggians – past and present for being the best group ever. You guys have trained me in so many techniques, suggested so many useful experiments and been such excellent friends. A special thank you to Dr. Rafael Lucena and Dr. Maria Alcaide. You have always been there to help me with my research whenever I was stuck. You pushed me to do better every day and cheered for me when I succeeded.

I am thankful to the undergrads who helped me with my project: Logan Fisher, Tanakorn Janlaor (Will), Tiffany Huynh and Griffin Milligan. Your work was crucial to the data presented in this thesis work. Logan and Will assisted with some parts of the data shown here in Chapter 4, Tiffany contributed to parts of Chapters 2 and 3 and Griffin helped with some parts of Chapter 3.

I would also like to thank my thesis committee: Dr. Douglas Kellogg, Dr. Seth Rubin and Dr. Carrie Partch for their continued support and guidance.

To my colleagues: Drs. Michelle Tjia and Lotti Brose, thank you for your friendship, support and the endless chats we have had over coffees and lunches. Grad school would have been less fun without you both.

I would also like to thank Dr. Ben Abrams, Director of UCSC Life Sciences Microscopy Center for his help and support with all the microscopy experiments.

The text of this dissertation contains excerpts from the following material uploaded on BioRxiv and is currently submitted to Molecular Biology of the Cell (MBoC) for publication: Akshi Jasani, Tiffany Huynh, Douglas R. Kellogg. "Growth-dependent activation of protein kinases links cell cycle progression to cell growth" doi: https://doi.org/10.1101/610469. Tiffany Huynh partially contributed to Figures 2.5 and 2.7. Doug Kellogg supervised the entire research.

DEDICATION

I dedicate this dissertation with all my love to my husband Swair.

I will forever be grateful that I met you in 8th grade. We became friends and never looked back.

CHAPTER 1: OVERVIEW

Growth for the sake of growth is the ideology of the cancer cell.
~ Edward Abbey

Growth is a fundamental feature of all living cells. In its very basic form, cell growth can be defined as the accumulation of biomass in the form of an increase in its macromolecular content, all of which leads to an increase in its physical size. Thus, cell size is the most direct readout of cell growth. Perhaps one of the most astonishing features of all cells is an ability to maintain size homeostasis within the population. Thus, all cells within a given cell type fit within a narrow size distribution. Not only do cells possess the ability to maintain a constant cell size, they also have the ability to grow or shrink in response to various external/internal stimuli. This "cellular plasticity" has repercussions not only at the cellular level, but also at the organismal level. For instance, fruit flies fed with a nutrient-restricted diet are visibly smaller than flies fed a nutrient-rich diet (Edgar, 2006).

Cell growth plays a crucial role at the time of cell division. In general, before a cell divides, the cell must ensure that it roughly doubles in size so that the resulting daughter cells are born at the same size as the mother, thereby ensuring size homogeneity in the cell population. Normally, the growth phases (G1 and G2) interspersed between two mitotic cycles is when cell growth typically happens. Failure to ensure a tight coordination between cell growth and cell division disrupts normal functioning of the cell and is a common manifestation in a variety of diseases. For instance, cancer cells typically display size heterogeneity. In fact, the further the cancer has progressed, the more abnormalities that cells display in their nuclear : cytoplasmic ratios (Sokoloff, 1922).

How is it that cells regulate their own growth? What we realize so far is that cells must have the ability to somehow "measure" their own growth. Moreover, they are also able to gauge environmental conditions and regulate their size accordingly. Another key question is how do cells coordinate their growth with cell cycle progression? Through this thesis, I will try to answer some of these questions using budding yeast as the model system.

Cell size checkpoints ensure key cell cycle transitions occur only when sufficient growth takes place

Perhaps the earliest study to lay down the foundations for the concept of "cell size control" were performed in *Amoeba proteus* in 1928 by Hartmann *et al*. Hartmann periodically performed partial cytoplasmic amputations in amoeba and noticed that the amoeba failed to divide even as they resumed growth. Further, they also reported that while repeatedly amputated amoeba failed to divide for months, the un-amputated control amoeba underwent 56 successive cell divisions (Hartmann, 1926). These experiment were subsequently validated by Prescott *et al.* where they also reported that such amputated cells displayed a decrease in nuclear volume, a delay in cell division accompanied by a reduction in growth rate (Prescott, 1956). Further, *Prescott et al.* also observed that amoeba cells that have advanced sufficiently into the cell cycle will finish their cell cycle, albeit at a much slower rate, even if growth is perturbed by shifting them to non-nutrient conditions. This seminal work by Hartmann and Prescott gave us three critical pieces of information: (i) cells need to grow to a certain extent, or achieve a threshold size before they can commit to the cell cycle, leading to the idea of a size "checkpoint", (ii) once the size checkpoint has been passed, cells

will finish dividing even if their growth is perturbed, although they will do so at a much slower rate, and (iii) nutrient conditions affect the rate of cell division. Together, these findings indicated for the first time that cell growth and cell division are tightly linked.

In the 1970s, the pioneering works of Paul Nurse and Leland Hartwell catapulted the field of cell growth and cell division further. Hartwell and his associates discovered the existence of a growth checkpoint in early G1 that precedes the DNA checkpoint in S-phase, which is a rate-limiting step for budding yeast cells to commit to a new round of cell division. They observed that when cells finish cytokinesis, the daughter cell produced is much smaller than the mother cell. In the subsequent G1, the daughter cell thus spends a much longer time than the mother cell to reach to a similar "critical cell size" before it can fully commit to the cell cycle (Hartwell and Unger, 1977; Johnston et al., 1977a). This transition point in G1 referred to as "START" was the first experimentally demonstrated size checkpoint. In agreement with the works of Prescott and Hartmann, these studies similarly revealed that cell growth and cell division are well-coordinated processes. Mutants deficient in the cell cycle or cells arrested in G1 using the mating pheromone would continue to grow even as the cell cycle was halted. Conversely, interrupting cell growth by nutrient-deprivation caused cells to finish the cell cycle with very small daughter cells and arrest in the subsequent G1. Not surprisingly, the START checkpoint is regulated by the G1 cyclins, which drive the cells into a cell division cycle, thereby ensuring that the cells have grown sufficiently before they commit to cell division (Carter and Sudbery, 1980; Cross, 1988; 1990; Richardson et al., 1989).

A similar study in fission yeast revealed another size checkpoint at G2 that is dependent on the Wee1 kinase (Nurse, 1975). Cells where the Wee1 kinase was

inactivated divided at half the cell size as wildtype cells. In the subsequent study, Fantes and Nurse demonstrated that cell size rather than the amount of time spent growing was the key determinant of this checkpoint (Fantes and Nurse, 1977). Moreover, the threshold size determined by this G2 checkpoint is actively modulated by the nutrients in which the cells are growing. More specifically, cells growing in nutrient-rich conditions need to grow more to reach to a higher size threshold compared to cells growing in nutrient-poor conditions. Furthermore, when cells are shifted from rich to poor nutrients, their cell cycle is accelerated, presumably due to the lowered threshold requirement in poor nutrients. With successive cell divisions in poor nutrients, the cell length at division gradually shrinks until they adopt the lower size threshold. Thus, fission yeast cells have the ability to actively reset their growth threshold in response to nutrient availability, a feature that would be useful for cells and organisms alike.

For the longest time, it was thought that the time spent growing in G1 prior to bud initiation was the only growth phase in budding yeast that was modulated in response to nutrient availability; the timing of growth in the subsequent phases (S, G2 and mitosis) was independent of the nutrient availability (Hartwell and Unger, 1977). By this assumption, the size of the daughter cell would then solely be dependent on growth rate set by the cells in the prevailing nutrient conditions. However, cells lacking all the key regulators of G1 still undergo robust cell size regulation in response to nutrient availability suggesting the possibility of growth regulation beyond G1 (Jorgensen and Tyers, 2004). Indeed, recent findings from our lab revealed that budding yeast cells growing in poor nutrient conditions compensate for the slow growth rate by prolonging the duration of mitosis, thereby ensuring their cells don't divide

prematurely in poor nutrients even if their size threshold is effectively reduced (Leitao and Kellogg, 2017a). This is especially important as Leitao found that a mature budding yeast cell acquires nearly 60% of its total cell volume during its growth as a bud in mitosis. Thus, any perturbations to mitotic bud growth could have severe consequences on cell size at maturity. These findings also suggest that cells must possess strong regulatory networks that measure bud growth and relay signals to the cell cycle machinery. It was later found that the phosphatase PP2A with its regulatory subunit Rts1 (yeast homolog of the B56 subunit) is the key regulator that influences mitotic duration and growth rate in mitosis in response to prevailing nutrient conditions (Leitao et al., 2019b). Cell growth thus seems to be measured at almost every phase in the cell cycle and the growth threshold actively established so that cell size in the population is homogenous.

Budding yeast display different growth phases throughout the cell cycle

Compared to other eukaryotes, the pattern of cell growth in budding yeast is quite unique in several ways. They divide in an asymmetric manner so that completion of a cell cycle leads to a large mother cell and a smaller daughter cell (Hartwell and Unger, 1977; Johnston et al., 1977a). Moreover, growth of the plasma membrane is a dynamic, integral part of cell growth and is regulated by the Cyclin-dependent kinase (Cdk1 in yeast) (McCusker et al., 2007; 2012; Moffat and Andrews, 2004). After a daughter cell is born, it undergoes a brief period of growth across its entire surface (isotropic cell growth) in G1 (Mitchison, 1958). Once sufficient growth has occurred, the daughter cell (now a new mother) commits to a round of cell division in late G1, wherein, growth of the mother cell stops and all new growth is directed to the formation

of a daughter bud (Mitchison, 1958; Tkacz and Lampen, 1972). From this point, growth is restricted solely to the daughter bud, where it initially grows in a polarized manner until G2 and growth is directed to the bud tip . At mitotic initiation, Cdk1 again signals a switch from polarized to isotropic growth in the daughter bud so that the bud continues to grow all across its cell surface throughout mitosis (Leitao and Kellogg, 2017a; Lew and Reed, 1993). Eventually, at completion of mitosis, membrane growth is polarized again to the site of cytokinesis, to aid in cell separation.

Typically, cells are expected to grow only during interphase and cease growth in mitosis. However, as explained in the previous section, budding yeast cells acquire nearly 60% of their total cell volume in mitosis (Leitao and Kellogg, 2017a). Other cell types do exhibit some membrane growth during mitosis but are not accompanied by an increase in cell volume. For instance, the syncytial *Drosophila* embryos develop membrane compartments called metaphase furrows to ensure faithful segregation of chromosomes (Lecuit and Wieschaus, 2000). But so far, understanding how mammalian cells grow has been relatively mysterious due to their constantly fluctuating cell shapes and membrane dynamicity. Budding yeast cells thus provide an excellent model to understand cell growth and how it influences cell cycle progression.

Membrane growth delivers key signaling lipids and proteins to the cell membrane

The plasma membrane is a highly dynamic organelle of the cell. The shape and surface area of the cell membrane are ultimately determined by the pattern of membrane growth and the relative rates of endo- and exo-cytosis. In fact, the

continued functioning of the secretory pathway that delivers vesicles for membrane formation is essential for normal ribosome biogenesis - the production of ribosomes; to increase the biosynthetic capacity of the cell (Li et al., 2000; Mizuta and Warner, 1994). Thus, plasma membrane growth is an essential driver of growth-related events in the cell and must therefore be precisely controlled. Furthermore, the lipid constitution in the inner and outer leaflets of the membrane is quite different and strongly influenced by various cell cycle proteins (Clarke et al., 2017; Roelants et al., 2015; Yamane-Sando et al., 2014).

There is growing evidence that signaling lipids enriched in local clusters at the plasma membrane could create niches for specific signaling events (Haupt and Minc, 2017; Kabeche et al., 2015). For instance, anionic phospholipids like phosphatidylserine (PS) are usually delivered by vesicle trafficking to the outer leaflet and eventually flipped to the cytosolic side by flippases (Pomorski et al., 2003). The negatively charged polar head groups of PS help generate locally-charged membrane regions, which recruit proteins with polybasic residues, creating a polarized cell (Haupt and Minc, 2017). Although PS is not an abundant phospholipid in the cell, it constitutes nearly 25 - 30% of the total phospholipid content in the plasma membrane (van Meer et al., 2008). It is thus plausible that delivery of such signaling lipids to the growing plasma membrane can generate “growth signals” that recruit and activate signaling proteins, which provide an indirect readout of cell growth and orchestrate timely progression through the cell cycle.

We previously showed that cessation of membrane growth by blocking the secretory pathway causes a pre-mitotic checkpoint arrest (Anastasia et al., 2012a). Anastasia *et al*. provided the first mechanistic link between membrane growth and

mitotic entry (**Fig. 1**). Briefly, this checkpoint is initiated when the inactive Rho1 GTPase is delivered to the growing bud tip in secretory vesicles where it gets activated by membrane-anchored Rho1 guanine-nucleotide exchange factor (GEFs) (Abe et al., 2003). Once at the membrane, Rho1 activates protein kinase C (Pkc1), which eventually interacts with the PP2A phosphatase, bound to the Cdc55 regulatory subunit (B55 homolog in yeast) and accessory Zds1/2 proteins (Jonasson et al., 2016; Kamada et al., 1996; Rossio and Yoshida, 2011a; Rossio et al., 2014; Wicky et al., 2011). Together, the $PP2A^{Cdc55}$-Zds1/2 complex activate the phosphatase Cdc25, which in turn activates Cdk1 for mitotic entry (Kumagai and Dunphy, 1991; Pal et al., 2008). Thus, gradual activation of Rho1-Pkc1 as vesicles are delivered to the growing bud tip provide an indirect readout of the extent of polar bud growth and dictate when cells could initiate mitosis. This pathway will be further studied and discussed in greater detail in chapter 4.

Figure 1: Inactive Rho1 delivered to the growing bud through vesicle trafficking initiates a growth-dependent signaling cascade for mitotic entry.
The model below summarizes the findings of (Anastasia et al., 2012a).

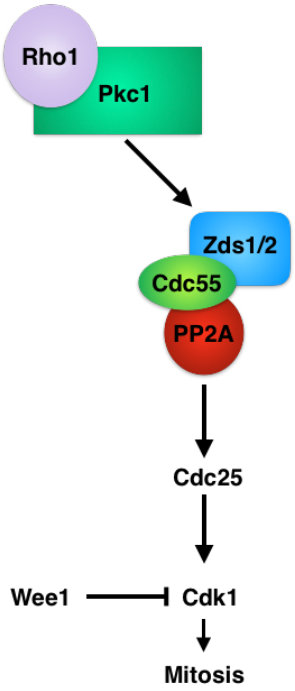

My work in chapters 2 and 3 implicate the related kinases Gin4 and Hsl1 in a similar mechanism, where the Gin4-related kinases could be getting activated in response to isotropic membrane growth upon binding to PS at the bud neck and then mediating mitotic progression once cells have undergone sufficient growth. This regulation is warranted since the growth rate of cells in mitosis almost quadruples compared to interphase and consequently cells acquire nearly 60% of their total volume during this time (Leitao and Kellogg, 2017a). Thus, strong regulatory processes must be enforced in this phase. Further, details are discussed in chapters 2 and 3.

Control of growth rate and cell size is interlinked and regulated by the conserved TORC2 network

The most obvious physical manifestation of cell growth is the increase in cell size. Emerging evidence from various systems suggest that the size of the cell at any given point in the cell cycle is a reflection of its growth rate in the preceding cell cycle phase as well as the amount of time spent growing (Cadart et al., 2018a; Ferrezuelo et al., 2012; Leitao and Kellogg, 2017a; Leitao et al., 2019b). Moreover, these processes need to be coordinated with other growth processes like the translational capacity of the cell so that cells undergo growth in the most efficient way possible (Knapp et al., 2019). External environmental factors such as nutrient availability also play a key role in setting the growth rate and size threshold of the cells such that in poor nutrients, the size threshold is lower than in rich nutrients, however, in the same nutrient conditions, larger cells grow much faster than smaller cells (Fantes and Nurse, 1977; Johnston et al., 1977b; Prescott, 1956). Thus, a cell's growth rate is regulated

by nutrient availability, which determines the size of the cell at maturity, which in turn will influence the growth rate of the cell. As a result, cells growing in poor nutrients will grow at a slower growth rate and acquire a smaller cell size compared their counterparts in rich nutrients. We found that these processes are coordinated like a well-oiled machine, with the conserved TORC2 signaling pathway at the helm, from yeast cells to human cells (Gonzalez and Rallis, 2017; Lucena et al., 2017b; Xie and Guan, 2011). Moreover, both Pkc1 and the Gin4-related kinases are upstream of the TORC2 pathway (Alcaide-Gavilán et al., 2018b; Leskoske et al., 2018). Thus, the proteins that sense the extent of cell growth are also well-positioned to influence growth rate by modulating TORC2 activity.

Models for cellular growth control

While the fact that cells possess intrinsic mechanisms for growth control is universally accepted, there are however, differing opinions as to what aspect of growth is actually being measured and how. Since cells come in different shapes and sizes, it has been relatively difficult for a single mechanism to be adaptable for all cell types. For a long time, the field of growth control favored the “sizer” or the “timer” models. The “sizer” model can be exemplified by fission yeast, where cells need to cross achieve a critical cell size to gain entry into mitosis (Nurse, 1975; Pan et al., 2014). In contrast, in a ”timer” model, cells are expected to grow for a fixed amount of time, so that large cells grow more than the smaller cells leading to cells of varying cell sizes (Allard et al., 2018a; Banerjee et al., 2017). Alternatively, a “dilution” model postulates that cells could be sensing their own volume by diluting/titrating the concentration of a

sensor protein present in a fixed amount, so that eventually when the protein is diluted sufficiently, the cell cycle progresses further (Schmoller et al., 2015).

Recently, the “adder” model has been receiving wide popularity in the field. This mechanism relies on the addition of a constant amount of cell growth in each cell cycle irrespective of the parent cell sizes. In this way, large cells grow less, and small cells grow more in each successive cell cycle until the sizes of all cells converge to an average size over time. This mechanism has been held widely applicable from bacteria to mammalian cells (Amir, 2014; Campos et al., 2014; Jun and Taheri-Araghi, 2014; Varsano et al., 2017). Moreover, the Gin4-based growth sensing model that I propose in the later chapters of this thesis could also be used to enforce an adder mechanism in yeast cells.

Growth control at the organ and organismal level

While the contents of this thesis mostly deal with growth control at the cellular level, it is important to understand that growth control also exists at the organ and organismal level. The size of an organ is regulated by a balance in the rates of cell growth, cell proliferation and cell death. Increases in organ size can thus be mediated by hypertrophy (increase in cell size) or hyperplasia (increase in cell number by cell proliferation). Even though cellular hypertrophy seems to be the most straightforward way to meet the demands of the body compared to undergoing additional rounds of cell division, the increased cell size serves the opposite function. If cells become too large, the metabolic demands of the cell would increase and transport of solutes in and out of the cell would become inefficient. It is perhaps for this reason, that various disease models exhibit irregular cell sizes. For instance, it is quite common for patients

of myocardial infarction that causes death of the cardiac tissues to have a compensatory increase in the size of the remaining cardiac cells in order to cope with the demands of the body. Consequently such patients often suffer from enlarged hearts or “ventricular hypertrophy”, which in turn, further increases the risk of myocardial infarction in patients (Nepper-Christensen et al., 2017). Control of cell size is thus critical at the organ level, although complicated by various factors. It is possible that a small subset of cells direct cellular proliferation throughout the entire organ (“top-down” mechanism). In other cases, the final size of the organ is determined by the local cell-cell signaling (“bottom-up” mechanism) (Hariharan, 2015). In either scenario, the challenge is to determine how the behavior of each cell in the organ is regulated so that collectively, the organ reaches the correct size.

One example of a signaling pathway that is implicated in organ growth regulation in mammals is the Hippo pathway. *In vivo* activation or inactivation of downstream Hippo pathway components caused changes in liver size (Zeng and Hong, 2008). A study found Par-1 (the Gin4 homolog in *Drosophila*) as a novel regulator of the Hippo pathway, where Par-1 overexpression resulted in an increased expression of Hippo target genes responsible for an increased cell proliferation (Huang et al., 2013). In a mechanism possibly similar to yeast Gin4, the Par proteins are known for establishing cell polarity in *Drosophila* and *C. elegans* as well as to facilitate asymmetric cell division (Jiang and Harris, 2019; Tabler et al., 2010). These findings suggest that the molecular signals that operate in yeast cells are most likely conserved across different species.

Concluding remarks

In all single and multicellular cells, growth control is established at the cellular level. Mechanisms that control cell growth not only ensure that growth scales with nutrient availability but also act as gatekeepers that allow cell proliferation only when a threshold amount of growth has occurred. But how exactly do cells measure their own growth? And how do they link cell growth to cell division? The following chapters will try to answer some of these questions.

CHAPTER 2 (submitted to MBoC) : Growth-dependent activation of protein kinases links cell cycle progression to cell growth

Introduction

Key cell cycle transitions occur only when sufficient growth has occurred. To enforce this linkage, cells must convert growth into a proportional signal that triggers cell cycle progression when it reaches a threshold. The molecular mechanisms by which cells generate proportional signals used to measure and limit growth have remained deeply mysterious.

In budding yeast, growth occurs in 3 distinct intervals that are characterized by different rates and patterns of growth (Ferrezuelo et al., 2012; Goranov et al., 2009; Johnston et al., 1977b; Leitao and Kellogg, 2017b; McCusker et al., 2007). The first interval occurs during G1 phase and is characterized by uniform growth over the cell surface. The second interval is initiated at the end of G1 phase when a new daughter cell emerges and undergoes polar growth. The third interval is initiated at entry into mitosis and is marked by a switch from polar bud growth to growth that occurs more widely over the bud surface. Bud growth continues throughout mitosis. The distinct size and shape of a yeast cell is ultimately defined by the extent of growth during each of these intervals.

Several observations suggest that maintenance of a specific cell size requires tight control over the duration and extent of bud growth (Leitao and Kellogg, 2017b). First, little growth occurs during G1 phase. For example, in cells growing in rich nutrients only about 20% of growth occurs during G1 phase. Rather, most growth occurs during mitosis, and the rate of growth in mitosis is approximately 3-fold faster than growth during the other intervals. Therefore, failure to tightly control the duration

and extent of bud growth, particularly during mitosis, would have large consequences for cell size.

Additional evidence that bud growth is tightly controlled comes from analysis of the effects of nutrients on cell growth and size. Shifting cells from rich to poor nutrients causes a reduced growth rate, as well as a large reduction in cell size (Johnston et al., 1977b; 1979). This proportional relationship between growth rate and cell size appears to hold across all orders of life. In budding yeast, a shift to poor nutrients has little effect on cell size at completion of G1 phase (Bean et al., 2006; Leitao and Kellogg, 2017b). Furthermore, mutant cells that lack all known regulators of cell size in G1 phase show robust nutrient modulation of cell size (Jorgensen and Tyers, 2004). In contrast, poor nutrients cause a large decrease in the extent of growth in both metaphase and anaphase, which causes daughter cells to complete cytokinesis at a substantially reduced size (Hartwell and Unger, 1977; Leitao and Kellogg, 2017b). Furthermore, the duration of growth in mitosis is increased in poor nutrients, which suggests that cells compensate for slow bud growth by increasing the duration of growth (Leitao and Kellogg, 2017b). These observations point to the existence of mechanisms that measure and modulate both the duration and extent of bud growth in mitosis.

A model in which the extent of bud growth is tightly controlled requires a molecular mechanism for measuring growth. In previous work, we found evidence that polar bud growth before mitosis is measured via growth-dependent hyperphosphorylation and activation of the protein kinase Pkc1 (Anastasia et al., 2012b). The data suggest a model in which vesicles that drive polar growth of the plasma membrane carry signaling molecules that drive activation of Pkc1 at the site of

membrane growth, thereby generating a signal that is proportional to the extent of growth. Here, we searched for proteins that could play a role in measuring growth during mitosis. A candidate-based approach identified 3 related kinases: Gin4, Hsl1 and Kcc4. We refer to these as Gin4-related kinases. Similar kinases are found in all eukaryotes. Observations reaching back over 30 years have suggested that Gin4-related kinases play roles in control of cell growth and size (Altman and Kellogg, 1997a; Barral et al., 1999; Ma et al., 1996; Okuzaki et al., 1997; Young and Fantes, 1987). For example, loss of Gin4-related kinases in both budding yeast and fission yeast causes a prolonged delay in mitotic progression (Altman and Kellogg, 1997a; Barral et al., 1999; Ma et al., 1996; Okuzaki et al., 1997; Young and Fantes, 1987). Growth continues during the delay, resulting in aberrant growth of large cells. These observations suggest that Gin4-related kinases could play roles in growth control. However, a caveat is that previous analysis of Gin4-related kinases utilized gene deletions that cause severe phenotypes. This made it difficult to discern which aspects of the phenotype are an immediate and direct consequence of loss of function, versus phenotypic effects that are the result of secondary defects accumulated over multiple generations. For example, there is evidence that loss of Gin4-related kinases causes defects in positioning the mitotic spindle, which could cause chromosome segregation defects and associated mitotic delays that lead to abnormally prolonged growth (Fraschini et al., 2006; Gihana et al., 2018; Grava et al., 2006). In this case, growth defects could be a secondary consequence of mitotic spindle defects. Similarly, previous studies have shown that mother cell size strongly influences growth and size of the daughter cell, which could mean that gradually accumulating defects in mother cell size over multiple generations could cause indirect effects on daughter cell growth

and size (Leitao and Kellogg, 2017b; Schmoller et al., 2015). An additional limitation of previous studies is that they hinted that Gin4-related kinases could be involved in growth control yet found no evidence that the activity of Gin4-related kinases is mechanistically linked to cell growth, which made it difficult to rule out alternative models.

Here, we utilized conditional alleles of the Gin4-related kinases to show that defects in control of bud growth are an immediate and direct consequence of inactivating Gin4-related kinases. We further show that Gin4-related kinases control the duration and extent of growth during metaphase, and that they do so partly via regulation of Cdk1 inhibitory phosphorylation. Finally, we show that Gin4-related kinases generate and/or relay growth-dependent signals that could be used to measure bud growth.

Results

Gin4-related kinases are required for normal control of bud growth during mitosis

Gin4 and Hsl1 are the most important Gin4-related kinases in budding yeast. Loss of either kinase alone causes defects in control of bud growth, whereas loss of both causes severe defects (Barral et al., 1999; Longtine et al., 2000). Loss of the Gin4 paralog Kcc4 has little effect. We therefore focused on Gin4 and Hsl1. To avoid the complications associated with long term inactivation of the Gin4-related kinases, we created auxin-inducible degron (AID) versions of Gin4 and Hsl1, which allowed us to define the immediate effects of inactivation (Nishimura et al., 2009). A strain carrying AID-tagged versions of both *GIN4* and *HSL1* had no size defects in the

absence of auxin (**Fig. S1 A**). Addition of auxin before mitosis in synchronized cells caused a large reduction in levels of Gin4-AID protein within 30 minutes (**Fig. S1 B**), as well as a delay in mitotic progression (**Fig. S1 C**).

Figure S1: Characterization of *gin4-AID* and *hsl1-AID* alleles.
(A) Wild type, *2xTIR1* control cells*, gin4-AID hsl1-AID 2xTIR1 cells* and *gin4-AID hsl1-AID swe1*Δ *2xTIR1* cells were grown overnight at room temperature in YPD and cell size distributions were analyzed with a Coulter counter. **(B)** Control cells and *gin4-AID hsl1-AID* cells growing in YPD were released from a G1 phase arrest. After release, the *gin4-AID hsl1-AID* cells were split into two aliquots and 0.5 mM auxin was added to one aliquot and an equivalent amount of the solvent for auxin was added to the other. Auxin was also added to the control strain. Samples were taken at the indicated intervals and the behavior of Gin4 was analyzed by western blot. All strains contain 2 copies of the *TIR1* gene (*2xTIR1*). **(C)** *gin4-AID hsl1-AID 2xTIR1* cells growing in YPD were released from a G1 phase arrest. After release, the cells were split into two aliquots and 0.5 mM auxin was added to one aliquot and an equivalent amount of the solvent for auxin was added to the other. Samples were taken at the indicated intervals and the behavior of Clb2 was analyzed by western blot.

A.

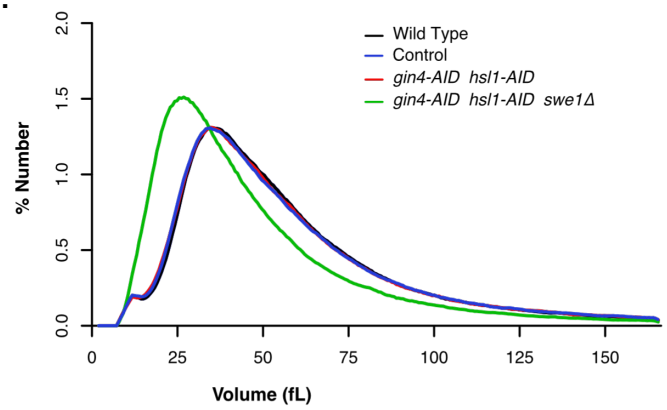
Wild Type
Control
gin4-AID hsl1-AID
gin4-AID hsl1-AID swe1Δ
% Number
0.0
0.5
1.0
1.5
2.0
0
25
50
75
100
125
150
Volume (fL)

B.

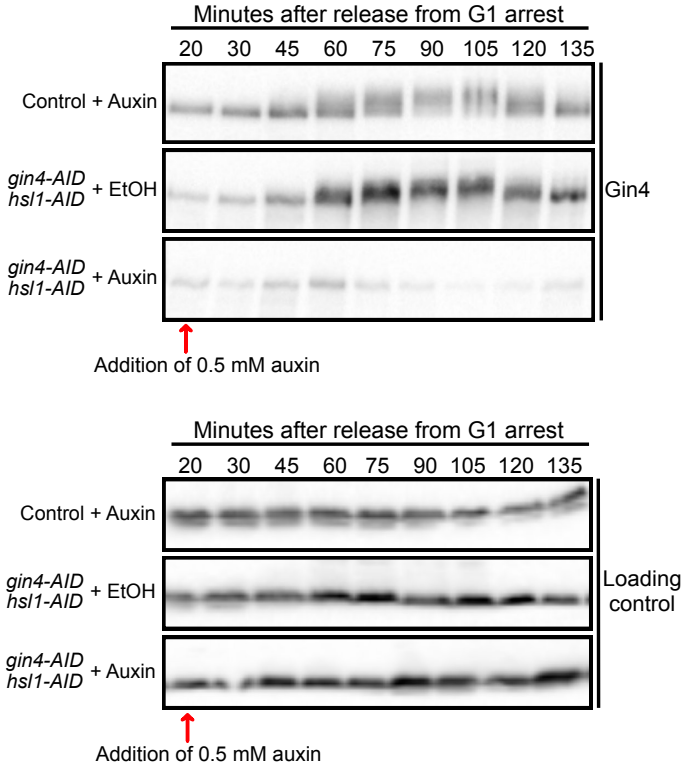
Minutes after release from G1 arrest
20 30 45 60 75 90 105 120 135
Control + Auxin
gin4-AID hsl1-AID + EtOH
gin4-AID hsl1-AID + Auxin
Gin4
Addition of 0.5 mM auxin
Minutes after release from G1 arrest
20 30 45 60 75 90 105 120 135
Control + Auxin
gin4-AID hsl1-AID + EtOH
gin4-AID hsl1-AID + Auxin
Loading control
Addition of 0.5 mM auxin

C.

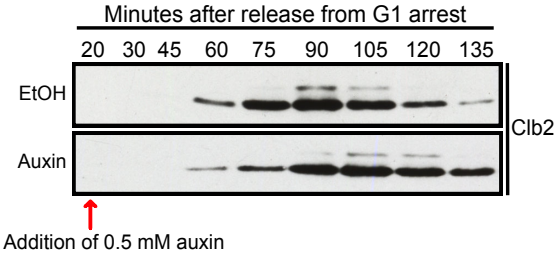
Minutes after release from G1 arrest
20 30 45 60 75 90 105 120 135
EtOH
Auxin
Clb2
Addition of 0.5 mM auxin

We first tested how conditional inactivation of Gin4 and Hsl1 influences bud growth and mitotic progression via live analysis of single cells. We included a fluorescently tagged spindle pole protein to monitor the duration of metaphase and anaphase (see Materials and Methods and (Leitao and Kellogg, 2017b)). The spindle poles in wild type and *gin4-AID hsl1-AID* cells were marked with different fluorescent tags, which allowed simultaneous imaging of both strains under identical conditions.

We analyzed the effects of *gin4-AID* or *hsl1-AID* alone, as well as the combined effects of *gin4-AID hsl1-AID*. Cells were released from a G1 arrest and auxin was added immediately before initiation of bud emergence, which ensured that Gin4 and Hsl1 were depleted by the time of mitotic entry. Bud size and mitotic spindle dynamics were then analyzed at 3-minute intervals to determine how loss of Gin4 and Hsl1 influenced bud growth and the duration of mitosis. Examples of wild type and *gin4-AID hsl1-AID* cells are shown in **Fig. 2.1 and Video 1**. Both cells undergo bud emergence at nearly the same time, but the wild type cell completes bud growth and exits mitosis while the *gin4-AID hsl1-AID* cell remains delayed in metaphase as the bud continues to grow. The *gin4-AID hsl1-AID* cell eventually completes mitosis, but at a substantially larger bud size than the wild type control cell. The daughter bud is more elongated in the *gin4-AID hsl1-AID* cell, which indicates a defect in control of polar growth.

Figure 2.1: Gin4 and Hsl1 are required for normal control of cell growth and size in mitosis.
Control cells and *gin4-AID hsl1-AID* cells were differentially marked with fluorescently-tagged mitotic spindle poles. Thus, control cells express *SPC42-mRuby2*. while the *gin4-AID hsl1-AID* cells express *SPC42-GFP*. Both strains include 2 copies of the *TIR1* gene. Cells growing in CSM were arrested with α factor and then mixed together before releasing from the arrest. Auxin was added to 0.5 mM at 20 minutes after release from arrest, which corresponds to approximately 30 minutes before bud emergence. Cells were then imaged at 3-minute intervals by confocal microscopy at 27°C. Bud emergence was used to set the zero timepoint. Key mitotic transitions are highlighted for each strain.

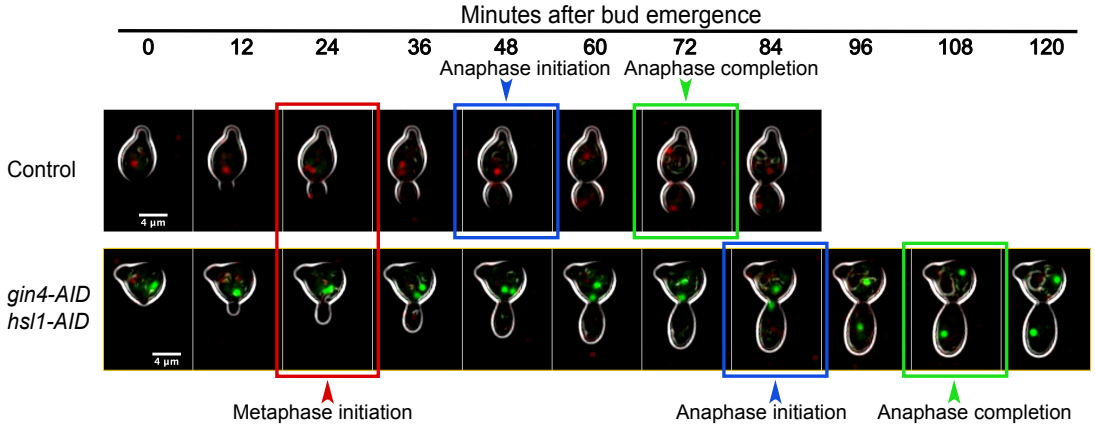

Quantitative analysis of multiple cells showed that destruction of Gin4 and/or Hsl1 caused an increase in the duration of metaphase but had no effect on the duration of anaphase (**Fig. 2.2 A**). Destruction of Gin4 and Hsl1 also caused an increase in bud size at completion of each mitotic interval (**Fig. 2.2 B**). The effects of *gin4-AID* and *hsl1-AID* were not additive (**Fig. 2.2, A and B**), which was surprising because *hsl1*Δ and *gin4*Δ have strong additive effects on cell size and shape (**Fig. S2 A** and (Barral et al., 1999)). This issue is addressed below.

In wild type cells, bud volume at completion of mitosis is proportional to growth rate during mitosis (Leitao and Kellogg, 2017b). *gin4-AID hsl1-AID* appeared to cause a partial loss of the proportional relationship between growth rate and cell size at completion of mitosis (**Fig. 2.2 C**). However, *gin4-AID hsl1-AID* did not cause significant effects on the growth rate of the daughter cell (**Fig. S2 B**).

Figure 2.2: Gin4 and Hsl1 are required for normal control of cell growth and size in mitosis.
Cells of the indicated genotypes were released from a G1 arrest and analyzed by confocal microscopy as described for Fig. 3 B. All strains included 2 copies of the *TIR1* gene. **(A)** Scatter plots showing the duration of metaphase and anaphase. **(B)** Scatter plots showing bud size at completion of metaphase and anaphase. **(C)** Plots showing cell size at completion of mitosis versus growth rate in mitosis for control cells and *gin4-AID hsl1-AID* cells. **(D)** Scatter plots showing the ratio of major axis to minor axis of the bud at completion of anaphase. For panels **A,B,D**, the mean and standard deviation for each strain are shown.

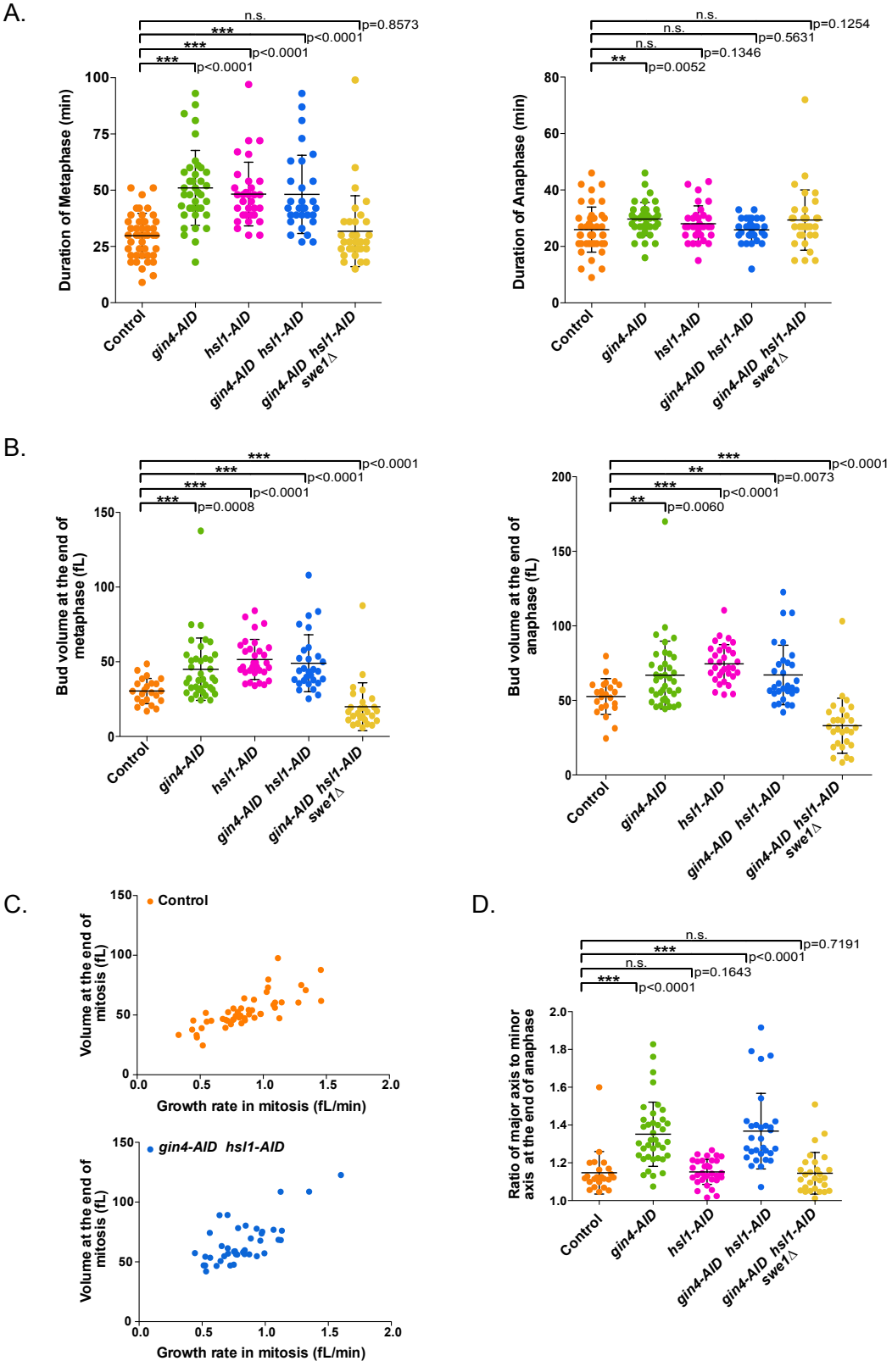
A.
Duration of Metaphase (min)
n.s. p=0.8573
*** p<0.0001
*** p<0.0001
*** p<0.0001
Duration of Anaphase (min)
n.s. p=0.1254
n.s. p=0.5631
n.s. p=0.1346
** p=0.0052
B.
Bud volume at the end of metaphase (fL)
*** p<0.0001
*** p<0.0001
*** p<0.0001
*** p=0.0008
Bud volume at the end of anaphase (fL)
*** p<0.0001
** p=0.0073
*** p<0.0001
** p=0.0060
Control
gin4-AID
hsl1-AID
gin4-AID hsl1-AID
gin4-AID hsl1-AID swe1Δ
C.
Control
gin4-AID hsl1-AID
Volume at the end of mitosis (fL)
Growth rate in mitosis (fL/min)
D.
Ratio of major axis to minor axis at the end of anaphase
n.s. p=0.7191
*** p<0.0001
n.s. p=0.1643
*** p<0.0001

Figure S2: Gin4 and Hsl1 control bud growth during mitosis.
(A) *gin4Δ, hsl1Δ, gin4Δ hsl1Δ, and gin4Δ hsl1Δ swe1Δ* cells were grown to log phase in YPD media at 25˚C and images were obtained using DIC optics. **(B)** A scatter plot showing the growth rate of the daughter buds during mitosis for the indicated genotypes. The growth rate (fL/min) was determined as the increase in bud volume from initiation of metaphase to the completion of anaphase, divided by the total time spent in metaphase and anaphase.

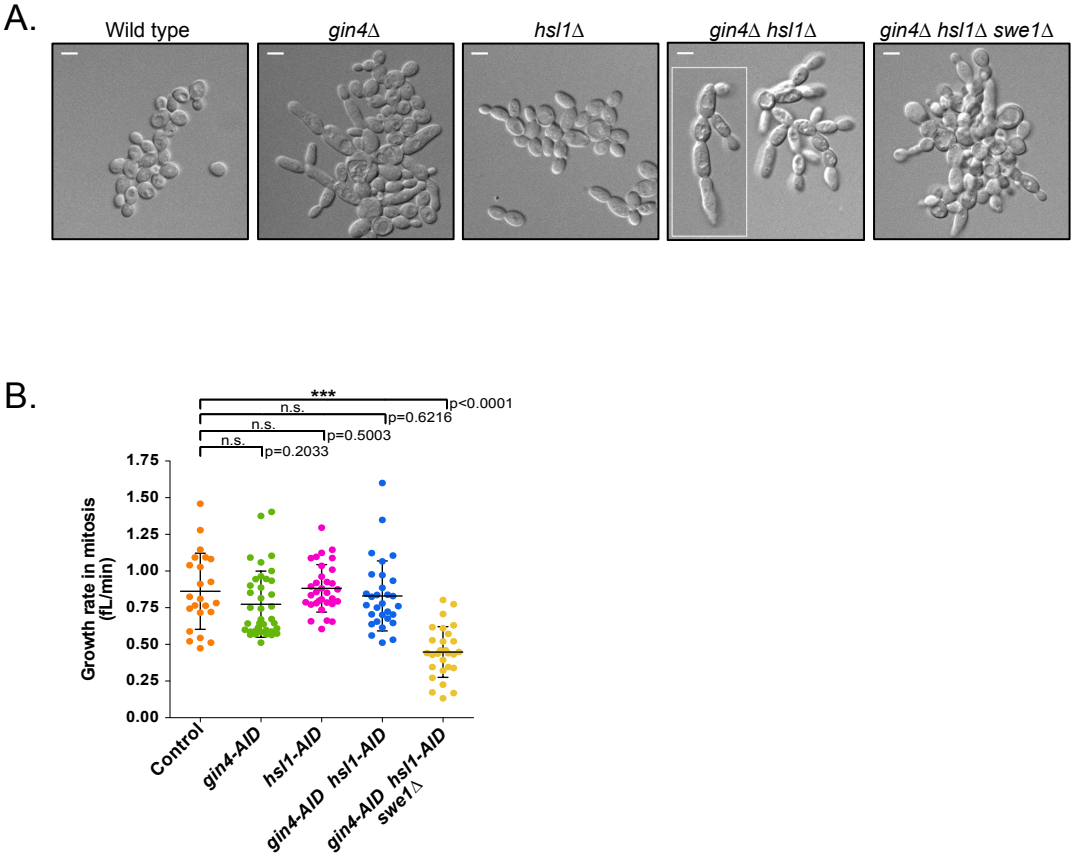

Inactivation of *gin4-AID* caused polar bud growth to continue in mitosis, whereas inactivation of *hsl1-AID* did not. This effect was quantified by measuring axial ratios of daughter buds at completion of anaphase (**Fig. 2.2 D**).

Previous studies found that *gin4*Δ and *hsl1*Δ cause defects in cytokinesis that lead to formation of clumps of interconnected cells (Altman and Kellogg, 1997a; Barral et al., 1999; Ma et al., 1996; Okuzaki et al., 1997). Consistent with this, we observed that *gin4-AID hsl1-AID* caused a failure in cell separation in nearly all cells following the first cell cycle after addition of auxin (**Video 2**). Previous studies also found that *gin4*Δ and *hsl1*Δ cause defects in spindle positioning (Fraschini et al., 2006; Grava et al., 2006; Gihana et al., 2018). We observed few defects in spindle positioning during the first cell division after addition of auxin to *gin4-AID hsl1-AID* cells. However, in the second cell division many cells showed aberrant movement of the metaphase spindle into the daughter cell before anaphase (**Video 2**).

Gin4-related kinases are required for normal control of mother cell growth

In wild type cells, little growth of the mother cell occurs after bud emergence (Ferrezuelo et al., 2012; McCusker et al., 2007). In *gin4-AID hsl1-AID* cells, however, mother cell growth often continued throughout the interval of daughter cell growth. Example plots of mother and daughter cell size as a function of time for wild type and *gin4-AID hsl1-AID* cells are shown in **Fig. 2.3 A**. Quantitative analysis revealed that *gin4-AID* and *hsl1-AID* had additive effects upon mother cell growth so that most *gin4-AID hsl1-AID* cells underwent abnormal mother cell growth (**Fig. 2.3 B**).

Figure 2.3: Gin4 and Hsl1 are required for normal control of mother cell growth.

Cells of the indicated genotypes were released from a G1 arrest and analyzed by confocal microscopy as described for Fig. 3 B. **(A)** A representative plot of mother and daughter cell size as a function of time. In each case, the daughter cell is the daughter of the mother cell shown in the same plot. **(B)** Scatter plots showing the net increase in mother cell volume from the time of bud emergence to completion of anaphase. The plot shows the mean and standard deviation for each strain.

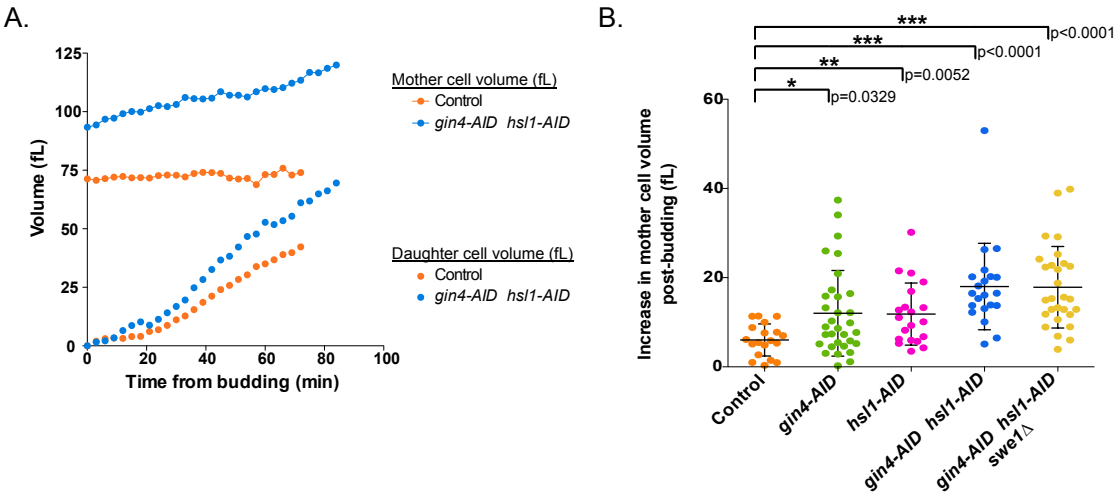

Previous work has shown that large mother cells drive a faster rate of daughter cell growth (Leitao and Kellogg, 2017b; Schmoller et al., 2015). As a result, the increased size of mothers in *gin4-AID hsl1-AID* cells would be expected to drive faster growth of daughter cells in subsequent cell divisions, leading to increased defects in cell growth and size in subsequent cell divisions. Thus, the role of Gin4 and Hsl1 in control of mother cell growth could help explain why prolonged loss of Gin4 and Hsl1 causes strong additive effects on cell growth and size. Defects in spindle positioning and cell separation could also cause defects that accumulate over multiple subsequent cell divisions. We found that the effects caused by *gin4-AID hsl1-AID* increased substantially with prolonged incubation in the presence of auxin, consistent with a model in which the terminal phenotype caused by *gin4*Δ *hsl1*Δ is the result of defects that accumulate over multiple cell cycles (**Fig. S3**).

Figure S3: The severity of the *gin4-AID hsl1-AID* phenotype increases with time.

Control cells and *gin4-AID hsl1-AID* cells were grown to log phase at room temperature in YPD medium and auxin was added to both strains. Both strains included 2 copies of the *TIR1* gene. DIC images of the cells were taken at the indicated times. Scale bar represents 5 μm.

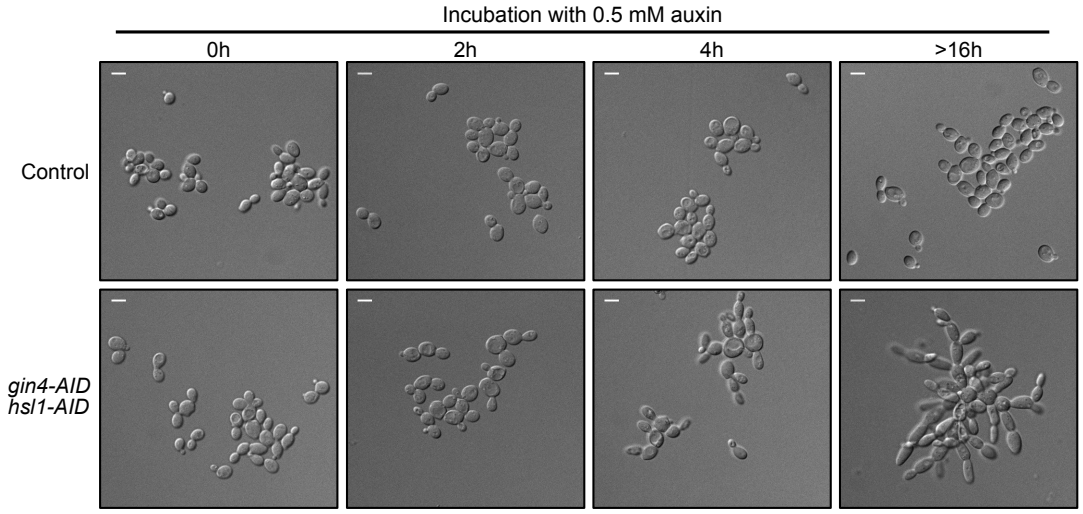

Gin4-related kinases influence the duration of growth in metaphase via inhibitory phosphorylation of Cdk1

Genetic analysis has shown that Gin4 and Hsl1 are negative regulators of Swe1, which is the budding yeast homolog of the Wee1 kinase that phosphorylates and inhibits mitotic Cdk1 (Longtine et al., 2000; Ma et al., 1996). Additional studies have shown that Swe1 influences the timing of mitotic entry as well as the duration of metaphase (Harvey and Kellogg, 2003; Leitao et al., 2019a; Lianga et al., 2013). We therefore tested whether Gin4 and Hsl1 influence metaphase duration via Swe1. To do this, we analyzed the effects of *swe1*Δ on bud growth and mitotic duration in *gin4-AID hsl1-AID* cells. This revealed that *swe1*Δ eliminated the prolonged metaphase delay caused by loss of Gin4 and Hsl1 (**Fig. 2.2 A**). Furthermore, *swe1*Δ caused daughter buds in *gin4-AID hsl1-AID* cells to complete metaphase and anaphase at sizes smaller than the wild type control cells (**Fig. 2.2 B**), and it eliminated the bud elongation caused by *gin4-AID* (**Fig. 2.2 D**). As reported previously, *swe1*Δ caused reduced growth rate, which is thought to be due to the decreased size of mother cells (**Fig. S2 B**)(Leitao et al., 2019a).

Several observations demonstrated that Gin4 and Hsl1 do not influence growth solely via Swe1. Previous studies found that *swe1*Δ cells have a shorter metaphase than wild type cells (Leitao et al., 2019a; Lianga et al., 2013). Here, we found that *swe1*Δ reduced the duration of metaphase in *gin4-AID hsl1-AID* cells, but it did not make the duration of metaphase in these cells shorter than metaphase in wild type cells. In addition, *swe1*Δ did not fully rescue growth defects caused by *gin4*Δ *hsl1*Δ (**Fig. S2 A**). Finally, *swe1*Δ did not eliminate inappropriate growth of mother cells in *gin4-AID hsl1-AID* cells (**Fig. 2.3 B**). Together, these observations demonstrate that

Gin4 and Hsl1 control bud growth during mitosis through Swe1-dependent and Swe1-independent mechanisms.

Gin4 and Hsl1 are required for full hyperphosphorylation of Swe1

We next investigated how Gin4 and Hsl1 control Swe1. In previous work, we showed that Swe1 undergoes complex regulation in mitosis (Harvey et al., 2011; 2005; Sreenivasan and Kellogg, 1999). In early mitosis, Cdk1 phosphorylates Swe1 on Cdk1 consensus sites, which activates Swe1 to bind and inhibit Cdk1. This form of Swe1, which we refer to as partially hyperphosphorylated Swe1, works in a systems-level mechanism that maintains a low level of Cdk1 during metaphase. Further phosphorylation events drive full hyperphosphorylation of Swe1, leading to release of Cdk1 and inactivation of Swe1. Swe1 is proteolytically destroyed at the end of mitosis; however, mutants that block Swe1 destruction have no effect on mitotic progression, so the function of Swe1 destruction remains unknown (Raspelli et al., 2011; Thornton and Toczyski, 2003).

A previous study suggested that *hsl1*Δ causes defects in phosphorylation of Swe1 but did not provide sufficient resolution of differently phosphorylated forms of Swe1 to determine which events were affected (Shulewitz et al., 1999). Here, we found that conditional inactivation of gin4-AID and hsl1-AID before mitosis in synchronized cells caused a failure in full hyperphosphorylation of Swe1 (**Fig. 2.4**). Similarly, addition of auxin to asynchronous *gin4-AID hsl1-AID* cells caused loss of fully hyperphosphorylated Swe1 within 30 minutes (**Fig. S4**). These data show that Gin4 and Hsl1 are required for generation of the fully hyperphosphorylated inactive

form of Swe1, consistent with genetic data showing that Gin4-related kinases are negative regulators of Swe1.

Figure 2.4: Gin4 and Hsl1 are required for full hyperphosphorylation of Swe1. Control cells and *gin4-AID hsl1-AID* cells growing in YPD were released from a G1 arrest at 25˚C and 0.5 mM auxin was added to both strains 20 min after release. Both strains included 2 copies of the *TIR1* gene. Samples were taken at the indicated intervals and the behavior of Swe1 and Clb2 was analyzed by western blot.

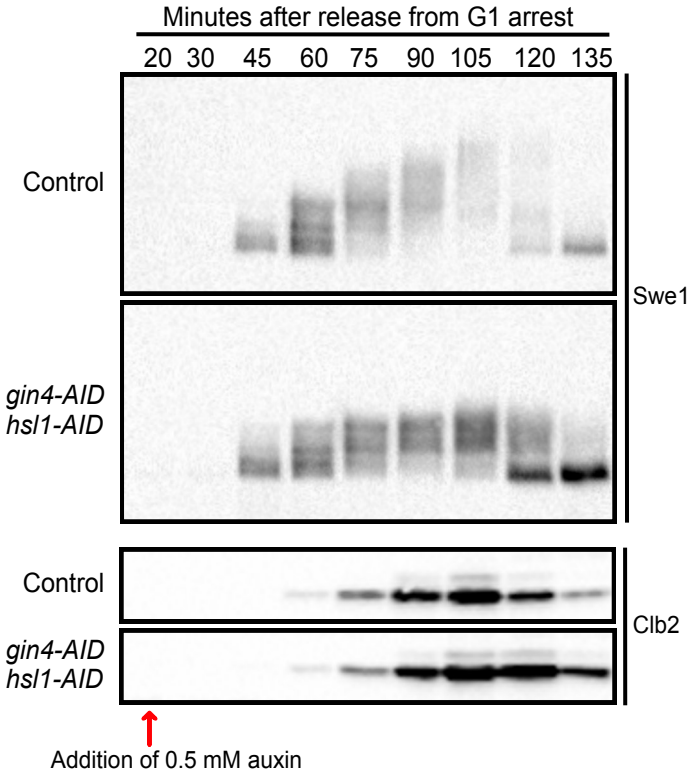

Figure S4: Swe1 is rapidly dephosphorylated in asynchronous cells upon inactivation of Gin4 and Hsl1.
gin4-AID hsl1-AID 2xTIR1 cells were grown to log phase in YPD and were then split into two aliquots. 0.5 mM auxin was added to one aliquot and an equivalent amount of the solvent for auxin was added to the other. Samples were taken at the indicated intervals and the behavior of Swe1 was analyzed by western blot. Anti-Nap1 was used as loading control.

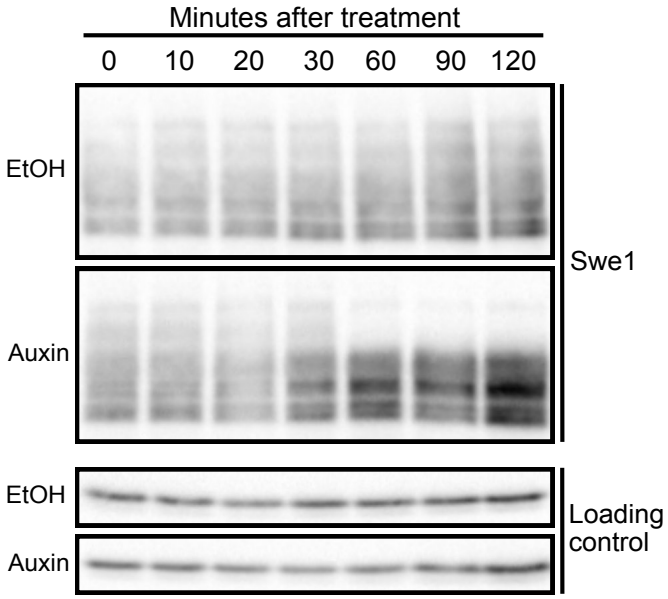

Hyperphosphorylation of Gin4 and Hsl1 is correlated with the extent of bud growth

We previously found that Gin4 undergoes gradual hyperphosphorylation and activation during bud growth, reaching peak activity in late mitosis as growth ends (Altman and Kellogg, 1997a). Thus, gradual phosphorylation and activation of Gin4 appears to be correlated with gradual bud growth, which suggests that growth-dependent activation of Gin4 could provide a proportional readout of the extent of bud growth. To begin to test this hypothesis, we first carried out additional experiments to determine whether hyperphosphorylation of Gin4 and Hsl1 is proportional to bud growth. To do this, we took advantage of the fact that the durations of both metaphase and anaphase are increased when cells are growing slowly on a poor carbon source, yet the extent of growth in mitosis is reduced (Leitao and Kellogg, 2017; Leitao et al., 2019). In other words, cells in poor carbon spend more time growing in both metaphase and anaphase, but complete mitosis at a reduced daughter bud size. Therefore, if hyperphosphorylation of Gin4 and Hsl1 is proportional to bud growth, the time required to reach full hyperphosphorylation should be increased in cells growing in poor carbon.

Wildtype cells growing in rich carbon (2% glucose) or poor carbon (2% glycerol, 2% ethanol) were released from a G1 arrest and phosphorylation of Gin4 and Hsl1 was assayed by western blot to detect phosphorylation events that cause electrophoretic mobility shifts. The same samples were also probed for the mitotic cyclin Clb2 as a marker for mitotic duration. Cells growing in poor carbon showed delayed mitotic entry and a prolonged mitosis compared to cells growing in rich carbon, as previously described (**Fig. 2.5, A and B**) (Leitao and Kellogg, 2017b). Gin4 is

present throughout the cell cycle, while Hsl1 is synthesized anew before mitosis and destroyed at the end of mitosis (Altman and Kellogg, 1997a; Barral et al., 1999). In both carbon sources, hyperphosphorylation of Gin4 and Hsl1 increased gradually during mitosis, with peak phosphorylation occurring near peak Clb2 levels. In addition, the interval during which hyperphosphorylation occurred was prolonged in poor carbon, consistent with the hypothesis that hyperphosphorylation of Gin4 and Hsl1 provides a readout of the extent of bud growth. Previous studies have shown that the increased duration of mitosis in poor carbon under these conditions is not an artifact caused by poor synchrony (Leitao and Kellogg, 2017b; Leitao et al., 2019a).

We also noticed that the maximal extent of phosphorylation of Gin4 and Hsl1 was reduced in poor carbon (**Fig. 2.5, A, B and C**). Thus, cells in poor carbon progress through mitosis with less hyperphosphorylation of Gin4 and Hsl1 than cells in rich carbon, which suggests that the maximal extent of hyperphosphorylation of Gin4 and Hsl1 reached during mitosis is proportional to the growth rate set by the carbon source. One interpretation of this observation is that the extent of hyperphosphorylation of Gin4 and Hsl1 required for mitotic exit is reduced in poor carbon, which allows cells to complete mitosis at a smaller bud size.

Figure 2.5: Hyperphosphorylation of Gin4 and Hsl1 is proportional to the extent of bud growth.

Wild type cells grown overnight in YPD **(A)** or YPG/E **(B)** were arrested with α factor. The cells were then released from the arrest at 25˚C and samples were taken at 10 min intervals. The behavior of Gin4, Hsl1-6XHA and Clb2 was assayed by western blot. **(C)** A direct comparison of the maximal extent of Gin4 phosphorylation in rich or poor carbon was made by comparing samples taken at peak Clb2 expression in each condition (90 min in rich carbon and 140 min in poor carbon). An anti-Nap1 antibody was used as a loading control.

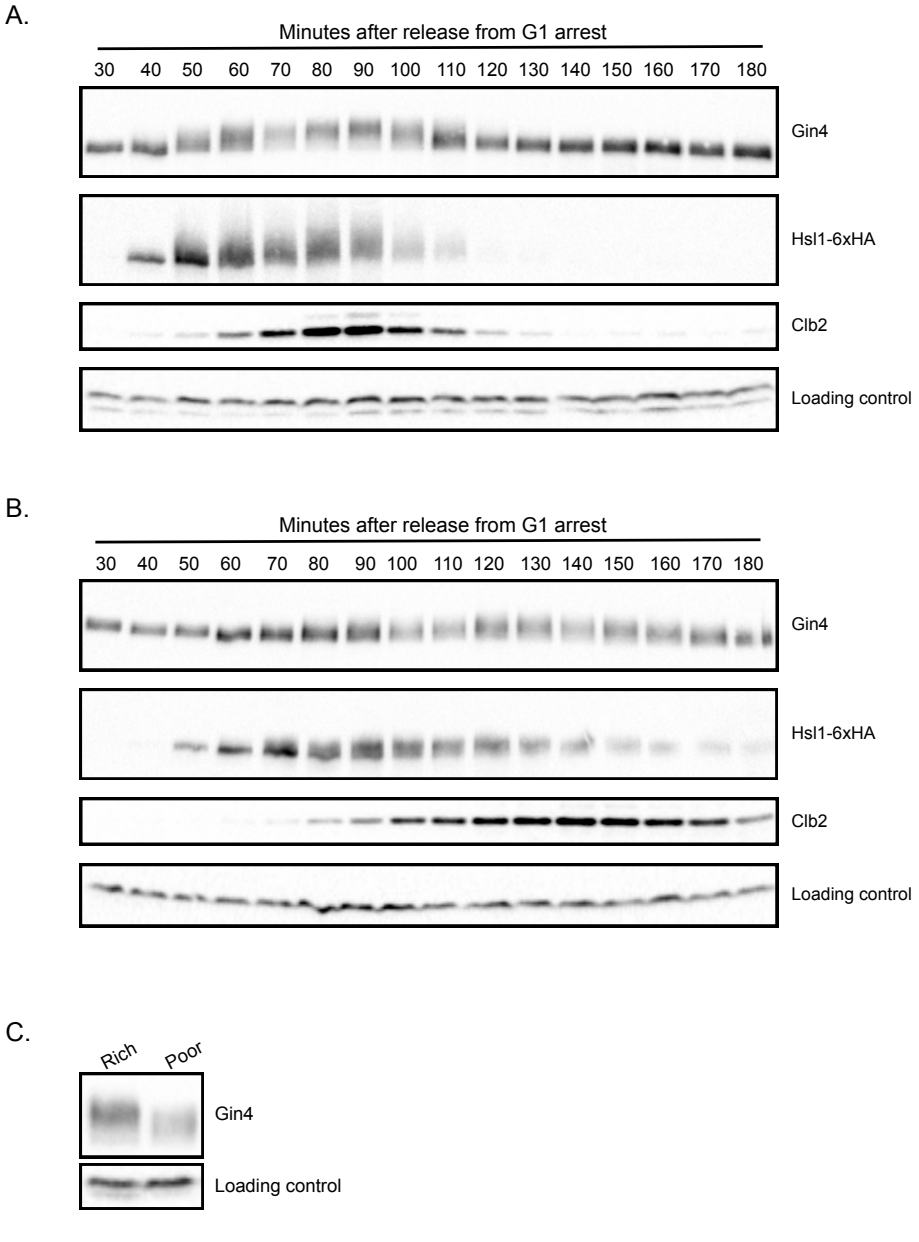

Hyperphosphorylation of Gin4 is dependent upon bud growth

We next tested whether hyperphosphorylation of Gin4 is dependent upon bud growth. To do this, we used a temperature-sensitive allele of *SEC6* (*sec6-4*) to block bud growth. Sec6 is a component of the exocyst complex, which is required at the plasma membrane for docking and fusion of vesicles that drive bud growth. In previous work, we showed that inactivation of Sec6 blocks bud growth and triggers an arrest in early mitosis (Anastasia et al., 2012b). The arrest is enforced by Swe1. Thus, *sec6-4 swe1*Δ cells fail to undergo bud growth yet enter mitosis and complete chromosome segregation before arresting in late mitosis. We therefore analyzed Gin4 phosphorylation in *sec6-4 swe1*Δ cells, which allowed us to distinguish whether effects of *sec6-4* were a consequence of a failure to undergo bud growth, or a failure in mitotic progression. As controls, we also analyzed Gin4 hyperphosphorylation in wild type and *swe1*Δ cells.

Cells were released from a G1 arrest and shifted to the restrictive temperature for the *sec6-4* allele before bud emergence. Gin4 phosphorylation was assayed by western blot (**Fig. 2.6 A**). The same samples were probed for Clb2 as a marker for mitotic progression (**Fig. 2.6 B**). The *sec6-4 swe1*Δ cells entered mitosis but arrested in late mitosis with high levels of mitotic cyclin, as previously reported (Anastasia et al., 2012b). Hyperphosphorylation of Gin4 failed to occur in the *sec6-4 swe1*Δ cells (**Fig. 2.6, A and C**). Direct comparison of the extent of Gin4 hyperphosphorylation in mitosis showed a complete loss of Gin4 phosphorylation (**Fig. 2.6 C**). Thus, hyperphosphorylation of Gin4 is dependent upon membrane trafficking events that drive bud growth.

Figure 2.6: Hyperphosphorylation of Gin4 is dependent upon bud growth. Wild type, *swe1*Δ and *swe1*Δ *sec6-4* cells were released from a G1 arrest in YPD at room temperature and shifted to the restrictive temperature (34˚C) 30 min after release from arrest. Samples were taken at the indicated intervals and the behavior of Gin4 **(A)** and Clb2 **(B)** was analyzed by western blot. **(C)** A direct comparison of the extent of Gin4 phosphorylation was made by loading samples from all three strains taken at 90 min (wild type), 80 min (*swe1*Δ) and 100 min (*sec6-4 swe1*Δ).

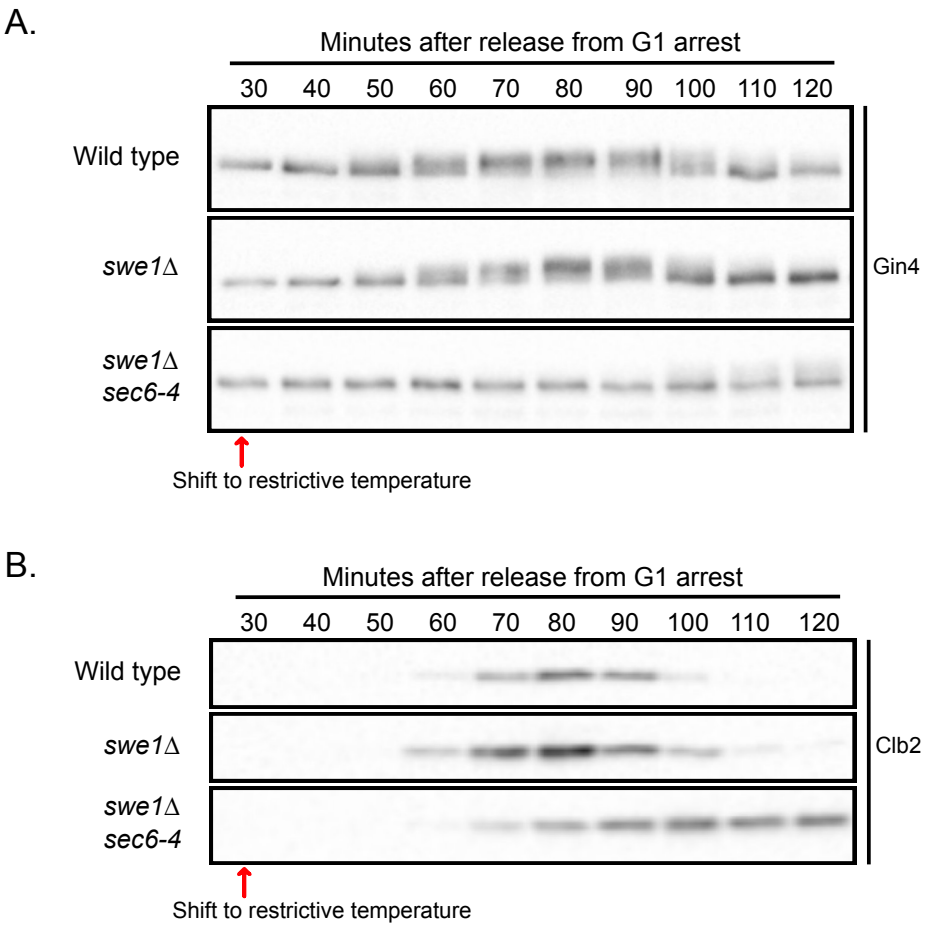

Proportional phosphorylation of Gin4 during bud growth requires binding to anionic phospholipids

We next investigated the mechanisms that drive hyperphosphorylation of Gin4-related kinases, since these could provide clues to how growth-dependent signals are generated and relayed. Both Gin4 and Hsl1 have well-defined C-terminal kinase associated 1 (KA1) domains, which bind phosphatidylserine and other anionic phospholipids (Moravcevic et al., 2010). Phosphatidylserine is a low abundance phospholipid that is preferentially localized to the growing bud (Ejsing et al., 2009; Fairn et al., 2011; Klose et al., 2012), and in vivo analysis suggests that phosphatidylserine is the most important effector for KA1 domains (Moravcevic *et al.*, 2010). Furthermore, binding of phosphatidylserine to kinases that contain KA1 domains can promote an open and active conformation of the kinase that could potentially drive autophosphorylation or phosphorylation by another kinase (Emptage et al., 2017; 2018; Wu et al., 2015). Together, these observations led us to hypothesize that phosphatidylserine delivered to the plasma membrane during bud growth could drive hyperphosphorylation of Gin4-related kinases, thereby generating a signal that is proportional to the extent of growth.

To test the hypothesis, we focused on Gin4. A version of Gin4 that lacks the KA1 domain (*gin4-ΔKA1*) failed to undergo hyperphosphorylation during bud growth (**Fig. 2.7 A**). Analysis of Clb2 levels in synchronized cells showed that *gin4-ΔKA1* cells exhibited normal timing of mitotic entry and an increased duration of mitosis (**Fig. 2.7 B**). The *gin4-ΔKA1* cells also showed increased cell size and an elongated bud phenotype similar to *gin4Δ* cells (**Fig. 2.7, C and D)**. *gin4-ΔKA1* in an *hsl1Δ* background caused a phenotype similar to *gin4Δ hsl1Δ* (**Fig. 2.7 D**). Finally, Gin4-

ΔKA1-GFP failed to localize to the bud neck normally and was observed primarily in the cytoplasm (**Fig. 2.7 E**), although weak localization to the bud neck could be detected in a fraction of cells, indicating that determinants outside the KA1 domain contribute to Gin4 localization to the bud neck (**arrowheads, Fig. 2.7 E**).

The KA1 domain could carry out functions required for Gin4 hyperphosphorylation that are independent of binding to anionic phospholipids. We reasoned that if binding to anionic phospholipids is the sole function of the KA1 domain, then replacing the KA1 domain with a heterologous phosphatidylserine binding domain should restore normal Gin4 activity. To test this, we replaced the KA1 domain with the bovine LactC2 domain, which shows no structural similarity to the KA1 domain (Moravcevic et al., 2010; Shao et al., 2008). The LactC2 domain was sufficient to restore proportional hyperphosphorylation of Gin4 during bud growth in *gin4-ΔKA1-LactC2* cells (**Fig. 2.7 A**). In addition, *gin4-ΔKA1-LactC2* cells showed normal mitotic timing, as well as normal cell size (**Fig. 2.7, B, C and D)**. Finally, the LactC2 domain restored normal bud neck localization to *gin4-ΔKA1* (**Fig. 2.7 E**). A previous study showed that deletion of the KA1 domain of Hsl1 causes reduced localization of Hsl1 to the bud neck, which can be rescued by addition of the LactC2 domain (Finnigan *et al.*, 2016).

Mutation of three amino acids in the LactC2 domain required for efficient binding to phosphatidylserine (*gin4-ΔKA1-LactC2^{AAA}*) (Yeung *et al.*, 2008) caused a failure in proportional phosphorylation of Gin4 (**Fig. 2.7 A**), as well as a phenotype similar to *gin4Δ* and *gin4-ΔKA1* (**Fig. 2.7, B, C and D**). The *LactC2^{AAA}* domain partially restored Gin4 localization to the bud neck, however, the amount of *gin4-ΔKA1-LactC2^{AAA}-GFP* at the bud neck was reduced relative to *GIN4-GFP* and *gin4-ΔKA1-*

LactC2-GFP (**Fig. 2.7 E and S5**). These data suggest that the delivery of anionic phospholipids to the membrane could drive gradual growth-dependent activation of Gin4-related kinases.

Figure 2.7: Proportional phosphorylation of Gin4 during bud growth requires binding to anionic phospholipids.
Cells of the indicated genotypes were released from a G1 arrest in YPD at 30˚C. The behavior of Gin4 **(A)** and Clb2 **(B)** was analyzed by western blot. In each strain, Gin4 constructs were marked with a 3xHA tag and detected with anti-HA antibody. The signal for *gin4-ΔKA1* and the LactC2 constructs was weaker, so these blots were exposed longer. Gin4-ΔKA1-3xHA was about 16 KDa smaller than the other proteins. **(C)** Cells of the indicated genotypes were grown in YPD overnight, diluted in fresh YPD, and then incubated for 5h at 30˚C. The size distribution for each strain was analyzed using a Coulter counter. **(D)** Cells of the indicated genotypes were grown to log phase in YPD at 25˚C and imaged by DIC optics. **(E)** Cellular localization of Gin4, Gin4-ΔKA1, Gin4-ΔKA1-LactC2 and Gin4-ΔKA1-LactC2^{AAA} fused to GFP at the C-terminus. All four strains were excited by the GFP-laser with identical settings at 100x magnification and displayed with the same brightness levels to compare relative levels of Gin4 localized to the bud neck. Gin4-ΔKA1-GFP shows mostly cytoplasmic localization with a small level of bud neck localization (white arrowheads). The brightfield images for each field are shown below. Scale bar represents 5 μm.

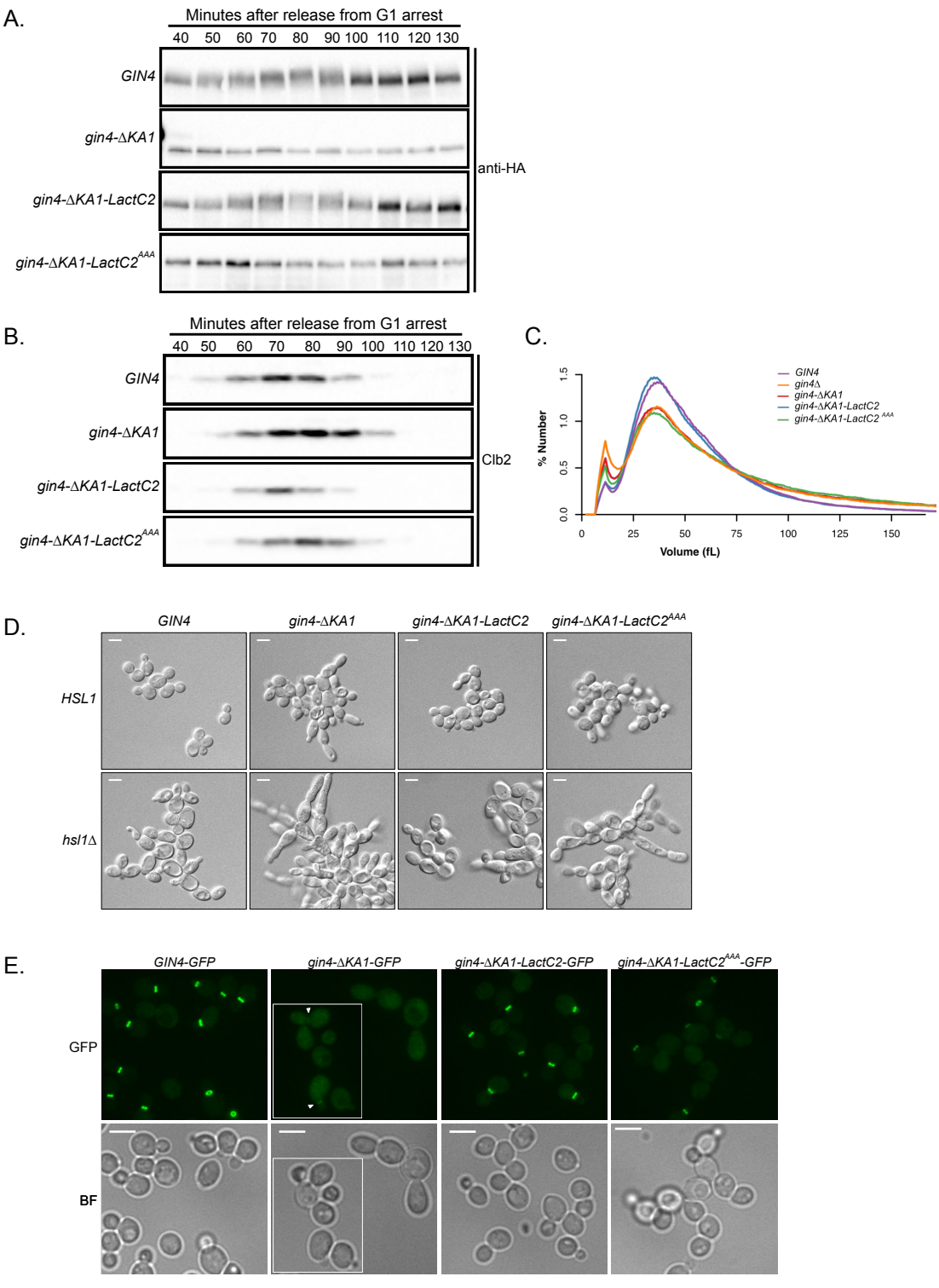
A.
Minutes after release from G1 arrest
40 50 60 70 80 90 100 110 120 130
GIN4
gin4-ΔKA1
gin4-ΔKA1-LactC2
gin4-ΔKA1-LactC2AAA
anti-HA
B.
Minutes after release from G1 arrest
40 50 60 70 80 90 100 110 120 130
GIN4
gin4-ΔKA1
gin4-ΔKA1-LactC2
gin4-ΔKA1-LactC2AAA
Clb2
C.
GIN4
gin4Δ
gin4-ΔKA1
gin4-ΔKA1-LactC2
gin4-ΔKA1-LactC2 AAA
% Number
0.0
0.5
1.0
1.5
0
25
50
75
100
125
150
Volume (fL)
D.
GIN4
gin4-ΔKA1
gin4-ΔKA1-LactC2
gin4-ΔKA1-LactC2AAA
HSL1
hsl1Δ
E.
GIN4-GFP
gin4-ΔKA1-GFP
gin4-ΔKA1-LactC2-GFP
gin4-ΔKA1-LactC2AAA-GFP
GFP
BF

Figure S5: Quantification of Gin4-GFP constructs at the bud neck.
Cells of the indicated genotypes were analyzed to determine the maximum pixel intensity for GFP fluorescence at the bud neck. The Y-axis on the scatter plot shows the maximum pixel intensity in arbitrary units after subtracting background signal.

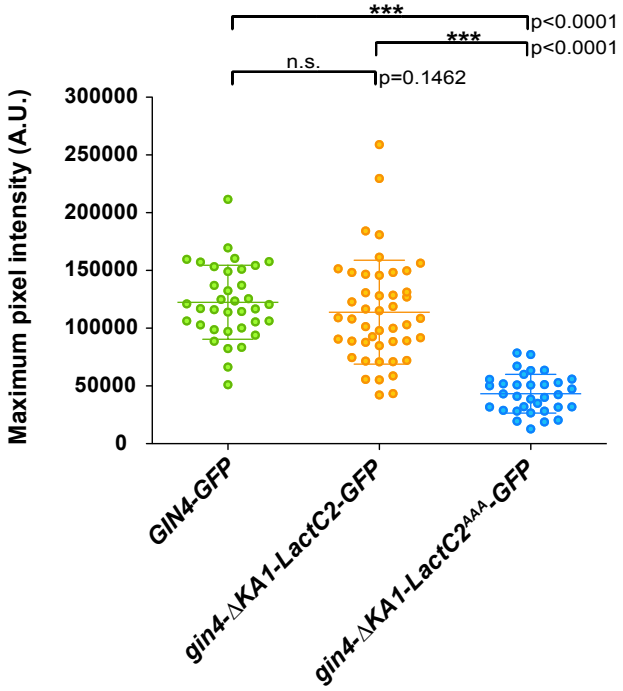

Discussion

Growth-dependent activation of Gin4-related kinases could link cell cycle progression to cell growth

Our results show that Gin4-related kinases have key properties expected of proteins that play roles in measuring cell growth. For example, we used the first conditional alleles of Gin4-related kinases to show that their loss causes inappropriate growth during a prolonged metaphase delay. Thus, cells that lack Gin4-related kinases behave as though they fail to properly detect that bud growth has occurred, consistent with a model in which they relay growth-dependent signals that report on the extent of growth. We also discovered that gradual hyperphosphorylation of Gin4-related kinases during bud growth is dependent upon and proportional to bud growth. In previous work, we showed that the kinase activity of Gin4 is dependent upon and proportional to Gin4 hyperphosphorylation (Altman and Kellogg, 1997a; Mortensen et al., 2002). Together, these observations suggest that the events that drive bud growth also drive growth-dependent hyperphosphorylation and activation of Gin4-related kinases. We therefore hypothesize that Gin4-related kinases generate and/or relay growth-dependent signals that are used to measure the extent of bud growth.

Growth-dependent signals could also be used to ensure that growth rate scales with cell size. Previous studies have pointed to close functional relationships between Gin4-related kinases and the TORC2 signaling network, a master regulator of cell growth that strongly influences growth rate (Alcaide-Gavilán et al., 2018a; Zapata et al., 2014). The Gin4-related kinases promote signaling in the TORC2 network and TORC2 signaling appears to scale with cell size during bud growth (Alcaide-Gavilán et al., 2018a). Thus, growth-dependent activation of Gin4-related kinases could drive

a gradual increase in TORC2 signaling that drives a gradual increase in growth rate as cells increase in size.

The maximal extent of Gin4 and Hsl1 hyperphosphorylation achieved in mitosis is reduced in poor nutrients. Thus, it appears that cells in poor nutrients require a lower threshold of Gin4/Hsl1 activity to progress through mitosis. We therefore hypothesize that reduction in cell size at completion of metaphase in poor nutrients (Leitao and Kellogg, 2017b) could be driven by nutrient-dependent signals that reduce the threshold activity of Gin4-related kinases required for mitotic progression.

Additional analysis will be needed to test these hypotheses. The use of biochemical reconstitution to define the molecular mechanisms that drive proportional phosphorylation of Gin4-related kinases will be a key step.

Gin4-related kinases influence the duration and extent of bud growth in metaphase

Previous analysis of the in vivo functions of Gin4-related kinases utilized gene deletions. A caveat of these studies was that gene deletions cause severe phenotypes that could be the outcome of cumulative defects gained over multiple generations. Therefore, it has not been possible to discern the immediate and direct consequences of loss of function of Gin4-related kinases. Indeed, our analysis of conditional alleles strongly suggests that a number of the previously observed phenotypes caused by deleting Gin4-related kinases are indirect effects that accumulate over multiple generations. Here, conditional alleles allowed us to rigorously define the functions of Gin4-related kinases. This showed that inactivation of Gin4 and Hsl1 causes aberrant growth during a prolonged metaphase delay but has little effect on the duration or

extent of growth in anaphase. In a previous study we found that extensive growth occurs during anaphase, and that the duration and extent of growth in anaphase is modulated by nutrients, which suggests that anaphase growth is regulated (Leitao and Kellogg, 2017b). Our results suggest that Gin4-related kinases are unlikely to control the anaphase growth interval. Growth in anaphase is also unlikely to be controlled by Cdk1-inhibitory phosphorylation (Leitao et al., 2019a). The mechanisms that control the duration and extent of growth in anaphase therefore remain mysterious.

Gin4-related kinases influence the location of growth

The effects of inactivating Gin4 and Hsl1 on the duration of growth in metaphase were not additive, which was surprising because *gin4*Δ and *hsl1*Δ show strong additive effects on cell size and shape (Barral et al., 1999). A potential explanation came from the discovery that loss of Gin4-related kinases causes inappropriate mother cell growth during mitosis. In this case, the effects were additive. Previous work found that large mother cells drive an increased growth rate in daughter cells (Leitao and Kellogg, 2017b; Schmoller et al., 2015). Thus, we hypothesize that increased size of mother cells caused by loss of Gin4 and Hsl1 drives an increased rate of growth that amplifies aberrant growth in subsequent divisions. However, other factors likely contribute to the additive effects of *gin4*Δ and *hsl1*Δ. For example, we observed severe spindle positioning defects in the second cell division after inactivation of Gin4 and Hsl1, which could cause prolonged mitotic delays that lead to further aberrant growth. Defects in growth control could also be amplified by failures in cytokinesis that create chains of conjoined cells in which the signals that control cell growth and size are no longer effectively compartmentalized.

Our studies also suggest that Gin4 and Hsl1 play different roles in controlling polar bud growth. Destruction of Gin4 caused excessive polar growth in the first cell cycle following destruction, whereas destruction of Hsl1 did not. In normal cells, the interval of polar growth is terminated by low level activation of Cdk1 at mitotic entry (Lew and Reed, 1993). However, low level activation of Cdk1 appears to occur normally in *gin4*Δ cells, albeit with a delay (Altman and Kellogg, 1997a). Moreover, the elongated buds and cell separation defects caused by *gin4*Δ are not fully rescued by *swe1*Δ. Together, these observations suggest that Gin4 influences polar growth at least partly via a mechanism that works downstream or independently of Cdk1. Previous work suggested that Gin4 binds and regulates Bnr1, a formin protein that controls the location of actin cables that deliver vesicles to sites of membrane growth (Buttery et al., 2012b). Bnr1 is localized to the bud neck, and loss of Bnr1 is thought to cause inappropriate polar growth because the actin cables that direct isotropic growth are lost (Gao and bretscher, 2010; Pruyne et al., 2004a). Thus, polar growth caused by loss of Gin4 could be due at least partly to misregulation of Bnr1. The fission yeast homolog of Gin4 also is also known to execute functions that are independent of Wee1 (Breeding et al., 1998).

Gin4-related kinases influence growth in metaphase partly via Cdk1 inhibitory phosphorylation

Early work suggested that Wee1 family members work solely at mitotic entry. However, more recent work in both vertebrates and yeast found that Wee1 also controls events after mitotic entry (Harvey et al., 2011; Lianga et al., 2013; Vassilopoulos et al., 2014; Toledo et al., 2015; Leitao et al., 2019)(Deibler and

Kirschner, 2010). In budding yeast, several studies suggested that the activity of Swe1 in metaphase could be controlled by the Gin4-related kinases; however, interpretation of the results was complicated by use of gene deletions (Altman and Kellogg, 1997a; Barral et al., 1999; Carroll et al., 1998; Sreenivasan and Kellogg, 1999; Sreenivasan et al., 2003). Here, conditional inactivation of Gin4 and Hsl1 provided definitive evidence that Gin4-related kinases influence the duration of metaphase via Cdk1 inhibitory phosphorylation. We also showed that loss of Gin4-related kinases causes a failure in full hyperphosphorylation of Swe1. Previous studies suggested that Gin4-related kinases from fission yeast can directly phosphorylate Wee1; however, there is no evidence yet that this is true in budding yeast (Coleman et al., 1993; Kanoh and Russell, 1998).

Careful analysis of the effects of conditional inactivation of Gin4-related kinases suggested that they do not influence the duration of metaphase solely via Swe1. Previous studies showed that the duration of metaphase in *swe1*Δ cells is shorter than in wild type cells (Leitao et al., 2019a; Lianga et al., 2013). Here, we found *swe1*Δ substantially reduced the metaphase delay caused by inactivation of Gin4-related kinases, but metaphase was still slightly prolonged relative to wild type cells.

Growth-dependent hyperphosphorylation of Gin4 requires binding to anionic phospholipids

We found that growth-dependent hyperphosphorylation of Gin4 and normal control of cell growth are both dependent upon the KA1 domain, which binds anionic phospholipids. We further discovered that growth-dependent phosphorylation of Gin4

occurs normally when the KA1 domain is replaced by a heterologous LactC2 domain that binds phosphatidylserine. Mutations in the LactC2 domain that reduce binding to phosphatidylserine also block growth-dependent phosphorylation of Gin4 and cause a failure in control of cell growth.

Hyperphosphorylation of both Gin4 and Hsl1 is dependent upon their kinase activity, which suggests that growth-dependent phosphorylation is due to autophosphorylation (Altman and Kellogg, 1997; Barral *et al.*, 1999). Moreover, previous studies have suggested that binding of anionic phospholipids to KA1 domains can drive formation of an open, active conformation (Wu *et al.*, 2015; Emptage *et al.*, 2017; 2018). Together, these observations suggest that anionic phospholipids delivered to the growing bud could generate a growth-dependent signal by binding and activating Gin4-related kinases. In this model, the Gin4-related kinases would be direct sensors of a critical event that drives cell growth (i.e. delivery of anionic phospholipids to the plasma membrane).

Alternative models are possible. For example, binding to anionic phospholipids could help bring Gin4-related kinases to the bud neck where they receive growth-dependent signals from other kinases. Distinguishing models will require a better understanding of the molecular mechanisms that drive growth-dependent phosphorylation of Gin4-related kinases.

The KA1 domain binds preferentially to phosphatidylserine but can also bind other anionic phospholipids, such as phosphatidylinositol (Moravcevic *et al.*, 2010; Wu *et al.*, 2015). In contrast, the LactC2 domain appears to bind only to phosphatidylserine (Shao *et al.*, 2008). The fact that the KA1 domain can be functionally replaced by the LactC2 domain therefore suggests that binding to

phosphatidylserine is sufficient to generate or relay a growth-dependent signal. Phosphatidylserine is a low abundance lipid that is preferentially localized to the growing bud (Fairn et al., 2011; Moravcevic et al., 2010). Phosphatidylserine is also preferentially localized to sites of membrane growth in fission yeast (Haupt and Minc, 2017).

Cells that completely lack phosphatidylserine can be made by deleting the CHO1 gene, which encodes the enzyme that catalyzes the last step in synthesis of phosphatidylserine. However, interpretation of the phenotype caused by loss of phosphatidylserine is complicated by several factors. First, loss of phosphatidylserine causes increased synthesis of phosphatidylinositol, an anionic phospholipid that could compensate for some functions of phosphatidylserine, including binding to KA1 domains (Hikiji et al., 1988; Matsuo et al., 2007). In addition, phosphatidylserine is a precursor in one of the major pathways used to synthesize phosphatidylethanolamine (Klug and Daum, 2014). In both budding yeast and fission yeast, cells that lack phosphatidylserine are barely viable (Hikiji et al., 1988; Matsuo et al., 2007). In fission yeast, the slow growth caused by loss of phosphatidylserine can be rescued by inclusion of ethanolamine in the growth media (Matsuo *et al.*, 2007). Cells grown under these conditions are abnormally large, consistent with the idea that growth-dependent signals generated by phosphatidylserine are used to determine when sufficient growth has occurred (Haupt and Minc, 2017).

Growth-dependent signaling suggests a broadly relevant mechanism for control of cell growth and size

Theoretical analysis has shown that cell size control can be achieved by an "adder" mechanism, in which a constant increment of growth is added during each cell cycle (Campos et al., 2014). In the adder model, cells measure growth, rather than size. Adder behavior has been reported in cells ranging from bacteria to vertebrates, yet a mechanistic explanation for how growth could be measured has remained elusive (Cadart et al., 2018b; Campos et al., 2014). Our discovery that growth-dependent events drive proportional activation of Gin4-related kinases suggests that they could work in an adder mechanism that measures bud growth. Our results further suggest that delivery of signaling lipids to sites of growth could be the critical event that is monitored to measure bud growth. This kind of growth-dependent signaling could be broadly relevant, as it would be readily adaptable to cells of diverse size and shape. It could also influence cell shape by controlling the extent of growth at specific locations on the cell surface. Further analysis of the mechanisms that drive growth-dependent signaling should yield new insights into control of cell growth and size.

Materials and Methods

Yeast strain construction, media, and reagents

All strains are in the W303 background (*leu2-3,112 ura3-1 can1-100 ade2-1 his3-11,15 trp1-1 GAL+ ssd1-d2*). The additional genetic features of strains are listed in Table 1. Cells were grown in YP medium (1% yeast extract, 2% peptone, 40 mg/liter adenine) supplemented with 2% dextrose (YPD), or 2% glycerol and 2% ethanol (YPG/E). For live cell imaging, cells were grown in complete synthetic medium (CSM) supplemented with 2% dextrose and 40 mg/ml adenine.

Gene deletions and C-terminal epitope tagging was performed by standard PCR amplification and homologous recombination (Longtine *et al.*, 1998; Janke *et al.*, 2004; Lee *et al.*, 2013). *gin4-ΔKA1-LactC2* constructs integrated at the GIN4 locus were created by gene splicing with overlap extension (Horton et al., 1990). Briefly, LactC2 fragments were PCR amplified from the plasmids pKT2100 or pKT1995 (Takeda et al., 2014) with 40bp of flanking sequence at the 5' end that was homologous to the GIN4 ORF just upstream of the KA1 domain (amino acids 1007-1142) using oligos Gin4-39 and Gin4-40 (Table 2). The 3xHA::His3MX6 fragment was amplified from pFA6a-3HA-His3MX6 (Longtine et al., 1998b) with 5' homology to the terminal sequence of LactC2 and 3' homology to the DNA sequence just downstream of the Gin4 ORF using primers Gin4-38 and Gin4-41. The two fragments were then gel purified, annealed to each other and elongated for 15 PCR cycles in the absence of primers, followed by PCR amplification using primers Gin4-38 and Gin4-39. The resulting fragments were then transformed into wild type cells and correct integrants were identified by western blotting with anti-HA antibody. To create the GFP-tagged versions of the *gin4-ΔKA1-LactC2* constructs, GFP-His3MX6 was amplified from

pFA6a-GFP-His3MX6 (Longtine et al., 1998b) and spliced to LactC2 as described above.

To generate strains with an AID tag on *GIN4* and/or *HSL1*, the *HSL1* gene was tagged at the C-terminus with an AID tag marked with KanMX6 in a parent strain that has two copies of the *TIR1* gene. The KanMX6 marker was then replaced by a *TRP1* marker. Next, a second AID tag marked with KanMX6 was incorporated at the *GIN4* locus. The *SPC42* gene in all four AID-tagged strains was fused to GFP at the C-terminus using standard PCR and homologous recombination. The parent strain that contains *2xTIR1* was used as the control strain and was modified to express endogenous SPC42 fused with yeast-optimized mRuby2 (yomRuby2). Auxin was dissolved in 100% ethanol to make a 50 mM stock solution.

Cell cycle time courses and Western blotting

Cell cycle time courses were carried out as previously described (Harvey et al., 2011b). Briefly, cells were grown to log phase at room temperature overnight in YPD or YPG/E to an optical density (OD_{600}) of 0.5 - 0.7. Cultures were adjusted to the same optical density and were then arrested in G1 phase by incubation in the presence of 0.5 µg/mL α factor at room temperature for 3 hours. Cells were released from the arrest by washing 3 times with fresh YPD or YPG/E. All time courses were carried out at 25˚C unless otherwise noted, and α factor was added back at 70 minutes to prevent initiation of a second cell cycle. For experiments involving auxin-mediated destruction of proteins, a single culture synchronized in G1 phase was split into two culture flasks and 0.5 mM auxin was added to one flask at 20 minutes after release from the G1 phase arrest. An equivalent volume of ethanol was added to the control flask.

For western blotting, 1.6 mL sample volumes were collected in screw cap tubes and centrifuged at 13,000 rpm for 30 sec. After discarding the supernatant, 200 µL acid washed glass beads were added to the tubes and the samples were frozen in liquid nitrogen. Cells were lysed in 140 µL sample buffer (65 mM Tris HCl, pH-6.8, 3% SDS, 10% glycerol, 50 mM sodium fluoride, 100 mM ß-glycerophosphate, 5% ß-mercaptoethanol, and bromophenol blue) supplemented with 2 mM PMSF immediately before use. For experiments involving immunoblotting for Gin4-AID proteins, the sample buffer also included the protease cocktail LPC (1 mg/mL leupeptin, 1 mg/mL pepstatin, 1 mg/mL chymostatin dissolved in dimethylsulfoxide; used at 1/500 dilution). Sample buffer was added to cells immediately after they were removed from liquid nitrogen and the cells were then lysed in a Mini-beadbeater 16 (BioSpec) at top speed for 2 min. After a brief centrifugation, the samples were placed in a boiling water bath for 5 min and were then centrifuged again at 13,000 rpm for 3 min before loading onto SDS-PAGE gels. SDS PAGE was carried out as previously described (Harvey et al., 2011b). 10% polyacrylamide gels with 0.13% bis-acrylamide were used for analysis of Gin4, Clb2, and Nap1 (loading control). 9% polyacrylamide gels with 0.14% bis-acrylamide were used for Hsl1 and Swe1 blots. Proteins were immobilized onto nitrocellulose membranes using wet transfers for 1h 45 min. Blots were probed with the primary antibody at 1-2 µg/mL at room temperature overnight in 5% milk in PBST (1x phosphate buffered saline, 250 mM NaCl, 0.1% Tween-20) with 0.02% sodium azide. All the primary antibodies used in this study are rabbit polyclonal antibodies generated as described previously (Altman and Kellogg, 1997a; Kellogg and Murray, 1995; Mortensen et al., 2002; Sreenivasan and Kellogg, 1999). Primary antibodies were detected by an HRP-conjugated donkey anti-rabbit secondary

antibody (GE Healthcare; # NA934V) incubated in PBST for 1h at room temperature. Blots were rinsed in PBS before detection via chemiluminescence using ECL reagents (Advansta; #K-12045-D50) with a Bio-Rad ChemiDoc imaging system.

Coulter counter analysis

Cell cultures were grown in 10 mL YPD medium to an OD_{600} between 0.4 - 0.6. Cells were fixed by addition of 1/10 volume of 37% formaldehyde to the culture medium followed by incubation at room temperature for 1h. Cells were then pelleted and resuspended in 0.5 mL PBS containing 0.02% sodium azide and 0.1% Tween-20 and analyzed on the same day. Cell size was measured using a Coulter counter (Channelizer Z2; Beckman Coulter) as previously described (Artiles et al., 2009; Jorgensen et al., 2002). Briefly, 40 µL of fixed cells were diluted in 10 mL diluent (Isoton II; Beckman Coulter) and sonicated for 5 pulses of approximately 0.5 second each at low power. The Coulter Counter data shown in the figures represents the average of 3 biological replicates that is each the average of 3 technical replicates. For **Fig. 7 C** the strains were grown to log phase overnight at room temperature, diluted to OD_{600} - 0.1 in 5 mL fresh YPD, and then incubated for 4-5 h at 30˚C to observe temperature-dependent phenotypes of the mutants.

Microscopy

For DIC imaging, cells were grown to log phase in YPD and fixed in 3.7% formaldehyde for 30 min and then resuspended in PBS with 0.1% Tween-20 and 0.02% sodium azide. Images were obtained using a Zeiss-Axioskop 2 Plus microscope fitted with a 63x Plan-Apochromat 1.4 n.a. objective and an AxioCam HR

camera (Carl Zeiss, Thornwood, NY). Images were acquired using AxioVision software and processed on Fiji (Schindelin et al., 2012).

For live cell time-lapse imaging, the control strain (DK3510) and AID-tagged strains (DK3307, DK3308, DK3327 or DK3330) were grown in CSM overnight to an OD_{600} of 0.1 - 0.2 and then arrested in G1 phase with α factor. The control and the AID-tagged strains were mixed in a 1.6 mL tube and then washed 3X in CSM prewarmed to 30˚C to release the cells from the G1 phase arrest. After resuspending the cells in CSM, approximately 200 µL cells were immobilized onto a concanavalin A-treated chambered #1.5 Coverglass system (Labtek-II; Nunc™#155409) for 5 min. Unbound cells were washed away by repeated washes with CSM. The cells were then incubated in 500 µL CSM at 27˚C for the duration of the imaging. Auxin was added to the cells to a final concentration of 0.5 mM 20 minutes after the first wash used to release the cells from the α factor arrest.

Scanning confocal images were acquired on a Zeiss 880 confocal microscope running ZEN Black software using a 63x/1.4 n.a. Plan Apo objective. The microscope was equipped with a heat block stage insert with a closed lid and exterior chamber for temperature control. The microscope was allowed to equilibrate at the set temperature of 27˚C for at least 1h to ensure temperature stability prior to imaging. Definite Focus was used to keep the sample in focus during the duration of the experiment. 1 x 2 tiled *z*-stack images were acquired every 3 min. Zoom and frame size were set to 0.8x magnification to achieve a consistent pixel area of 1024 x 1024 pixels in XY and pixel dwell time was 0.5 µs. Optical sections were taken for a total of 14 *z*-planes every 0.37 µm with frame averaging set to 2, to reduce noise. 488 nm laser power was set to 0.2 % and the 561 nm laser power was set to 1% to minimize cell damage.

The gain for GFP, RFP and bright field was set to 550, 750 and 325, respectively. The same gain settings were used for each experiment. GFP signal was acquired on a GaAsP detector and collected between 498 nm - 548 nm. Brightfield images were collected simultaneously. RFP signal was acquired on a GaAsP detector and collected between 577 nm - 629 nm.

Initiation of metaphase is defined as the time at which the spindle poles move to a distance of 1-2 uM apart in the mother cell (Leitao and Kellogg, 2017b). Initiation of anaphase is marked by further separation of spindle poles and migration of one spindle pole into the daughter cell. Completion of anaphase correspond to the time when the spindle poles reach their maximal distance apart.

To visualize the localization of Gin4 constructs fused to GFP, cells were grown in CSM overnight, fixed in 3.7% formaldehyde for 15 min, and then resuspended in 500 µL 1x PBST. Images were acquired on a spinning disk confocal microscope with a Solamere system running MicroManager* (Edelstein et al., 2014). The microscope was based on a Nikon TE2000 stand and Coherent OBIS lasers. We used a 100x/1.4 n.a. Plan Apo objective for **Fig. 6 E** and a 63x/1.4 Plan Apo objective for data collection in **Fig. S5**. Pixel sizes were 0.11 µm in X,Y and *z*-stack spacing was set to 0.5 µm with a total of 17 *z*-slices. GFP was excited at 488 nm and collected through a 525/50nm band pass filter (Chroma) onto a Hamamatsu ImageEMX2 EMCCD camera. Gain levels were set to 200 to maximize signal without hitting saturation. GFP and brightfield images were collected sequentially.

Image analysis

All images were analyzed on Fiji (Schindelin et al., 2012). For visualization of GFP-tagged Gin4 constructs, a sum projection of *z*-slices was used. Movies for the time-lapse were processed as previously described(Leitao and Kellogg, 2017b). The bright field images were processed using the "Find Focused Slices" plugin available on Fiji to create a stack with the focused slice +/- one slice for each timepoint. A *z*-projection with sum of slices was performed on this stack and then bud volumes were determined using the plugin BudJ (Ferrezuelo et al., 2012).

The timings of cell cycle events were determined as previously reported (Leitao and Kellogg, 2017b). Briefly, bud initiation was manually determined by the appearance of a protrusion on the surface of the mother cell. The initiation of metaphase was marked by the appearance of separation of spindle poles to 2-3 microns apart. Initiation of anaphase was marked by further separation of the spindle poles and segregation of one of the poles into the daughter cell. We defined completion of anaphase as the point at which the spindle poles reached their maximal distance apart.

For a quantitative comparison of the localization of GFP-tagged Gin4 constructs in **Fig. S5**, a *z*-projection with sum of slices was performed on the images and an elliptical ROI was drawn around the bud neck. The maximum pixel intensity was determined for each cell after subtracting the background pixel intensity.

Statistical analysis

Data acquired from the image analysis were plotted as scatter dot plots using GraphPad Prism. The scatter plots show the data distribution along with the mean and standard deviation for each strain. For all scatter dot plots, the unpaired t-test was

calculated using the Mann-Whitney test for non-Gaussian distributions and the two-tailed *p*-values have been mentioned.

Table 1: List of strains used in Chapter 2

Strain	Mating type	Genotype	Source
DK 186	a	*bar1Δ*	(Altman and Kellogg, 1997a)
DK 3418	a	*bar1Δ HSL1-6XHA::His3MX6*	This study
SH 24	a	*bar1Δ swe1Δ::URA3*	(Harvey and Kellogg, 2003)
DK 1600	a	*bar1Δ swe1Δ::His3MX6 sec6-4::KanMX6*	(Anastasia et al., 2012b)
DK 3510	a	*bar1Δ his3::His3MX6+TIR1 leu2::LEU2+TIR1 SPC42-yomRuby2::KanMX6*	This study
DK 3307	a	*bar1Δ his3::His3MX6+TIR1 leu2::LEU2+TIR1 SPC42-GFP::HphNTI gin4-AID::KanMX6*	This study
DK 3308	a	*bar1Δ his3::His3MX6+TIR1 leu2::LEU2+TIR1 SPC42-GFP::HphNTI hsl1-AID::TRP*	This study
DK 3327	a	*bar1Δ his3::His3MX6+TIR1 leu2::LEU2+TIR1 SPC42-GFP::HphNTI gin4-AID::KanMX6 hsl1-AID::TRP1*	This study
DK 3330	a	*bar1Δ his3::His3MX6+TIR1 leu2::LEU2+TIR1 SPC42-GFP::HphNTI gin4-AID::KanMX6 hsl1-AID::TRP1 swe1Δ::URA3*	This study
DK 3350	a	*bar1Δ GIN4-GFP:: His3MX6 SPC42-yomRuby2::KanMX*	This study
DK 3790	a	*bar1Δ gin4-ΔKA1-GFP::His3MX6 SPC42-yomRuby2::KanMX*	This study
DK 3351	a	*bar1Δ gin4-ΔKA1-LactC2-GFP:: His3MX6 SPC42-yomRuby2::KanMX*	This study
DK 3823	a	*bar1Δ gin4-ΔKA1-LactC2^{AAA}-GFP::His3MX6 SPC42-yomRuby2::KanMX*	This study

DK 888	a	*bar1Δ gin4Δ::LEU2*	(Mortensen et al., 2002)
HT159	a	*bar1Δ hsl1Δ::His3MX6*	This study
DK3784	a	*bar1Δ gin4Δ::LEU2 hsl1Δ::His3MX6*	This study
DK2158	a	*bar1Δ gin4Δ::LEU2 hsl1Δ::HphNTI swe1Δ::URA3*	This study
DK 373	a	*bar1Δ GIN4-3xHA::TRP1*	This study
DK 2822	a	*bar1Δ gin4-ΔKA1-3xHA::His3MX6*	This study
DK 3286	a	*bar1Δ gin4-ΔKA1-LactC2-3xHA:: His3MX6*	This study
DK 3295	a	*bar1Δ gin4-ΔKA1-LactC2^{AAA}-3xHA::His3MX6*	This study
DK3621	a	*bar1Δ GIN4-3xHA::TRP1 hsl1Δ::HphNTI*	This study
DK3624	a	*bar1Δ gin4-ΔKA1-3xHA::His3MX6 hsl1Δ::HphNTI*	This study
DK3627	a	*bar1Δ gin4-ΔKA1-LactC2-3xHA:: His3MX6 hsl1Δ::HphNTI*	This study
DK3630	a	*bar1Δ gin4-ΔKA1-LactC2^{AAA}-3xHA::His3MX6 hsl1Δ::HphNTI*	This study

Table 2: List of primers used in Chapter 2

Primer Name	Primer sequence (5' to 3')
Gin4-39	TGTGCAAAAAATTAGGGAAAAAAATGCTGGCTCGCAGGCATG CACTGAACCCCTAGGCCT
Gin4-40	ACAGCCCAGCAGCTCCACT
Gin4-41	GCACAACCGTATCACCCTGCGAGTGGAGCTGCTGGGCTGTC GGATCCCCGGGTTAATTAA
Gin4-38	AACGAAGGAGACAAAACATGATTGCATTACATTAGCACTAGA ATTCGAGCTCGTTTAAAC

Table 3: List of plasmids used in Chapter 2

Plasmid Name	**Details**	Source
pKT1995	pRS306-GFP-LactC2^{AAA}-URA3	(Takeda et al., 2014)
pKT2100	pRS306-GFP-LactC2-URA3	(Takeda et al., 2014)
pAID1	AID-tagging genes at the C-terminus; Kanamycin resistance	(Nishimura et al., 2009)

pTIR2	Plasmid containing the osTIR1 under the GPD1 promoter. After PmeI digestion, recombines at the *HIS3* locus	(Nishimura et al., 2009)
pTIR4	Plasmid containing the osTIR1 under the GPD1 promoter. After PmeI digestion, recombines at the *LEU2* locus	(Nishimura et al., 2009)
pFA6a-yomRuby2::KanMx	Yeast-optimized (yo) mRuby2	(Lee et al., 2013a)

Supplementary information:

Video 1: Time-lapse imaging of *2xTIR1* and *gin4-AID hsl1-AID* cells.
The two strains were mixed together prior to imaging as described in Materials and methods. The spindle pole bodies were differentially tagged in the two strains. The cells in top right corner show *2xTIR1* cells with mRuby2-tagged SPC42 and the cells in the bottom left corner show *gin4-AID hsl1-AID* with GFP-tagged SPC42. The *gin4-AID hsl1-AID* cells undergo a prolonged metaphase delay with polarized bud growth while the *2xTIR1* cells begin the next cell cycle. The cells were imaged using time-lapse confocal microscopy with image acquisition every 3 min. The movie was converted to AVI format using Fiji and shows the time-lapse at a speed of 5 frames per second (fps). Scale bar represents 5 µm.

Video 2: *gin4-AID hsl1-AID* cells show spindle pole and cytokinesis defects.
A tile showing *2xTIR1* cells with mRuby2-tagged SPC42 and *gin4-AID hsl1-AID* cells with GFP-tagged SPC42 imaged together. Cells were imaged using time-lapse confocal microscopy with image acquisition every 3 min. The *gin4-AID hsl1-AID* cells exhibit defects in bud separation and results in the formation of cell chains. These defects are also accompanied by spindle defects (magenta arrows) in the second cell cycle. The movie was converted to AVI format using Fiji and shows the time-lapse at a speed of 5 fps.

CHAPTER 3 (unpublished) : Additional experiments related to Chapter 2

In this chapter I will show additional experiments that explore the role of Gin4 in regulating cell growth, and the underlying molecular signals that regulate Gin4 activity. These experiments were performed in support of or in addition to Chapter 2.

Results

Gin4 influences the location of cell growth most likely by regulating the formin Bnr1

In chapter 2, I showed that inactivation of the Gin4-related kinases caused a loss of cell growth control such that the daughter bud continues to grow in a polar manner during mitosis, while the mother cell undergoes inappropriate isotropic growth even after bud initiation (**Fig. 2.1-2.3**). The continuation of mother cell growth throughout the cell cycle was especially surprising since it had not been reported previously, even though large cell size was a commonly observed phenotype for cells lacking the Gin4-related kinases. Moreover, my data also showed that these effects were regulated by the Gin4-related kinases in a Swe1-independent pathway. So, I sought to explore effectors downstream of Gin4 that could help explain this observation.

There are two formin proteins in budding yeast: Bni1 and Bnr1 that are homologous to the mammalian formins (Chesarone et al., 2010). Formins help nucleate actin cables for the delivery of secretory vesicles to the sites of growth. (Pruyne et al., 2004b). These actin cables are organized into two kinds of structures in yeast: (i) cables formed along the mother-bud axis that drive growth of the daughter bud and, (ii) cables that are directed to the bud neck to facilitate the formation of the actomyosin ring at cytokinesis (Ozaki-Kuroda et al., 2001; Vallen et al., 2000). Bni1 is

a downstream effector of the Rho GTPase Cdc42 (which establishes the site of bud emergence) and also interacts with the polarisome complex to help establish cell polarity and bud growth (Evangelista et al., 1997; Sagot et al., 2002). Inactivation of Bni1 causes loss of cell polarity and cells are thus more spherical (Ozaki-Kuroda et al., 2001). On the other hand, Bnr1 is tethered to the septin proteins at the bud neck, and helps organize actin cables that link the mother cell to the bud neck. (Pruyne et al., 2004b). *bnr1*Δ mutants have no significant defects in bud growth but hyperactivation of Bnr1 has been observed to cause the formation of hyperelongated buds (Chesarone et al., 2009).

Interestingly, Gin4 is essential for the localization and activation of the Bnr1 protein (Buttery et al., 2012a). Since my data indicated that inactivation of Gin4 caused cell growth defects and that formins are essential for proper cell growth, I hypothesized that Gin4 inactivation causes inappropriate cell growth through misregulation of Bnr1 and/or Bni1. Here, I utilized the auxin-inducible degron for Gin4. Inactivation of Gin4 using 1 mM auxin caused a nearly complete dephosphorylation of Bnr1 within 60 mins in asynchronous populations (**Fig. 3.1 A**). Although Gin4 regulation of Bni1 had not been previously reported, the proportion of dephosphorylated:phosphorylated Bni1 gradually increased upon Gin4 inactivation beginning at 60 mins (**Fig 3.1 B**). Overall, the data suggest that inactivation of Gin4 could be most likely causing misappropriate cell growth through Bnr1 and perhaps also Bni1, although more experiments will be needed to validate these findings.

Figure 3.1: Inactivation of Gin4 affects the formins Bnr1 and Bni1.
Log phase cultures of *gin4-AID* cells expressing either 3xHA-tagged Bnr1 **(A)** or Bni1 **(B)** were split into half and treated with either 1 mM auxin or an equivalent volume of ethanol. The cultures were then incubated in a shaking water bath at 25˚C and samples were collected at the timepoints indicated. The harvested samples were probed by western blotting using a polyclonal HA antibody. Nap1 was used as a loading control

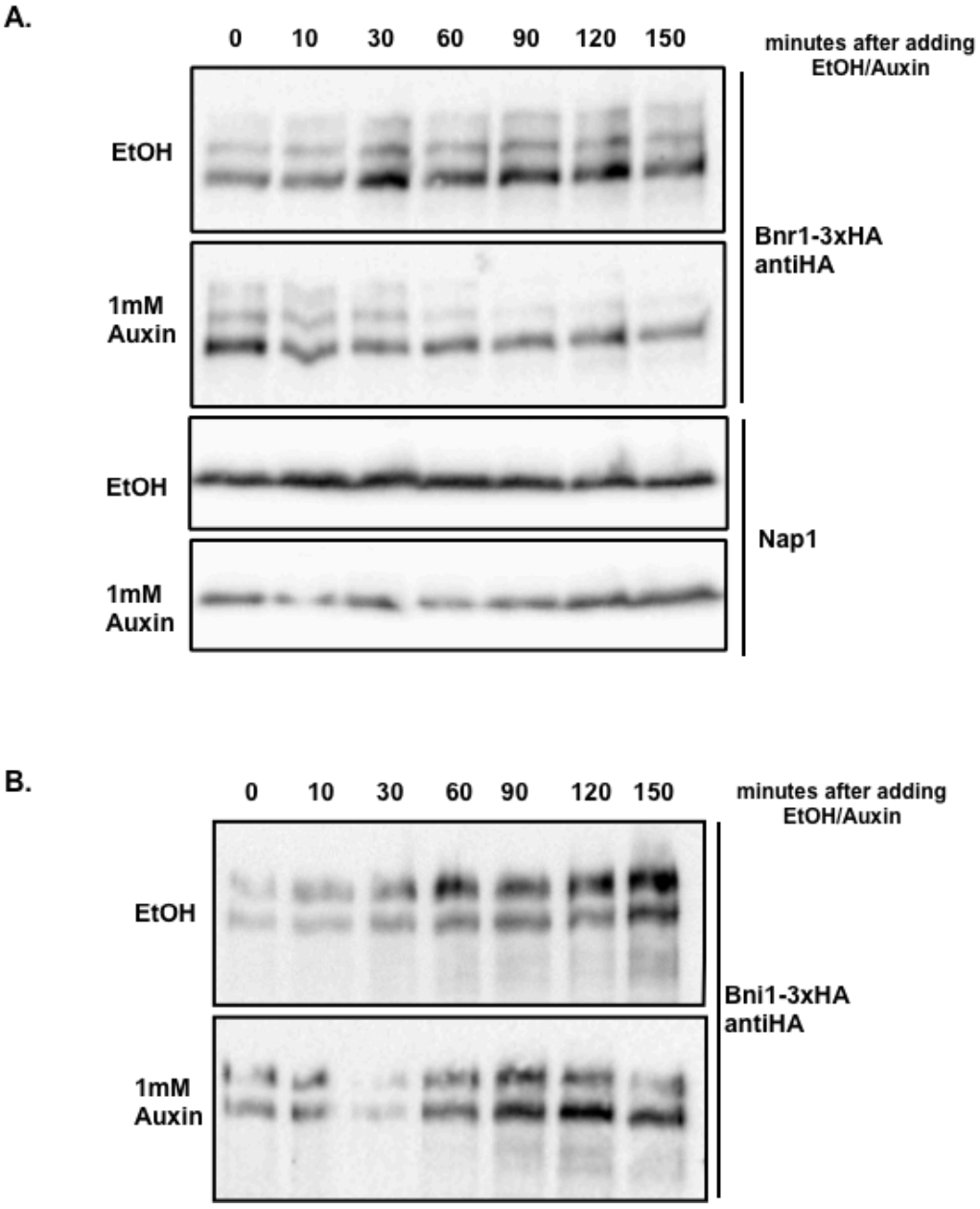

Anchoring Gin4 to the plasma membrane helps restore partial Gin4 function

In chapter 2, I showed that the C-terminal KA1 domain of Gin4 is essential for binding to anionic phospholipids, which could be generating a growth-dependent activation signal that promotes Gin4 hyperphosphorylation, possibly through its autophosphorylation. Alternatively, the KA1 domain could be critical in simply localizing Gin4 to the bud neck so that Gin4 can receive growth-dependent signals from other kinases. If the latter case is true, then cells lacking the KA1 domain of Gin4 could still have normal bud growth and mitotic progression as long as Gin4 can localize to the bud neck. One approach to tether Gin4 to the plasma membrane in the absence of the KA1 domain is by substituting the KA1 domain of endogenous GIN4 with the CAAX motif (KCAIL) at the C-terminus. The CAAX motif is a series of amino acids (C= Cysteine, A= any aliphatic amino acid, X= L or E , for recognition by the enzyme geranylgeranytransferase), which when fused to the C-terminus of any protein, promotes its prenylation and consequently helps anchor the prenylated protein to the membrane. This approach has been used to synthetically tether various proteins to the membrane (Berchtold and Walther, 2009; Meca et al., 2019; Tang et al., 2014). Here, I used KCAIL as the CAAX motif where, addition of the lysine helps improves the efficiency of the CAAX motif.

In log phase cells, fusing the CAAX box to *gin4-ΔKA1* partially restored phosphorylation of Gin4 (**Fig. 3.2 A**). Moreover, *gin4-ΔKA1-CAAX* cells also rescued the large size phenotype seen in *gin4-ΔKA1* cells (**Fig. 3.2 B and Fig. 2.7 C**). In addition, the *gin4-ΔKA1-CAAX* cells had normal cell morphology (data not shown).

I also analyzed the cell cycle dynamics of *gin4-ΔKA1-CAAX* cells during a time course. Gin4-ΔKA1-CAAX shows a very subtle phosphorylation shift and smear at

135 mins (**Fig. 3.2 C**; arrowheads) compared to the log phase cells. Moreover, while Clb2 expression began at the same time in both strains, mitotic progression was delayed in the *gin4-ΔKA1-CAAX* cells (**Fig. 3.2 D**) even though Gin4-ΔKA1-CAAX partially localizes to the bud neck (**Fig. 3.2 E**; arrowheads). Together, the data suggest that while anchoring Gin4 to the plasma membrane is sufficient to restore some functions of Gin4 such as normal growth phenotype of the buds, it failed to ensure a timely mitotic progression.

Figure 3.2: Anchoring Gin4 to the plasma membrane helps restore partial Gin4 function.
(A) Wildtype, *gin4-ΔKA1-3xHA* and *gin4-ΔKA1-KCAIL* (labeled as *gin4-ΔKA1-CAAX)* cells were grown to log phase and samples were collected to probe for Gin4 by western blotting. **(B)** Wildtype and *gin4-ΔKA1-KCAIL* cells were grown in YPD overnight and the cell sizes were measured for the population by Coulter counter. **(C and D)** The same strains were also synchronized in G1 using α-factor and released from the G1 arrest. The cultures were then incubated in a shaking water bath at 22˚C. Samples were collected at the indicated timepoints and probed for Gin4 **(C)** and the mitotic marker Clb2 **(D)**. **(E)** The indicated strains were fixed in formaldehyde and immunostained for Gin4 and DAPI.

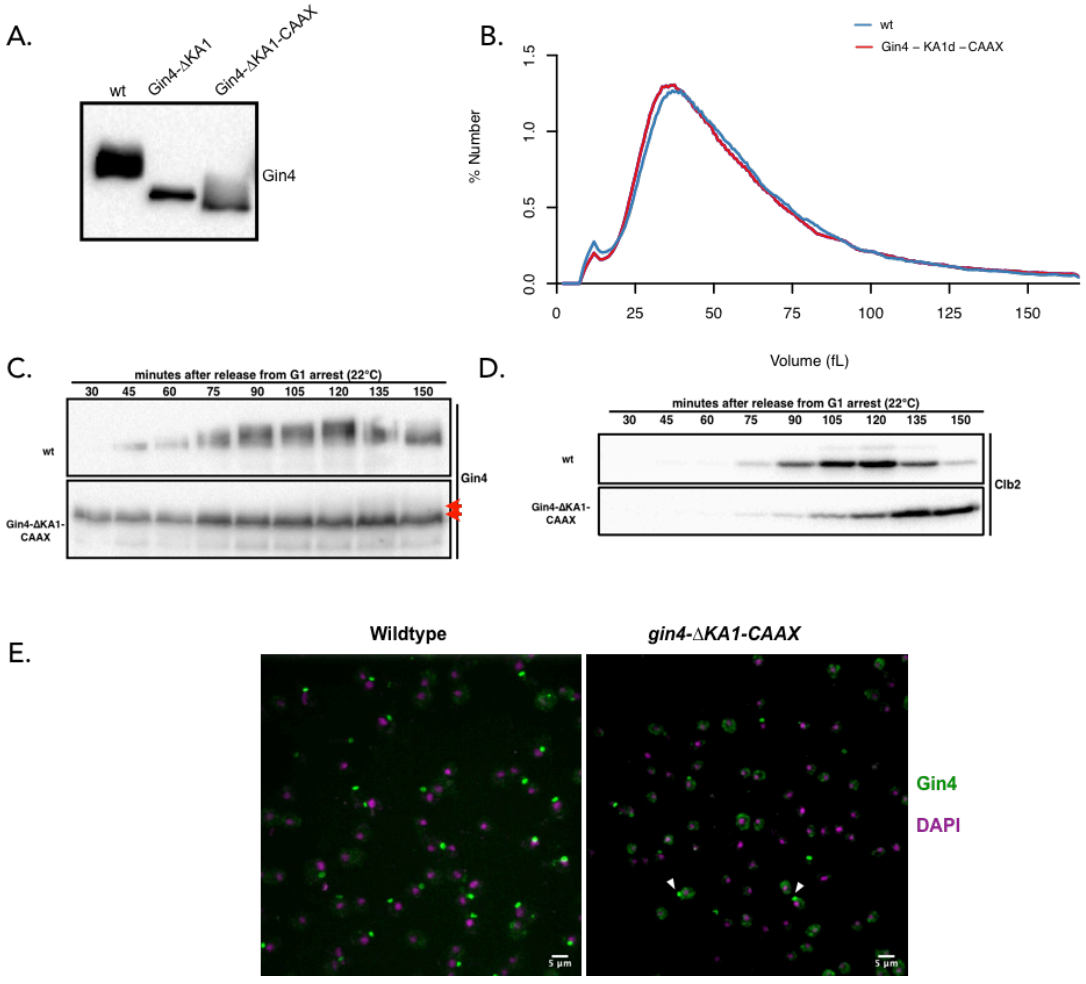

Dephosphorylation of Gin4 at the end of mitosis is dependent on the Cdc14 phosphatase

Our lab previously found that Gin4 phosphorylation and its kinase activity peak in mitosis, roughly coinciding with the timing of the metaphase-anaphase transition (**Fig. 2.5** and (Altman and Kellogg, 1997a)). Gin4 is subsequently dephosphorylated and remains so until the next cell cycle. So far, it is not clear how Gin4 is dephosphorylated at the end of mitosis and if the timing of this dephosphorylation affects mitotic progression.

We sought to identify the phosphatase that dephosphorylates Gin4 in late mitosis. In a candidate phosphatase screen, I found that inactivation of the Cdc14 phosphatase caused rapid hyperphosphorylation of Gin4 within 20 minutes (**Fig. 3.3 A**). Cdc14 seemed a promising candidate since it is the primary phosphatase that drives exit from mitosis (Bloom et al., 2011; Visintin et al., 1998). Inactivation of Cdc14 caused a prolonged mitosis and failure to dephosphorylate Gin4 in a timely manner (**Fig. 3.3 B**). Together, the data confirm that dephosphorylation of Gin4 is dependent on Cdc14 phosphatase.

Figure 3.3: Dephosphorylation of Gin4 at the end of mitosis is dependent on the Cdc14 phosphatase.
(A) Wildtype and *cdc14-1* cells were grown in in YPD overnight and then shifted to the restrictive temperature of 34˚C. Samples were collected at the indicated timepoints and probed for Gin4 by western blotting. **(B)** Cells of the indicated genotype were arrested in G1 using α-factor, released in YPD and then shifted to the restrictive temperature 10 minutes after the release from G arrest. Samples were collected at the indicated timepoints and probed for Gin4 and Clb2.

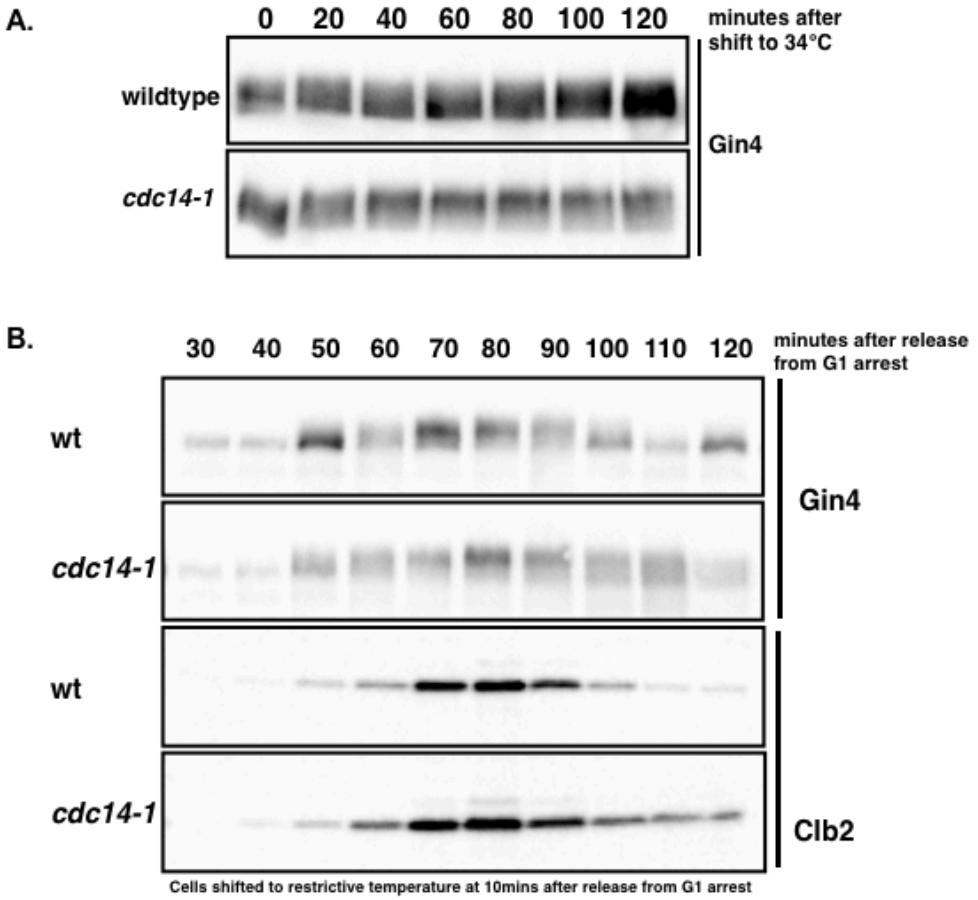

I next sought to determine how failure to dephosphorylate Gin4 affects mitotic progression. While there are reports of positive interactions in other models, Gin4 has never been shown to directly bind Swe1 in budding yeast (Guzmán-Vendrell et al., 2015; Opalko et al., 2019). Despite the lack of physical data, my results from chapter 2 showed that lack of Gin4-related kinases caused Swe1 to remain in a partially phosphorylated state (**Fig. 2.4**), which corresponds to the hyperactive form of Swe1. These data suggest a model in which the gradual increase in Gin4 activity during mitosis causes a corresponding increase in Swe1 phosphorylation leading to its inactivation, which allows cells to transition from metaphase to anaphase. Swe1 is ultimately degraded by the anaphase promoting complex (APC) (McMillan and Lew, 1999; Sia et al., 1998).

I assayed Swe1 phosphorylation during the cell cycle after inactivation of Cdc14. Previous studies demonstrated a direct interaction between Cdc14 and Swe1 and that Swe1 dephosphorylation is driven by Cdc14 *in vitro* (Raspelli et al., 2015). Here, inactivation of Cdc14 caused Swe1 to undergo a more extensive hyperphosphorylation that persisted for the duration of mitosis (**Fig. 3.4**). It is likely that the failure to degrade Swe1 causes cells to delay in mitosis. Based on results from **Fig, 3.3** and **3.4**, this could be explained in one of two ways : Cdc14 opposes normal hyperphosphorylation of Swe1 by Gin4, so that when Cdc14 is inactivated, Gin4 hyperphosphorylate Swe1. Conversely, inactivation of Gin4 should cause premature Swe1 dephosphorylation by Cdc14. Alternatively, Cdc14 could bind and inhibit Gin4 activity, and upon Cdc14 inactivation, Gin4 would become hyperactive causing Swe1 hyperphosphorylation. To test these hypotheses, I analyzed the effect of Cdc14 inactivation in *gin4*Δ mutants. Swe1 failed to become fully dephosphorylated

and persisted in a partially phosphorylated state throughout the cell cycle even as cells exited from mitosis (**Fig 3.4 A and B**). These data point to the idea that Cdc14 fails to interact directly with Swe1 in the absence of Gin4, although more *in vitro* experiments will be needed to corroborate these findings.

Figure 3.4 Cdc14-mediated Swe1 dephosphorylation fails to occur in *gin4*Δ mutants.
Wildtype, *cdc14-1* and *cdc14-1 gin4*Δ cells were arrested in G1, released from the G1 arrest at 25˚C and then shifted to 34˚C at 45 minutes. Samples were collected at the indicated timepoints and probed for Swe1 **(A)** and Clb2 **(B)** by western blotting.

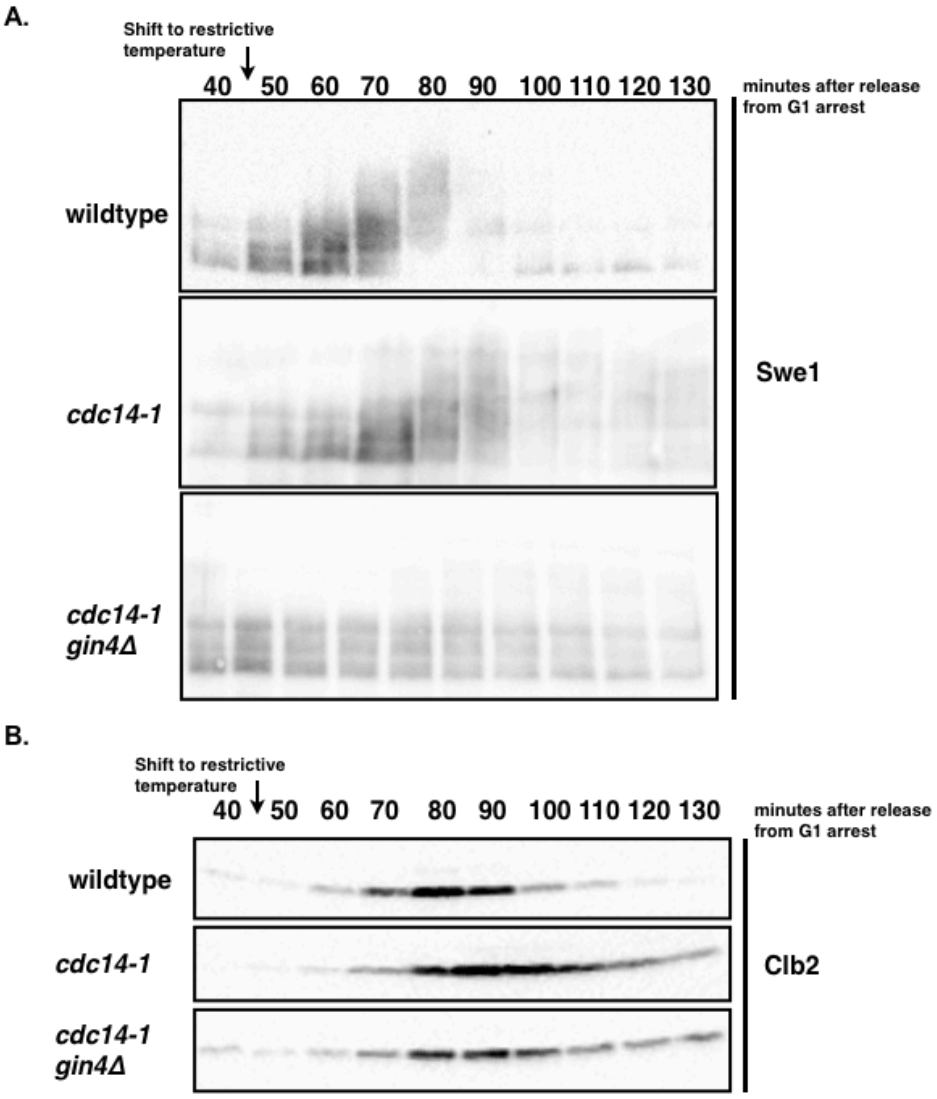

Gin4 (Cdr2) hyperphosphorylation in fission yeast is proportional to cell growth

To test whether the Gin4-based growth sensing model could be applicable to other models, I investigated the behavior of Cdr2 (Gin4 homolog) in fission yeast as cells go through two successive cell cycles. Cells expressing endogenous Cdr2 with a 3xHA-epitope tag were synchronized through centrifugal elutriation to harvest small sized cells and were then incubated at 25˚C in a shaking water bath. Samples were collected every 20 minutes until cells underwent two successive rounds of septation. These samples were then probed for Cdr2-3xHA by western blotting and the septation index was used to confirm cell synchrony (**Fig**. **3.5**). Similar to Gin4, Cdr2 undergoes gradual hyperphosphorylation, reaching peak phosphorylation at 100 and 240 minutes, followed by subsequent dephosphorylation by 120 and 260 minutes respectively. The timing of dephosphorylation coincided with the time at which almost 50% of the cells exhibit septation, indicating that they have undergone cytokinesis (Lucena et al., 2017a). Together, these data indicate that Cdr2 has the potential to act as a growth sensor in fission yeast through a model very similar to the Gin4-related kinases.

Figure 3.5: Cdr2 hyperphosphorylation in fission yeast is proportional to cell growth.
Fission yeast cells expressing Cdr2-3xHA were grown to log phase overnight in YES media and elutriated to harvest small-sized cells. They were then incubated in a shaking water bath at 25˚C and samples were collected for western blotting and calcofluor staining every 20 minutes for 5 hours. **(A)** Samples were probed for Cdr2-3xHA using a polyclonal HA antibody by western blotting. **(B)** The percentage of septated cells at each timepoint was determined by calcofluor staining. n=200 for each timepoint.

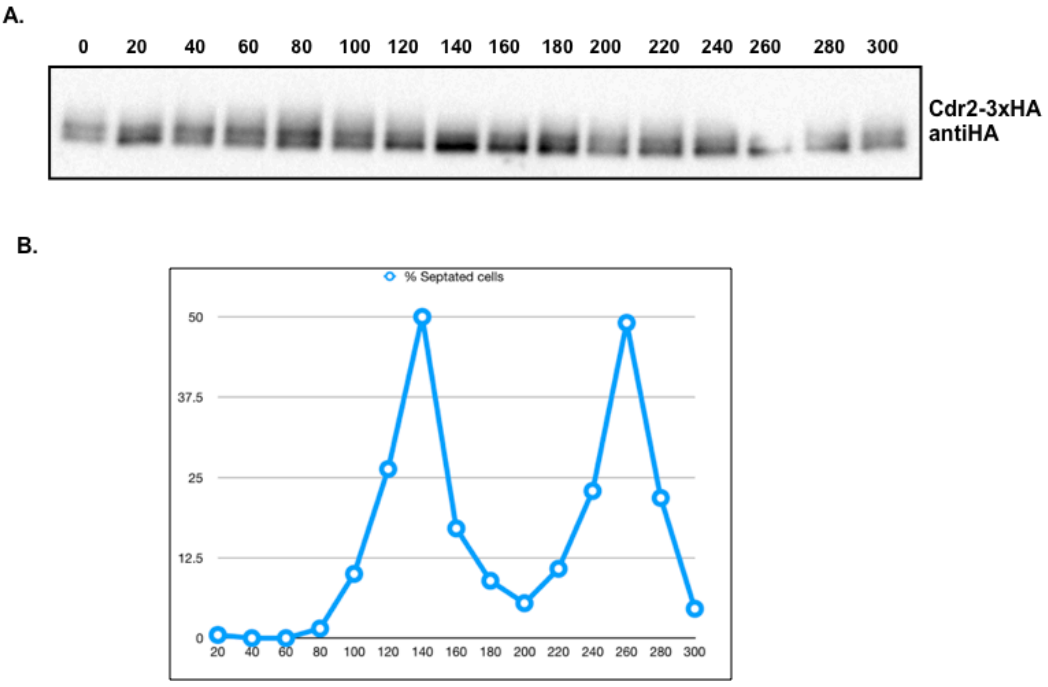

Discussion

In this chapter, I demonstrated that Gin4 inactivation causes complete dephosphorylation of the Bnr1 formin within 1 hour of auxin addition, while dephosphorylation of Bni1 happens to a lesser extent. Previous reports have shown a direct interaction between Bnr1 and Gin4 and that Gin4 is essential for the recruitment of Bnr1 to the bud neck (Buttery et al., 2012a). Moreover, defects in *gin4*Δ mutants can be rescued by overexpression of Bnr1. Together, these findings support a model where loss of the Gin4-related kinases cause misdirected growth of the mother cell through defects in the Bnr1-mediated actin cable network.

My data further show that the purpose of binding to anionic phospholipids is not simply to have Gin4 localized to the bud neck but is also necessary for Gin4 to be in prime position to receive lipid signals via their KA1 domains so that they can be relayed to mitotic regulators. The data show that substituting the KA1 domain with the CAAX motif partially restored Gin4 localization to the bud neck, which was sufficient to restore normal growth of the buds. This could be most likely attributed to the restored assembly of the septin collar and the associated Bnr1 formin that is Gin4-dependent (Buttery et al., 2012a; Li et al., 2012; Longtine et al., 2000; 1998a). Interestingly, the study also showed that cells expressing a Gin4 construct that lacks its kinase domain still show normal Bnr1 localization at the bud neck. Combining these findings, the normal cell size distributions for *gin4-ΔKA1-CAAX* cells suggest that Bnr1 probably binds to the region of Gin4 that links the N-terminal kinase domain to the C-terminal KA1 domain. Indeed, studies in the fungi *Candida albicans* (*ca*) have found that a similar intermediate domain in *ca*Gin4 is necessary for assembling the septin collar, which in turn, is essential for the recruitment of Bnr1 in budding yeast (Au Yong

et al., 2016). Even as the *gin4-ΔKA1-CAAX* cells had normal cell size distributions in the cell population, they still displayed a delayed mitotic progression. These findings indicate that *gin4-ΔKA1-CAAX* cells most likely have a reduced growth rate, suggesting that the KA1 domain could also be essential in functions independent of membrane anchoring. The Gin4-related kinases have been previously shown to control growth rate via the TORC2 signaling as discussed previously in Chapter 2 (Alcaide-Gavilán et al., 2018a). Since the CAAX motif only partially restores Gin4 localization to the bud neck, Gin4 is either not in the correct conformation or Gin4 localized to the cytoplasm could be misregulating other proteins such as those in the TORC2 pathway. Nonetheless, the data support a model where the KA1 domain of Gin4 has two functions that are decoupled in the CAAX constructs: (i) regulating growth rate and timing of mitotic progression and, (ii) measuring cell growth most likely through its interactions with signaling lipids.

I then searched for signals that inactivate Gin4 in late mitosis. We found that Gin4 dephosphorylation is dependent on the Cdc14 phosphatase. Cdc14 and Gin4 have been demonstrated to directly interact with each other *in vitro* (Au Yong et al., 2016; Bloom et al., 2011). In fact, a nucleolar-localizing domain was identified in *ca*Gin4 that associates with Cdc14. In this study, Gin4 responded to Cdc14 inactivation rapidly in asynchronous cells. During the cell cycle, Cdc14 inactivation affected both Gin4 and Swe1. My preliminary findings in this study revealed that Swe1 remained partially hyperphosphorylated despite Cdc14 inactivation in *gin4Δ* mutants. This was surprising since Cdc14 has been previously shown to bind to and dephosphorylate Swe1 *in vitro*. These findings lead to a model where Cdc14 could be first driving inactivation of Gin4, diverting Gin4 activity away from Swe1, consequently

promoting Cdc14-driven Swe1 dephosphorylation. Moreover, it could also suggest that Swe1 needs to first be hyperphosphorylated in a Gin4-dependent manner, followed by a subsequent inactivation or alternatively, Swe1 activity is modulated by the Cdc14-Gin4 complex. Understanding the interplay between these three proteins might be more complicated than previously thought and requires further validation. In either case, the tight regulation of Gin4 and Swe1 by Cdc14 could help ensure that the events of mitosis: sufficient bud growth and proper chromosome segregation are tightly coordinated before cells can exit from mitosis in a timely manner.

Finally, I also demonstrated that the fission yeast homolog of Gin4: Cdr2 undergo gradual hyperphosphorylation during the cell cycle in a manner similar to Gin4. Unlike budding yeast, there is no cell growth during mitosis. Thus, cells attain their full size at the end of G2. But similar to Gin4, Cdr2 also regulate Wee1 activity (Allard et al., 2018b; Guzmán-Vendrell et al., 2015; Opalko et al., 2019) Cdr2 is thus an excellent candidate for functioning as a growth sensor. In fact, various reports already favor a Pom1-Cdr2-Wee1 gradient model as the basis of cell size sensing in fission yeast (Bhatia et al., 2014; Martin and Berthelot-Grosjean, 2009; Pan et al., 2014). Briefly, Pom1 localized to the cell tips inhibits Cdr2 activity, which is essential for inhibiting Wee1 activity. Thus, small sized cells are expected to have high Wee1 activity that suppresses mitotic entry. However, as cells grow larger, Pom1 is diffused further away from the middle of the cell, creating a concentration gradient that allows gradual activation of Cdr2. Wee1 is subsequently inactivated in short bursts by inhibitory Cdr2 phosphorylation that allows mitotic entry. While there are differing opinions in the field about what aspect of cell size (cell length, surface area or volume) is the key determinant of the gradient model, the similarities between the Cdr2-based

gradient model and our Gin4 model make our currently proposed Gin4 model highly promising. However, unlike the gradient model, our Gin4 model argues that it is cell growth rather than cell size that is measured by cells.

Materials and Methods

Yeast strain construction, media, and reagents

All strains are in the W303 background (*leu2-3,112 ura3-1 can1-100 ade2-1 his3-11,15 trp1-1 GAL+ ssd1-d2*). The additional genetic features of strains are listed in Table 4. Cells were grown in YP medium (1% yeast extract, 2% peptone, 40 mg/liter adenine) supplemented with 2% dextrose (YPD), or 2% glycerol and 2% ethanol (YPG/E).

Gene deletions and C-terminal epitope tagging was performed by standard PCR amplification and homologous recombination (Longtine *et al.*, 1998; Janke *et al.*, 2004; Lee *et al.*, 2013). *gin4-ΔKA1-CAAX* constructs integrated at the GIN4 locus were created by gene splicing with overlap extension (Horton et al., 1990). Briefly, primers encoding KCAIL (CAAX box) fragments were PCR amplified with approximately 40bp of flanking sequence at the 5' end that was homologous to the GIN4 ORF just upstream of the KA1 domain (amino acids 1007-1142) using oligos Gin4-74 (TGTGCAAAAAATTAGGGAAAAAAATGCTGGCTCGCAGGCAAAATGT GCTATTTTGTGA*GGCGCGCC*ACTTCTAAA) and Gin4-38 (**Table 2**) that amplifies the 3'UTR of Gin4 immediately after the stop codon, followed by the KanMX6 resistance cassette. The resulting fragments were then transformed into wild type cells and correct integrants were identified by western blotting with the Gin4 antibody.

To generate strains with a 3xHA-epitope tag on BNR1/BNI1, standard PCR amplification and homologous recombination was performed in the *gin4-AID 2xTIR1* parent strain. Auxin was dissolved in 100% ethanol to make a 50 mM stock solution and used at a concentration of 1 mM in this chapter.

The SH 918 strain (*cdc14-1)* (SLJ250/DOM143) temperature-sensitive strain and its control strain (DOM90) were both obtained from the lab of David Morgan (Jaspersen et al., 1998). The *cdc14-1* mutation was identified as G323D by sequencing.

Cell cycle time courses and Western blotting

Cell cycle time courses were carried out as previously described (Harvey et al., 2011b) and in Chapter 2 of this thesis. For experiments involving Gin4 degradation via auxin addition, cells were grown to log phase to an optical density (OD_{600}) of 0.7 and the single culture was split into two culture flasks. 1 mM auxin was added to one flask and an equivalent volume of ethanol was added to the control flask. 1.6mL samples were collected at various times and probed by western blotting.

In the temperature shift experiments involving Cdc14 inactivation, cells were grown to log phase overnight to an OD_{600} of 0.4-0.5 and shifted to the restrictive temperature of 34˚C for log phase experiments. In cell cycle time courses, cells were synchronized in G1 using alpha-factor as previously described in Chapter 2. After release from the G1 arrest, cells were grown at room temperature and shifted to 34˚C either at 10 mins or 45 mins post release from G1 arrest. Samples were then collected at the indicated time points.

Western blotting was performed exactly as described in Chapter 2 of this thesis. For experiments involving analysis of Bnr1-3xHA and Bni1-3xHA, the samples were lysed in sample buffer supplemented with the protease cocktail LPC (1 mg/mL leupeptin, 1 mg/mL pepstatin, 1 mg/mL chymostatin dissolved in dimethylsulfoxide; used at 1/500 dilution). SDS-PAGE was carried out as previously described (Harvey

et al., 2011b) and in Chapter 2 of this thesis. 10% polyacrylamide gels with 0.13% bis-acrylamide were used for analysis of Gin4, Clb2, and Nap1 (loading control). 9% polyacrylamide gels with 0.14% bis-acrylamide were used for Bnr1, Cdr2-3xHA and Swe1 blots. 7.5% polyacrylamide gels with 0.17% bis-acrylamide were used for probing Bni-3xHA. Proteins were transferred via wet transfer onto nitrocellulose membranes. Blots were probed with various rabbit polyclonal primary antibodies at a final concentration of 1-2 µg/mL at room temperature overnight in 5% milk in PBST (1x phosphate buffered saline, 250 mM NaCl, 0.1% Tween-20) with 0.02% sodium azide. Primary antibodies were detected by an HRP-conjugated donkey anti-rabbit secondary antibody (GE Healthcare; # NA934V) incubated in PBST for 1h at room temperature. Blots were rinsed in PBS before detection via chemiluminescence using ECL reagents (Advansta; #K-12045-D50) with a Bio-Rad ChemiDoc imaging system.

Coulter counter analysis

Cell size analysis was performed as previously described in Chapter 2 using a Beckman coulter counter.

Immunostaining

Cells were fixed in 3.7% formaldehyde for 30 mins and washed in PBST. The cells were then prepared for immunostaining by digesting the cell wall using zymolyase prepared in PBST-azide supplemented with 2 mM PMSF+ 5 mM β-mercaptoethanol. Cells were digested at 30˚C until about 90% cells lose their shiny appearance under the microscope, indicating loss of the cell wall. Cells were then washed twice and resuspended in PBST-azide. A 15 µL cell suspension was added to printed slides

treated with 10 µL if 1 mg/mL poly-L-lysine and allowed to adhere for 5 min. The cells were blocked with PBST supplemented with 4% BSA and incubated in a humid chamber for 20 min, followed by incubation with the Gin4 primary antibody for 30 min. The unbound primary antibody was removed by 4x5 min washes with PBST + 4% BSA and then treated with FITC-labeled rabbit secondary antibody for 30 min in the dark. After 4x5 min washes with PBST + 4% BSA, the samples were DAPI-stained for 2 min, washed 3x and then mounted in mounting solution (Vectashield). A coverslip was placed on the slide and the edges were sealed.

Microscopy

The immunostained cells were visualized on a spinning disk confocal microscope with a Solamere system running MicroManager* (Edelstein et al., 2014). The microscope was based on a Nikon TE2000 stand and Coherent OBIS lasers. We used a 63x/1.4 Plan Apo objective for data collection. FITC staining was visualized using the GFP laser that was excited at 488 nm and collected through a 525/50nm band pass filter (Chroma) onto a Hamamatsu ImageEMX2 EMCCD camera.

Synchronization of *S. pombe* cells by centrifugal elutriation

The fission yeast cells were synchronized by centrifugal elutriation as previously described in (Lucena et al., 2017a). Briefly, *cdr2-HA* cells obtained from the lab of Kathy Gould were grown overnight to log phase in 3 L of YES media at 30˚C. Centrifugal elutriation was performed at 25˚C using a Beckman J6-MI centrifuge. After the elutriation, small-sized cells synchronized in G2 were resuspended in fresh YES media to an OD of 0.2 at 25˚C and samples were collected every 20 min for western

blotting and fixing for septation index. Cells were assayed for synchrony by measuring septation index using calcofluor staining as described in (Lucena et al., 2017a).

Table 4: List of strains used in Chapter 3

Strain	Mating type	Genotype	Source
DK 186	a	*bar1Δ*	(Altman and Kellogg, 1997a)
DK 3734	a	*bar1Δ gin4-ΔKA1-KCAIL::KanMX6*	This study
DK 2822	a	*bar1Δ gin4-ΔKA1-3xHA::His3MX6*	Chapter 2 of this study
SH 917	a	*bar1Δ* (isogeneic control for SH 918)	DOM 90 from Morgan lab
SH 918	a	*bar1Δ cdc14-1*	DOM 143 (Jaspersen et al., 1998)
DK 3353	a	*bar1Δ cdc14-1 gin4Δ::His3MX6*	This study
DK 4021	a	*bar1Δ his3::His3MX6+TIR1 leu2::LEU2+TIR1 gin4-AID::TRP1 BNR1-3xHA::KanMX6*	This study
DK 4022	a	*bar1Δ his3::His3MX6+TIR1 leu2::LEU2+TIR1 gin4-AID::TRP1 BNI1-3xHA::KanMX6*	This study
DK 3839		*cdr2-HA::KanR*	KGY 1628 from the lab of Kathy Gould (Breeding et al., 1998)

CHAPTER 4 (unpublished) : Rho1 and PP2A^{Cdc55}-Zds1/2 fine-tune Pkc1 activity to set a growth-threshold for mitotic entry

Introduction

Cell growth in budding yeast is tightly controlled. From the time of bud inception in late G1, cell growth is targeted to the incipient bud in a polarized manner so that growth is restricted to the tip of the growing bud. This continues until cells enter mitosis at which point, bud growth is directed across entire surface of the bud in an isotropic manner (Lew and Reed, 1993). The decision to switch from polar to isotropic growth is coupled to the timing of mitotic initiation. The time of mitotic entry in turn, is controlled by the Swe1 (budding yeast homolog of Wee1) kinase and Cdc25 phosphatase by regulating the activation of the mitotic Cdk1-cyclin complex (Gould and Nurse, 1989; Kumagai and Dunphy, 1991). Deletion of SWE1 causes cells to enter mitosis prematurely at a smaller bud size, while deletion of CDC25 results in a prolonged G2 phase where the bud continues to grow in a polar manner. These findings suggested a model in which Swe1 and Cdc25 respond to signals that control cell size. However, the upstream signals that link the activity of Wee1 and Cdc25 to cell growth or size have remained unknown, so the model has remained controversial.

Previous work from our lab identified a link between membrane growth and mitotic entry in budding yeast. We found that disrupting membrane growth with a temperature-sensitive allele of the exocyst protein SEC6 (*sec6-4)* arrests cells at G2 by a pathway that is Swe1-dependent (Anastasia et al., 2012a; Novick et al., 1996). Based on our findings, we proposed a "**growth-dependent signaling hypothesis**", which predicts that the delivery of secretory vesicles to the growing bud initiates a checkpoint signal that is proportional to the extent of membrane growth. The signal is

initiated when inactive Rho1 GTPase is delivered to the growing bud tip through the secretory pathway, where, it is activated by Rho1 guanine nucleotide exchange factor (GEFs) (Abe et al., 2003). Active Rho1 then binds and activates Pkc1 and this information is relayed down through a signaling cascade (Qadota et al., 1996). The downstream effector molecules, in turn, "read" the extent of growth to regulate Swe1 and Cdc25 activity, ultimately leading to mitotic entry. In this case, Zds1/2 proteins receive activating signals from Rho1-Pkc1 (Anastasia et al., 2012a; Jonasson et al., 2016; Rossio and Yoshida, 2011a; Rossio et al., 2014; Wicky et al., 2011; Yasutis and Kozminski, 2013). In association with protein phosphatase 2A (PP2A) bound to the Cdc55 regulatory subunit, Zds1/2 mediate the interaction between Pkc1 and $PP2A^{Cdc55}$, which leads to the phosphorylation of Cdc55 by Pkc1, thereby activating $PP2A^{Cdc55}$ (Thai et al., 2017). The activated $PP2A^{Cdc55}$-Zds1/2 complex then activates Cdc25 and inhibits Swe1 to allow activation of Cdk1, leading to mitotic entry (Harvey et al., 2011a; Pal et al., 2008). The following experiments show further evidence of how growth signals regulate Pkc1 activity and the critical proteins that modulate Pkc1 function.

Results

The timing of Pkc1 phosphorylation correlates with the duration of polar bud growth

Previous work from our lab demonstrated that Pkc1 gets rapidly dephosphorylated in response to an arrest of membrane growth and that overexpression of Pkc1 can drive cells through a G2 checkpoint arrest caused due to inactivation of bud growth (Anastasia et al., 2012a). These data indicate that Pkc1

phosphorylation and/or its activity could be an indirect readout of membrane growth. If this assumption is true, then Pkc1 phosphorylation could correlate to bud growth.

To test this hypothesis, I grew wildtype cells in rich carbon (2% dextrose) or poor carbon (2% glycerol + 2% ethanol) so that they grow at different rates. These cells were synchronized in G1 and then released to assay Pkc1 phosphorylation during the cell cycle. I assayed Pkc1 and the mitotic marker Clb2 by western blotting (**Fig. 4.1**). The blots show that Pkc1 undergoes gradual hyperphosphorylation in rich nutrients as seen by the gradual upward shift in Pkc1 bands due to lowered electrophoretic mobility. Moreover, Pkc1 becomes fully hyperphosphorylated simultaneously with the peak in Clb2 levels and subsequently dephosphorylated as Clb2 level drop. In poor nutrients, Pkc1 showed a similar trend, albeit, at a rate slower than cells growing in rich nutrients. Together, these data further support the idea that the timing of Pkc1 phosphorylation correlates with bud growth.

Figure 4.1: The timing of Pkc1 phosphorylation correlates with the duration of polar bud growth.
Cells were grown overnight either in YPD (rich nutrients) or YEP supplemented with 2% glycerol + 2% ethanol (poor nutrients), arrested in G1 using α-factor and then released from the arrest in fresh media at 25˚C. Samples were collected at the indicated timepoints and probed for Pkc1 and Clb2 by western blotting.

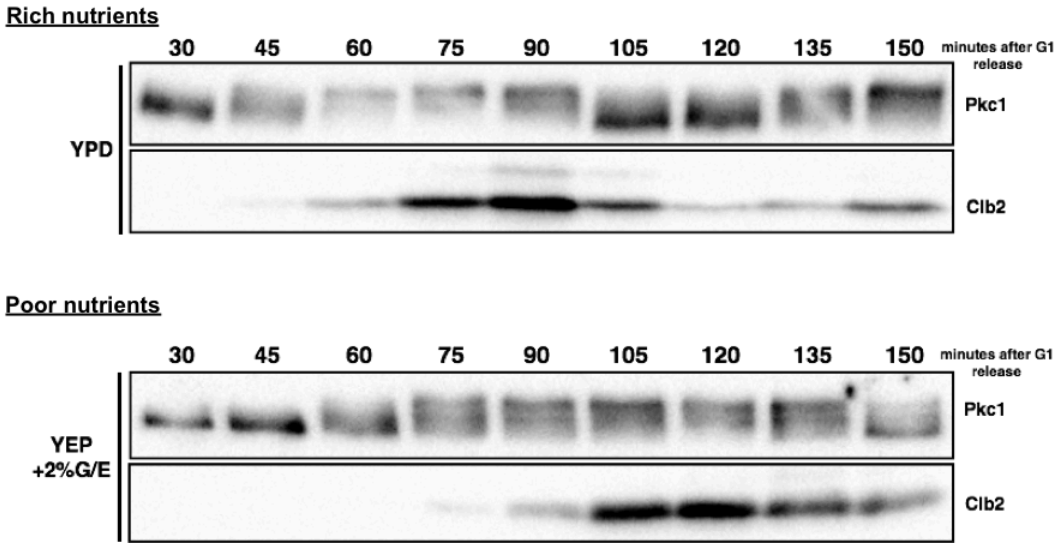

Pkc1 localizes to the growing bud tip during early polar growth and subsequently dissociates

Since bud growth is polarized and restricted to the bud tip, I wanted to track the localization of Pkc1 during this period of growth. Previous reports have shown that Pkc1 is also localized to the bud tip, however, evidence was lacking due to technical limitations in microscopic techniques and overexpression of fluorescently-tagged Pkc1 that could also cause mislocalization (Andrews and Stark, 2000; Denis and Cyert, 2005). Moreover, it is not known if Pkc1 remains localized to the bud tip throughout the duration of polar bud growth. I therefore fluorescently-tagged endogenous PKC1 with mRuby2, a yeast-optimized red fluorescent protein (RFP) derivative that has been shown to have a higher photostability and improved brightness over other RFPs (Lee et al., 2013b). PKC1 was tagged at the N-terminus, since conventional C-terminal tagging of PKC1 interfered with protein function due to the presence of the kinase domain at the C-terminus. As previously reported, Pkc1 does in fact, localize to the bud tip (**Fig. 4.2**), which further supports the notion of Pkc1 being an ideal candidate for a growth sensor.

Next, I monitored the localization of Pkc1 in live cells to determine if Pkc1 is localized to the growing bud tip for the entire duration of polar bud growth (**Fig. 4.3**). Pkc1 localizes to the bud site even before the emergence of a visible bud. However, it quickly dissociates from the bud tip even before cells enter mitosis (as seen by the separation of separated GFP-tagged spindle pole bodies) and later localizes to the bud neck. Thus, contrary to our prediction, Pkc1 gradually dissociates from the bud tip as cells progress through polar bud growth. One caveat here is that the Pkc1 signal appears to be getting photobleached over time and hence, cannot be quantified.

Nonetheless, Pkc1 is well-positioned to monitor bud growth. Further experiments will be necessary to validate these observations.

Figure 4.2: Pkc1 localizes to the growing bud tip during early polar growth. Cells expressing mRuby2-Pkc1 and Spc42-GFP were grown overnight in complete synthetic media (CSM) supplemented with 2% dextrose, arrested in G1 and then released from the G1 arrest. Live cells were imaged and tracked through one cell cycle. The figure shows a yeast cell at the time of bud inception in bright field and using the RFP detector channel. The white arrow indicates Pkc1 localization at the incipient bud site.

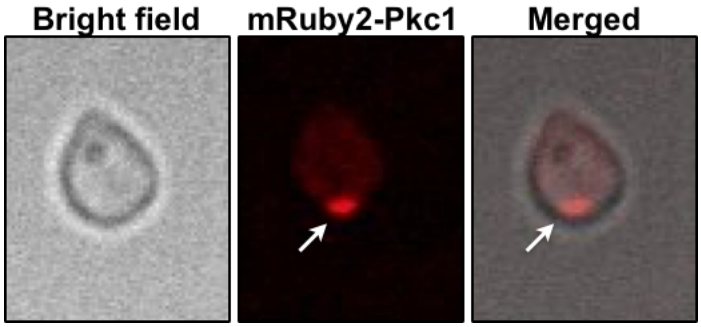

Figure 4.3: Pkc1 localizes to the growing bud tip during early polar growth and subsequently dissociates.
Cells expressing mRuby2-Pkc1 and Spc42-GFP were grown overnight in complete synthetic media (CSM) supplemented with 2% dextrose, arrested in G1 and then released from the G1 arrest. Live cells were imaged every 4 min and tracked through one cell cycle. The figure shows the montage of a representative yeast cell from the time of bud inception until they reach metaphase.

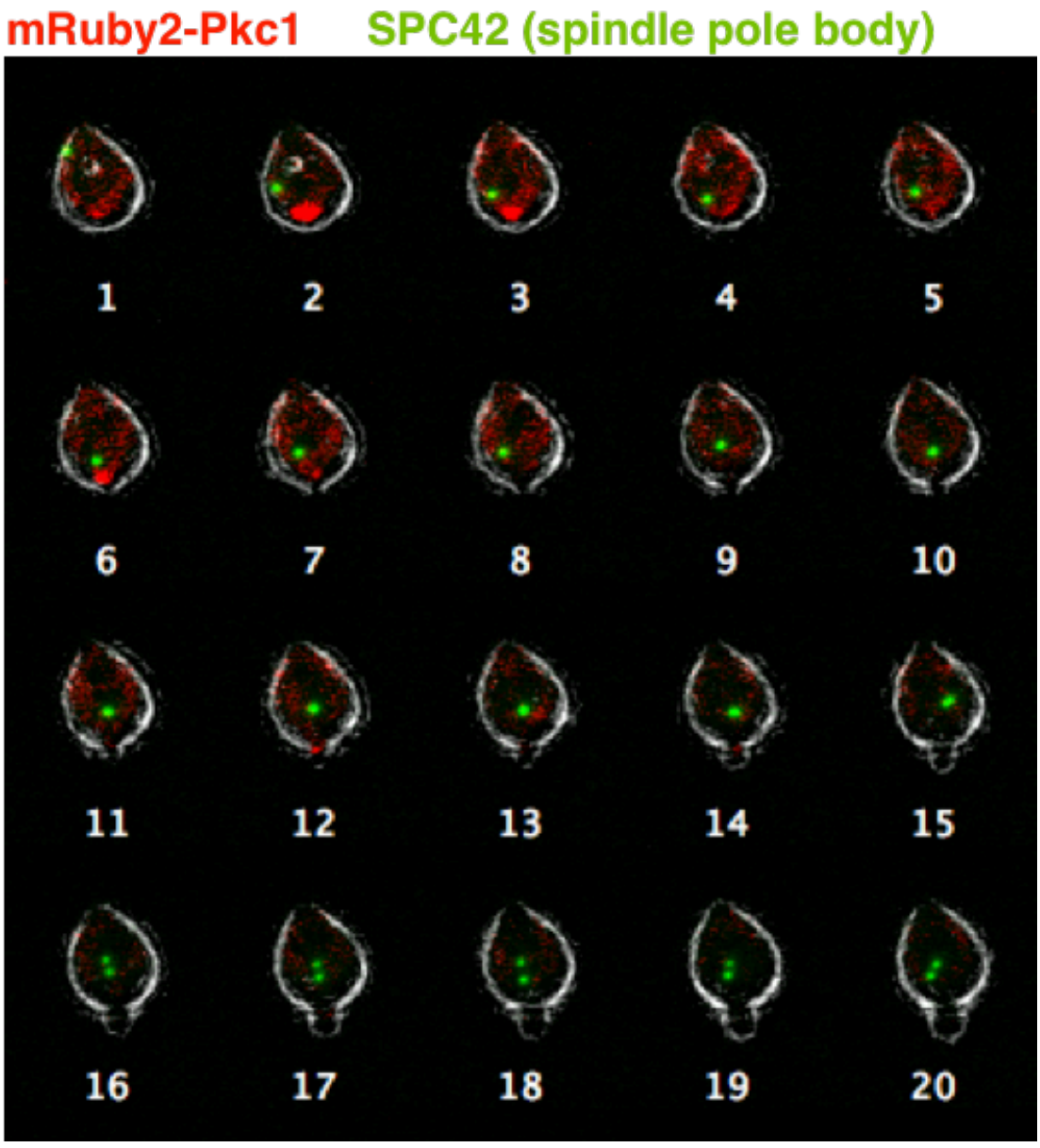

Pkc1 hyperphosphorylation is likely caused due to another kinase

Pkc1 is an atypical protein kinase C and the only protein kinase C archetype found in budding yeast compared to the numerous PKCs found in vertebrate cells (Parker et al., 1998). Studies in mammalian and yeast cells suggest that Pkc1 typically autophosphorylates itself after an initial priming phosphorylation by the kinase PDK (Inagaki et al., 1999). I showed above in **Fig. 4.1** that Pkc1 is gradually hyperphosphorylated in a manner proportional to polar bud growth. So, I next tested if Pkc1 autophosphorylates itself in response to bud growth. To test this, we created a kinase-dead version of Pkc1 (K853A), hereafter referred to as $Pkc1^{KD}$ with a point mutation that renders it catalytically inactive (Gray et al., 1997). *pkc1*Δ cells have defects in their cell wall formation and hence, are osmotically unstable and difficult to work with (Levin and Bartlett-Heubusch, 1992). So, we integrated the $PKC1^{KD}$ gene tagged with a 3xHA-epitope in wildtype cells at the LEU2 gene locus. This allowed us to selectively observe the behavior of $Pkc1^{KD}$ during the cell cycle, using the 3xHA epitope and compare their behavior to wildtype Pkc1 also tagged with 3xHA that served as the isogeneic control. To our surprise, we noticed that despite being kinase-dead, $Pkc1^{KD}$ still displayed a similar hyperphosphorylation compared to wildtype Pkc1-3xHA (**Fig. 4.4**). This indicates that (i) either Pkc1 hyperphosphorylation is caused due to another kinase, (ii) or, the endogenous Pkc1 cross-phosphorylates $Pkc1^{KD}$. In either case, further testing needs to be done to verify this observation.

Figure 4.4: Pkc1 hyperphosphorylation is likely caused due to another kinase. Cells expressing wildtype 3xHA-Pkc1 or 3xHA-Pkc1^{KD} integrated at the LEU2 gene locus were arrested in G1 and then tracked through the cell cycle after release from the arrest. Samples were collected at the indicated timepoints and probed by western blotting using HA and Clb2 antibodies.

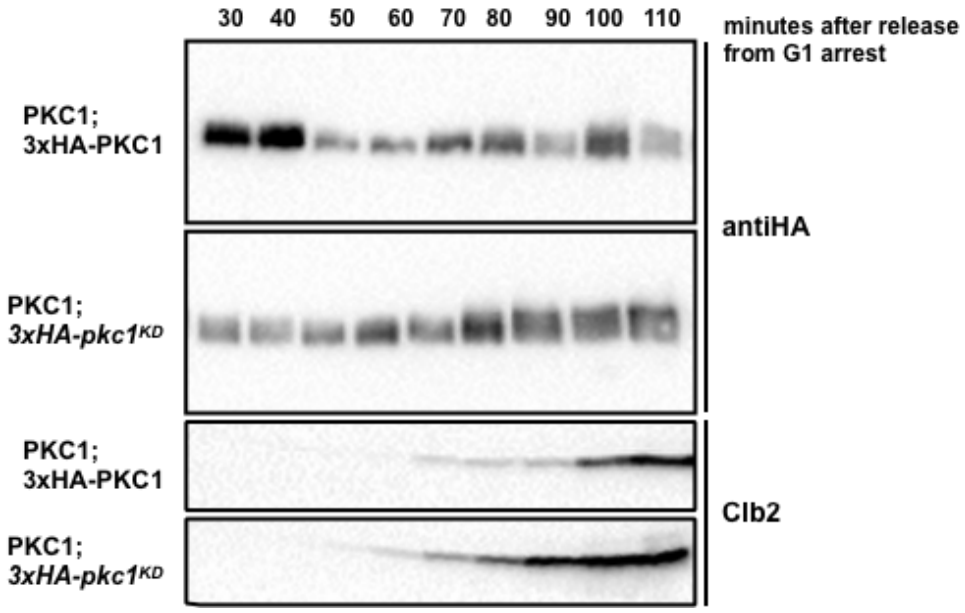

Pkc1 exhibits peaks kinase activity when it is partially phosphorylated

We saw previously that Pkc1 is gradually hyperphosphorylated during the cell cycle with maximal phosphorylation correlated with peak Clb2 levels (**Fig. 4.1**). Changes in the phosphorylation state of Pkc1 without associated changes in protein levels might be indicative of a change in its protein activity. So, I next tested if Pkc1 activity changed during the cell cycle and if so, determine when its activity peaks. Based on our current hypothesis, we would predict that since Pkc1 is upstream of the Swe1/Cdc25 checkpoint proteins, Pkc1 should be most active at or around G2-M phase transition.

To test this theory, I harvested cells at ten-minute intervals from G1-synchronized cells and immunoprecitated 3xHA epitope-tagged Pkc1 under physiological conditions. I then assayed the activity of immunoprecipitated Pkc1 using a generic substrate Histone H1 (Altman and Kellogg, 1997b) in the presence of radiolabeled gamma-ATP (γP32-ATP) (**Fig. 4.5 A**). Consistent with **Fig. 4.4**, we noticed that while the $Pkc1^{KD}$ controls do not possess kinase activity, they still appear to be phosphorylated. In the case of wildtype Pkc1, we observed that its kinase activity gradually increases during the cell cycle with peak activity at 60 mins followed by a gradual decline in activity. Comparing these activity levels to the phosphorylation state of Pkc1, we found that Pkc1 is maximally active when it is only partially phosphorylated (**Fig. 4.5 B**). Moreover, the timing of peak activity coincides with the beginning of Clb2 expression. Together, these data suggest that Pkc1 activity is indeed the highest at the G2-M phase transition.

We failed to observe Pkc1 autophosphorylation on the autoradiogram (not shown), which suggests that either Pkc1 autophosphorylation is not responsible for

creating the electrophoretic mobility shifts usually associated with Pkc1 or that it is too weak to be detected via autoradiography.

Figure 4.5: Pkc1 exhibits peaks kinase activity when it is partially phosphorylated.
Cells expressing or 3xHA-Pkc1 were arrested in G1 and after release from the arrest, samples were collected for immunoprecipitation-kinase assay **(A)** western blotting **(B)**. Untagged wildtype and 3xHA-Pkc1^{KD} cells were used as controls. **(A)** The samples were immunoprecipitated using a polyclonal HA antibody and assayed for kinase activity using histone H1 and radiolabeled ATP. The samples were then run on an SDS-PAGE gel and probed for the amount of phosphorylated Histone H1 on an autoradiogram (top panel) and immunoprecipitated Pkc1 using monoclonal HA antibody (bottom panel). **(B)** 1.6mL samples collected simultaneously with the samples in **(A)** were probed by western blotting for HA-tagged Pkc1 (top panel) and the mitotic marker Clb2 (bottom panel).

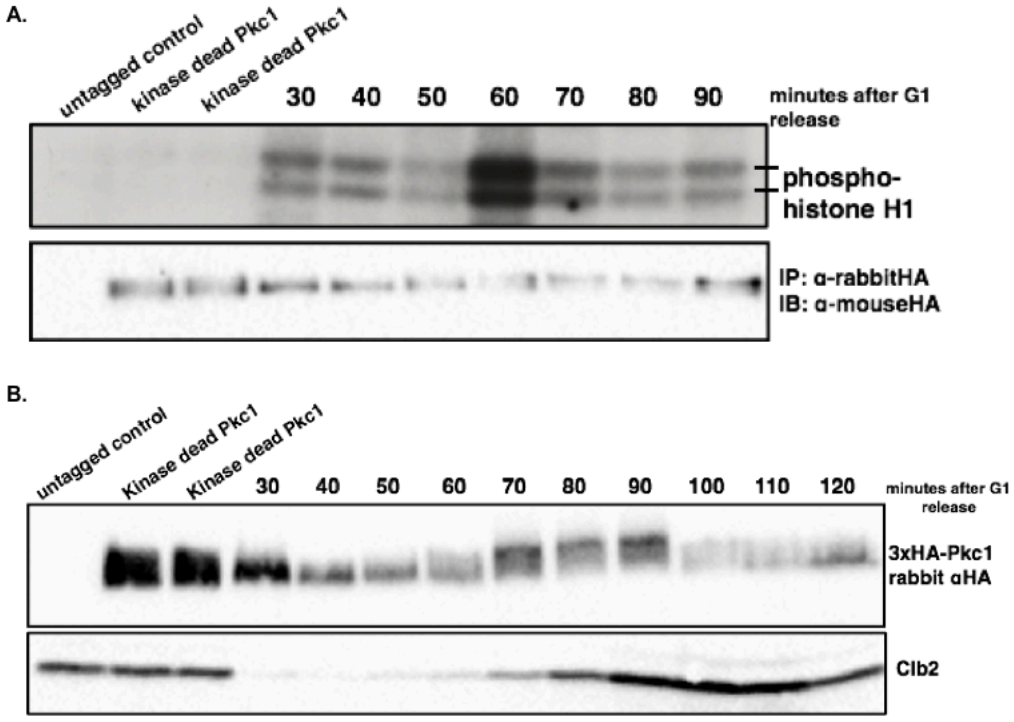

Inhibiting binding interactions between Rho1 and Pkc1 affect bud growth and delay the timing of mitotic entry

I next started looking at effectors that could modulate Pkc1 activity during the cell cycle. For this, we focused on two candidates: (i) Rho1 GTPase and, (ii) anionic phospholipids like phosphatidylserine (PS). Rho1 GTPase has been shown previously to interact with and modulate Pkc1 activity by our lab and others (Anastasia et al., 2012a; Kamada et al., 1996; Schmitz et al., 2002). Moreover, inactive Rho1 is delivered to the growing bud in secretory vesicles. Upon docking at the bud tip, Rho1 is activated by GEFs, where it further binds and activates Pkc1 (Abe et al., 2003; Kono et al., 2012). We have also previously shown that overexpression of Rho1 can drive cells through a mitotic arrest induced by membrane growth inhibition (Anastasia et al., 2012a). Together, the data support the idea that gradual activation of the Rho1-Pkc1 complex could be used as an indirect readout of the extent of membrane growth that could be relayed downstream to mitotic checkpoint proteins.

To test this theory, I used a PKC1 point mutant (L54S) in the N-terminal HR1 domain of PKC1 that perturbs binding interactions between Rho1 and Pkc1 (Denis and Cyert, 2005; Schmitz et al., 2002). This point mutation makes cells sensitive to higher temperatures (**Fig. 4.6 A**). Moreover, daughter buds exhibit growth defects and are elongated. These defects accumulate over cell generations and older mother cells display large vacuoles (**Fig. 4.6 B**).

Figure 4.6: Characterizing the PKC1 (L54S) mutant.
(A) Serial dilution assays were performed for isogeneic wildtype and Pkc1 (L54S) expressing cells, spotted on YPD and incubated at room temperature (RT), 30˚C, 34˚C and 37˚C. Cell growth was imaged after 36 hours. **(B)** Cells of the indicated genotype were grown overnight at 30˚C, fixed and observed at 63x magnification under bright-field.

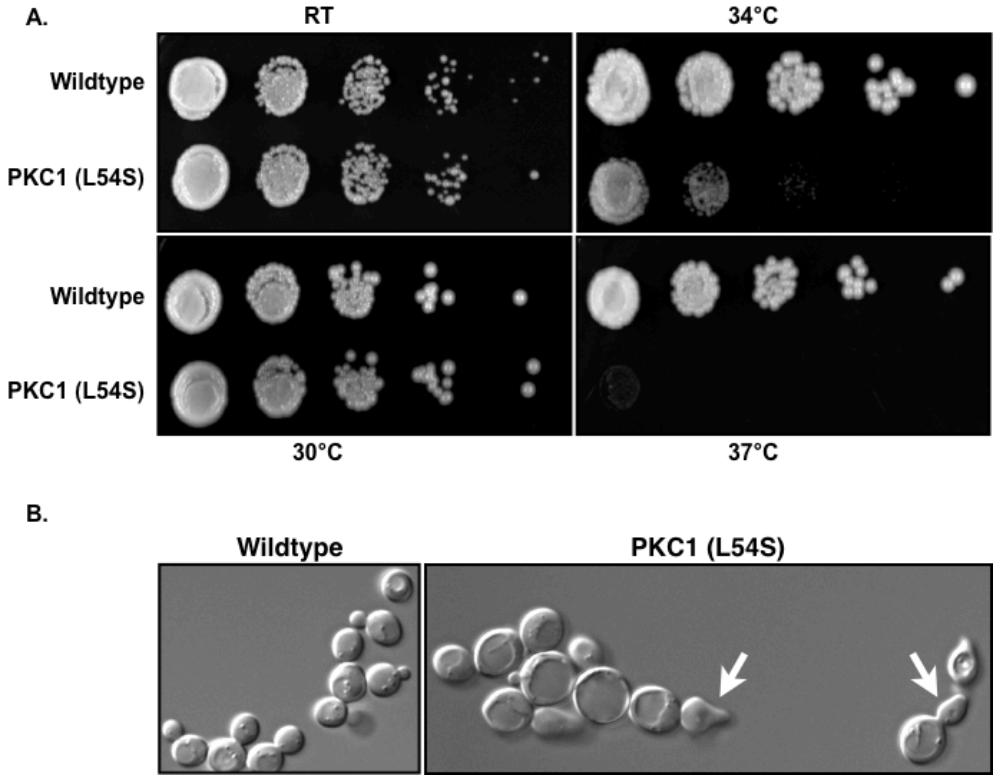

I next assessed the effect of this point mutation on Pkc1 phosphorylation and cell cycle kinetics. I performed the time course at 34˚C to enhance the temperature-sensitive phenotype of the point mutant. The analysis revealed that while Pkc1 (L54S) begins to become phosphorylated at the same time as wildtype Pkc1; however, the extent of phosphorylation is greatly reduced (**Fig. 4.7 A**). Moreover, Pkc1 (L54S) never becomes fully hyperphosphorylated as its wildtype counterpart. Abrogating binding to Rho1 also causes an almost 10-20 minute delay in mitotic entry and a prolonged mitosis. This delay is not caused due to defects in bud initiation as seen by the similar budding indices for both strains (**Fig. 4.7 B**). These findings suggest that binding of Rho1 to Pkc1 is necessary for normal bud growth. Moreover, in agreement with **Fig. 4.5**, the data further supports the idea that Pkc1 is more active when it is partially phosphorylated, causing a delay in mitotic entry and prolonged mitosis.

Figure 4.7: Lack of binding to Rho1 causes a failure in Pkc1 hyperphosphorylation and delays the timing of mitotic entry.
Cells of the indicated genotype were released from a G1 arrest and samples were collected at the indicated timepoints. **(A)** The samples were probed for Pkc1 and Clb2 by western blotting. **(B)** A second set of samples were collected for fixing at the same time and the percentage of budded cells was calculated for each of the indicated timepoints. n= minimum of 200 cells at each timepoint.

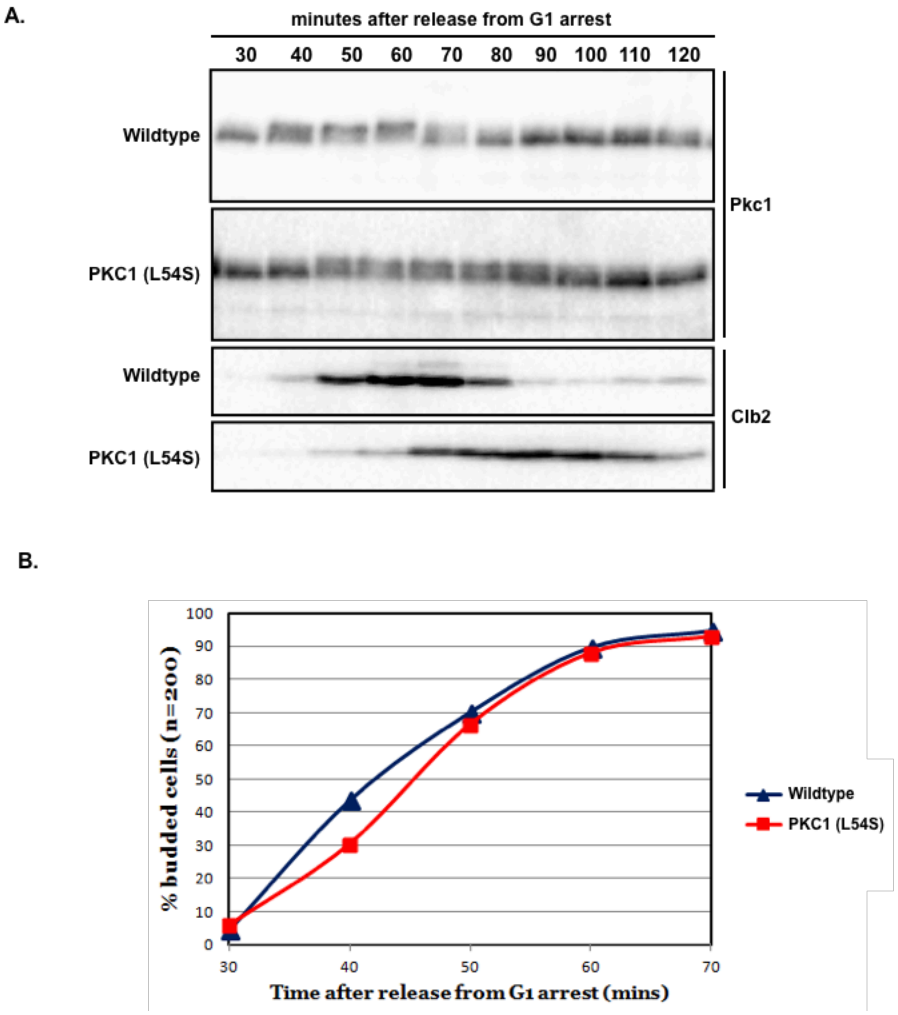

Phosphatidylserine is necessary for Pkc1 hyperphosphorylation

While vertebrate PKCs require additional effectors like diacylglycerol (DAG) and Ca^{2+}, phosphatidylserine alone is sufficient to stimulate yeast Pkc1 *in vitro* to a similar level as DAG (Kamada et al., 1996; Nomura and Inoue, 2017; Nomura et al., 2017). To test the role of PS on Pkc1 phosphorylation, previous work from our lab analyzed *cho1*Δ mutants, which encode the enzyme that synthesizes PS. We found that Pkc1 fails to become hyperphosphorylated in the *cho1*Δ mutants (Jesse Clarke, PhD thesis, UCSC, 2017).

Since Rho1 and PS are both effectors of Pkc1, I wanted to test the contributing effects of PS and Rho1 on Pkc1. More specifically, could Rho1 drive Pkc1 phosphorylation in cells lacking PS? This would help answer the series of events occurring at the bud tip that help measure bud growth.

Cells were grown in YEP+2% glycerol/ethanol and then induced with galactose to activate the GAL1-driven constitutively active Rho1 (Rho1*) in wildtype or *cho1*Δ log phase cells. As mentioned previously, Pkc1 remains mostly dephosphorylated in *cho1*Δ cells (**Fig 4.8 A**). Surprisingly, overexpression of Rho1 drove Pkc1 to a partially phosphorylated state, which could potentially be the most active form of Pkc1 (**Fig. 4.5**). However, it failed to do so in the *cho1*Δ cells. In order to determine the implications of Rho1 overexpression, I also assayed for Mih1 (budding yeast Cdc25 homolog) dephosphorylation. Our previous work showed that Rho1* can drive dephosphorylation of Mih1 even in cells undergoing a G2/mitotic arrest (Anastasia et al., 2012a). We saw a similar effect here (**Fig. 4.8 B**). Moreover, Rho1 induction also drove Mih1 dephosphorylation in *cho1*Δ cells. Together, the data suggest that while

Rho1* can drive Mih1 dephosphorylation in wildtype and *cho1*Δ cells, it fails to regulate Pkc1 in the absence of PS.

Figure 4.8: Phosphatidylserine is necessary for Pkc1 hyperphosphorylation. Cells of the indicated genotype were grown overnight in YEP supplemented with 2% glycerol + 2% ethanol. After collecting the 0 min timepoint, the cells were then supplemented with 2% galactose to induce Rho1* overexpression. Samples were collected at 30, 60, 90 and 120 min post galactose addition and probed for Pkc1 **(A)** and Mih1 **(B)**.

A.

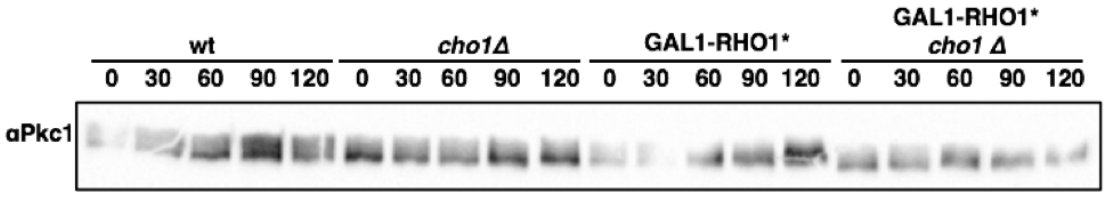

B.

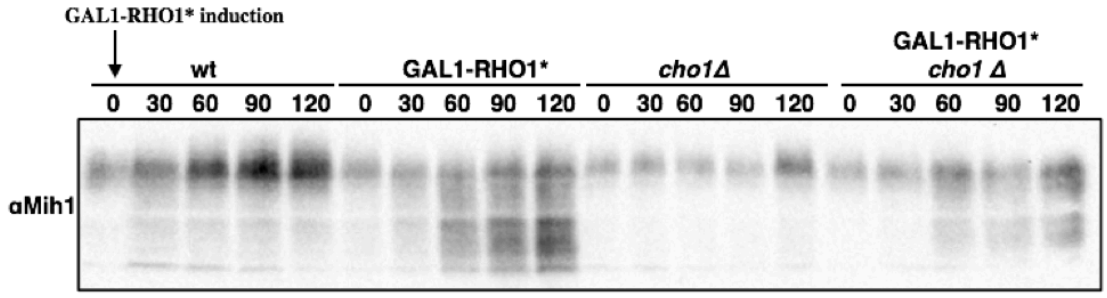

Rho1 drives Pkc1 dephosphorylation in a Cdc55-dependent manner

A recent study showed that the Zds1/2-PP2A^{Cdc55} complex was an effector of Rho1, although a direct interaction between purified Rho1 and Zds1/2 was not detected (Jonasson et al., 2016). Based on our work, it is very likely that Rho1 interacts with the Zds1/2-PP2A^{Cdc55} complex through Pkc1, especially since Pkc1 has already been shown to have strong binding interactions with the Zds1/2-PP2A^{Cdc55} (Rossio and Yoshida, 2011b; Rossio et al., 2014; Thai et al., 2017; Yasutis and Kozminski, 2013). To understand how Rho1* could drive hyperphosphorylated Pkc1 to a partially dephosphorylated state (**Fig. 4.8 A**), I tested if the Rho1-dependent Pkc1 dephosphorylation happened via PP2A^{Cdc55}.

Log phase cells were induced with galactose to overexpress Rho1* either in wildtype cells or cells expressing a temperature-sensitive mutant of CDC55: *cdc55-ts.* The cells were immediately shifted to the restrictive temperature (34˚C) to inactivate CDC55 and then assayed for Pkc1 phosphorylation (**Fig. 4.9**). Inactivation of Cdc55 caused Pkc1 to become fully hyperphosphorylated. As observed in the previous **Figure 4.8 A**, Rho1* overexpression indeed caused the different Pkc1 phosphoforms to collapse into the partially phosphorylated form. However, the same effect was not observed when Cdc55 was inactivated, suggesting that Rho1 drives Pkc1 dephosphorylation probably through increasing the interaction between Pkc1 and PP2A^{Cdc55}. Whether Zds1/2 are essential for this interaction has not been tested yet.

Figure 4.9: Rho1 drives Pkc1 dephosphorylation in a Cdc55-dependent manner. Cells of the indicated genotype were grown overnight in YEP supplemented with 2% glycerol + 2% ethanol. After collecting the 0 min timepoint, the cultures were supplemented with 2% galactose (to stimulate Rho1* overexpression) and simultaneously shifted to 34˚C to inactivate Cdc55. Subsequent samples were collected at 30, 60 and 90 min and probed for Pkc1 by western blotting.

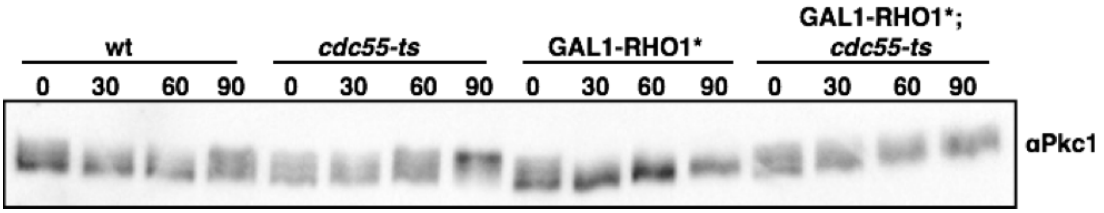

Discussion

Pkc1 measures polar bud growth to regulate the time of mitotic entry

Budding yeast cells undergo polarized growth directed to the bud tip from the time of bud inception to the end of G2 phase. Until recently, the molecular signals that measure and regulate this period of growth and coordinate the timing of mitotic entry so as to ensure that cells enter mitosis only when sufficient growth has occurred, have remained elusive. In this chapter, I analyzed the potential role of Pkc1 as a sensor for measuring polar bud growth. Pkc1 is well-positioned at the growing bud tip to receive growth signals in the form of activated Rho1 and phosphatidylserine upon delivery of secretory vesicles (Abe et al., 2003; Andrews and Stark, 2000; Kono et al., 2012). During the cell cycle, Pkc1 is gradually phosphorylated and the timing of this phosphorylation correlates well with the timing of bud growth. In both rich and poor nutrients, Pkc1 reached full hyperphosphorylation, albeit at a slower rate in poor nutrients. This was in stark contrast to the pattern of Gin4/Hsl1 phosphorylation observed in chapter 2 (**Fig. 2.5**). This can be probably explained by the observation that Pkc1 appeared to be maximally active in the partially phosphorylated state rather than the fully hyperphosphorylated state. Thus, in poor nutrients, the delayed timing of hyperphosphorylation suggested a more hyperactive Pkc1 until cells entered mitosis. It also leads to the idea that Pkc1 is inactivated when fully hyperphosphorylated. Together, these suggest a model where Pkc1 maintains itself in the hyperactive (partially phosphorylated state) form as a means to delay mitotic entry until sufficient polar bud growth has occurred.

Working model : PS, Rho1 and PP2A^{Cdc55}-Zds1/2 regulate Pkc1 activity

We also sought to determine how Rho1, PS and PP2A^{Cdc55}-Zds1/2 affected Pkc1 activity. Here overexpression of hyperactive Rho1 drove Pkc1 to the partially phosphorylated state that is dependent on PP2A^{Cdc55}. Rho1 has been previously shown to increase Pkc1 activity *in vitro* (Kamada et al., 1996). Consistent with our model and previous findings, this would suggest that overexpression of Rho1* would drive cells into mitosis prematurely. Indeed, overexpression of Rho1* can circumvent a G2 arrest caused due to inactivation of membrane growth (Anastasia et al., 2012a). It was thus not surprising when perturbing interactions between Rho1 and Pkc1 caused a delay in mitotic entry accompanied by defects in bud growth and large cell sizes. One caveat here is that the Pkc1 (L54S) mutant fails to be localized to the bud tip and mis-localizes primarily to the cytoplasm with some Pkc1 still localizing to the bud neck (Denis and Cyert, 2005). The observed growth defects and cell cycle delays along with the failure in Pkc1 hyperphosphorylation could then simply be attributed to Pkc1 not being in the correct location to orchestrate these events. This could also suggest that Rho1 may be required to keep Pkc1 localized to the membrane, where it could receive additional growth signals.

PS is gradually delivered to the outer membrane leaflet of the bud tip and then flipped to the inner membrane by flippases Dnf2/3 (Pomorski et al., 2003). While absence of the flippases had no significant effect on Pkc1 phosphorylation, deletion of CHO1 caused a failure in Pkc1 hyperphosphorylation. Moreover, the cell cycle is severely delayed. Surprisingly, *cho1*Δ cells overexpressing Rho1* showed no changes in Pkc1 phosphorylation but still caused normal Mih1 dephosphorylation as expected from Rho1 overexpression, indicating that Rho1 could bypass Pkc1 to drive

Mih1 dephosphorylation. While both Rho1 and PS are essential to increase Pkc1 activity *in vitro*, it could also suggest that PS and Rho1 have different roles in regulating Pkc1. It was recently shown that the binding interactions between Rho1 and Pkc1 were significantly decreased in *cho1*Δ mutants (Nomura et al., 2017). Also, autophosphorylation of mammalian Pkc βII is necessary for the protein to dissociate from the plasma membrane (Feng and Hannun, 1998). These findings suggest that PS could be essential in anchoring Pkc1 to the membrane, either inducing a conformational change that drives Pkc1 autophosphorylation or helping Pkc1 to be in proximity of other kinases that phosphorylate it (**Fig. 4.10**). Pkc1 phosphorylation could then promote increased interactions with Rho1 and/or its dissociation from the plasma membrane. Further, the Rho1-Pkc1 complex could then associate with $PP2A^{Cdc55}$-Zds1/2, both of which are known to interact with $PP2A^{Cdc55}$-Zds1/2. Whether the interaction between Rho1 and $PP2A^{Cdc55}$-Zds1/2 is dependent on the presence of Pkc1 has not been determined yet. In either scenario, binding to $PP2A^{Cdc55}$-Zds1/2 could oppose Pkc1 phosphorylation, keeping it hyperactive and delaying mitotic entry (Jonasson et al., 2016). We have previously shown that Pkc1 phosphorylates both Cdc55, the regulatory subunit of PP2A, and Zds1/2 at multiple sites (Thai et al., 2017). It is very likely that hyperactive Pkc1 eventually phosphorylates Cdc55 and Zds1/2, diverting $PP2A^{Cdc55}$-Zds1/2 activity towards activation of Mih1. However, phosphorylation-site mutants in CDC55 had no detectable phenotype indicating that the interactions between Pkc1 and $PP2A^{Cdc55}$ are more complicated than previously thought. One caveat here is that the coverage from the phosphosite mapping was very limited, so the lack of a detectable phenotype could

be attributed to the lack of finding relevant phosphosites. Nonetheless, we will need further experimentations to validate these claims.

The model proposed in this chapter is still preliminary and will need extensive work. Pkc1 has known roles in regulating the rates of ribosome biogenesis and interacting with the TORC network (Nomura and Inoue, 2015). Moreover, defects in mammalian PKCs are implicated in a variety of cancers 4. Overall, our data strongly support Pkc1 as a growth sensor that measures polar bud growth and orchestrates mitotic entry only when buds acquire the right size.

Figure 4.10: Proposed model for Pkc1 activation and growth-dependent entry into mitosis.
(1.) Addition of PS to the inner leaflet of the plasma membrane recruits Pkc1 to the membrane and this binding drives gradual phosphorylation of Pkc1. **(2.)** Increasing Pkc1 phosphorylation might promote its interactions with Rho1 as it gets delivered to the membrane, and together, the Rho1-Pkc1 complex dissociate from the membrane. **(3.)** Rho1-Pkc1 now interact with the $PP2A^{Cdc55}$-Zds1/2 complex. $PP2A^{Cdc55}$ opposes Pkc1 hyperphosphorylation keeping Pkc1 in an active state to delay mitotic entry. **(4.)** When Pkc1 is sufficiently activated, it phosphorylates Cdc55, diverting $PP2A^{Cdc55}$ activity away from Pkc1 and directing its activity towards activation of Mih1, which helps initiate mitosis.

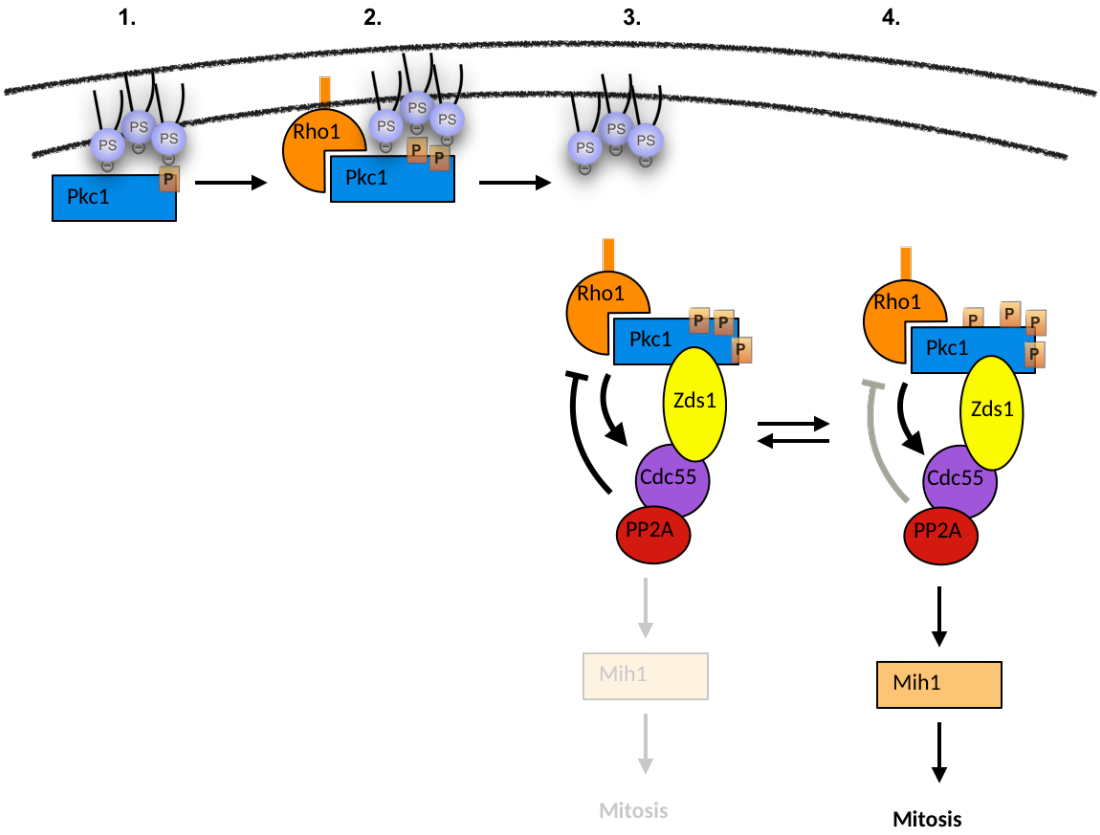

Materials and Methods

Yeast strain construction, media, and reagents

All strains are in the W303 background (*leu2-3,112 ura3-1 can1-100 ade2-1 his3-11,15 trp1-1 GAL+ ssd1-d2*). The additional genetic features of strains are listed in Table 5. Cells were grown in YP medium (1% yeast extract, 2% peptone, 40 mg/liter adenine) supplemented with 2% dextrose (YPD), or 2% glycerol and 2% ethanol (YPG/E). For live cell imaging, cells were grown in complete synthetic medium (CSM) supplemented with 2% dextrose and 40 mg/ml adenine.

Gene deletions and C-terminal epitope tagging was performed by standard PCR amplification and homologous recombination (Longtine *et al.*, 1998; Janke *et al.*, 2004; Lee *et al.*, 2013). To generate mRuby2-PKC1 under the control of the endogenous PKC1 promoter, DNA fragments encoding the PKC1 promoter, yeast-optimized mRuby2 ORF and PKC1 ORF were amplified with 50bp overlapping-flanking DNA sequences, gel-extracted, and column purified, mixed in equal amounts and transformed in yeast cells along with a yeast cen-vector YCplac33 (URA3) linearized using AflII. The overlapping sequences ensured that the plasmid is assembled at the restriction-digested sites such that the mRuby2 tag is at the N-terminus of PKC1 ORF immediately after the PKC1 promoter. The plasmid was then extracted from yeast, the newly assembled PKC1 insert digested from the vector backbone using the same restriction sites and then ligated to an integrating vector YIplac128 (LEU2). The resulting plasmid was re-transformed into a yeast diploid strain expressing only a single copy of PKC1. The diploids were sporulated to isolated haploid yeast cells with the endogenous PKC1 gene deleted and simultaneously expressing mRuby2-PKC1 at the LEU2 locus. A similar approach was used for

generating 3xHA-PKC1. To create the kinase-dead mutant of Pkc1 (K853A), we used the Agilent QuikChange II XL Site-Directed Mutagenesis Kit, according to the suggested protocol.

Cell cycle time courses and Western blotting

Cell cycle time courses were carried out as previously described (Harvey et al., 2011b) and in Chapter 2 of this thesis. Briefly, cells were grown overnight at room temperature in YPD or YPG/E to an optical density (OD_{600}) of 0.5 - 0.7. The cultures were arrested in G1 phase by incubation in the presence of 0.5 µg/mL α-factor at room temperature for 3 hours. Cells were released from the arrest by washing 3 times with fresh YPD or YPG/E. All time courses were carried out at 25˚C unless otherwise noted, and α factor was added back at 70 minutes to prevent initiation of a second cell cycle.

For experiments related to galactose-induced overexpression of Rho1*, all strains were grown overnight at room temperature in YPG/E at room temperature till they reached an OD_{600} of 0.5-0.6. The un-induced sample was collected and immediately induced with 2% galactose. The culture flasks were either incubated in a shaking water bath at 25˚C or shifted to the restrictive temperature of 34˚C (for *cdc55*-4) at the time of galactose addition. Samples were then collected at various intervals as indicated in the experiment.

Western blotting was performed exactly as described in Chapter 2 of this thesis. SDS-PAGE was carried out as previously described (Harvey et al., 2011b) and in Chapter 2 of this thesis. 10% polyacrylamide gels with 0.13% bis-acrylamide were used for analysis of Pkc1, Mih1 and Clb2. Proteins were transferred via wet transfer

onto nitrocellulose membranes. Blots were probed with various rabbit polyclonal primary antibodies at a final concentration of 1-2 µg/mL at room temperature overnight in 5% milk in PBST (1x phosphate buffered saline, 250 mM NaCl, 0.1% Tween-20) with 0.02% sodium azide. Primary antibodies were detected by an HRP-conjugated donkey anti-rabbit secondary antibody (GE Healthcare; # NA934V) incubated in PBST for 1h at room temperature. Blots were rinsed in PBS before detection via chemiluminescence using ECL reagents (Advansta; #K-12045-D50) with a Bio-Rad ChemiDoc imaging system.

Serial dilution spot assays

To characterize the PKC1 (L54S) strain, cells were grown overnight in YPD to an OD_{600} of 0.5. A series of 10-fold dilutions were prepared, spotted on YPD plates and grown at 25˚C, 30˚C, 34˚C and 37˚C.

Microscopy

For live cell time-lapse imaging of Pkc1, cells were grown in CSM overnight to an OD_{600} of 0.1 - 0.2 and then arrested in G1 phase with α factor. After an incubation period of 3h 30 min, the cells were then washed 3x in CSM prewarmed to 30˚C to release the cells from the G1 phase arrest. After resuspending the cells in CSM, about 3-4 µL cells were mixed with 10 µL media and gently layered onto CSM-agar pads prepared on glass slides (#1.5mm). A coverslip was placed on the slide and sealed with wax to prevent evaporation. The cells were visualized on a spinning disk confocal microscope with a Solamere system running MicroManager* (Edelstein et al., 2014). The microscope was based on a Nikon TE2000 stand and Coherent OBIS lasers. We

used a 63x/1.4 Plan Apo objective for data collection. The spindle poles were observed using the GFP laser and mRuby2-Pkc1 was visualized with the RFP channel.

IP-kinase assay

The assay was performed as described previously in (Altman and Kellogg, 1997a). Briefly, cells were arrested in G1 with alpha factor as mentioned previously and 50 mL samples were collected at each timepoint after release from the G1 arrest. The cells were resuspended in 1 mL media and transferred to a 2 mL wide-bottomed screw cap tube. The cells were pelleted, the supernatant was discarded, and the cell pellet was frozen in liquid nitrogen after addition of 500 µL acid-washed glass beads. Cells were lysed in 300 µL lysis buffer (50 mM Tris, pH- 7.6, 1 M NaCl, 1 mM EGTA, 1 mM MgCl2, 0.25% TritonX-100, 10% glycerol, 50 mM BGP, 50 mM NaF, 2 mM PMSF) in a Biospec Multibeater-8 and beaten at top speed for 25 s. The tubes were incubated on ice for 5 min, centrifuged for 5 min and 250 µL of the supernatant was transferred to a fresh tube. The process was repeated with 300 µL of fresh buffer and the two supernatants were pooled and centrifuged again and transferred again to a fresh tube.

Anti-HA beads were prepared by binding polyclonal rabbit HA antibody to protein A beads (Bio-Rad laboratories) in PBS overnight at 4˚C on a rotator (5 µg antibody/10 µL beads per sample). The beads were washed several times with lysis buffer (without PMSF), and 450 µL of each lysate was incubated with 10 µL protein A beads in 0.6-ml tubes on a rotator for 1 h at 4˚C. The beads were washed three times in lysis buffer, and two times in kinase buffer (50 mM HEPES, 2 mM MgCl2, 0.1% Tween-20, 10% glycerol) with a transfer to fresh tubes after the fifth wash. After the

final wash, the bound protein was eluted using 0.5 mg/mL HA-dipeptide resuspended in kinase buffer (2x20µL elutions) after incubation at 30˚C for 15 min and 15µL of the eluate was collected each time. For each sample, 20 µL eluate was mixed with 10 µL kinase buffer (supplemented with 1 mM DTT, 450 µM ATP, P32-labeled ATP and 1 µg Histone H1 substrate). The kinase reaction was carried out at 30˚C for 20 min with intermediate gentle vortexing. The reaction is stopped by the addition of 10 µL of 4x sample buffer and denaturation in a boiling water bath for 5 min. For autoradiography, 25 µL of the sample reaction was loaded on a 15% polyacrylamide gel. The top portion of the gel was used for immunoblotting Pkc1 using monoclonal HA antibody and the bottom portion was used for detecting phosphorylated histone H1 on an autoradiogram.

Table 4: List of strains used in Chapter 3

Strain	Mating type	Genotype	Source
DK 186	a	*bar1Δ*	(Altman and Kellogg, 1997a)
DK 3134	a	*bar1Δ pkc1Δ::His3MX6 leu2::mRuby2-PKC1 +LEU2 SPC42-GFP::KanMX6*	This study
DK3198	a	*bar1Δ pkc1Δ::His3MX6 leu2::3xHA-PKC1+LEU2*	This study
DK 3257	a	*bar1Δ pkc1Δ::His3MX6 leu2::3xHA-pkc1(K853R)+LEU2*	This study
DK2901	a	*bar1Δ pkc1::His3MX6 leu2::PKC1+ LEU2*	This study. The integrating plasmid was a gift from Dr. HP Schmitz (Schmitz et al., 2002)
DK 2902	a	*bar1Δ pkc1::His3MX6 leu2:pkc1(L54S)+ LEU2*	This study. The integrating plasmid was a gift from Dr. HP Schmitz (Schmitz et al., 2002)
DK 1651	a	*bar1Δ ura3:: GAL1-rho1(Q68H)*	(Anastasia et al., 2012a)
DK 3214	a	*bar1Δ cho1Δ::KanMX6*	This study
DK 4023	a	*bar1Δ cho1Δ::KanMX6 ura3:: GAL1-rho1(Q68H)*	This study
DK 177	a	BAR1	(Altman and Kellogg, 1997a)
DK 1496	a	BAR1 *cdc55-4::HIS5*	(Harvey et al., 2011b)
DK 1755	a	BAR1 *ura3:: GAL1-rho1(Q68H)*	This study
DK1757	a	BAR1 *ura3:: GAL1-rho1(Q68H) cdc55-4::HIS5*	This study

References

Abe, M., Qadota, H., Hirata, A., and Ohya, Y. (2003). Lack of GTP-bound Rho1p in secretory vesicles of Saccharomyces cerevisiae. The Journal of Cell Biology *162*, 85–97.

Alcaide-Gavilán, M., Lucena, R., Schubert, K.A., Artiles, K.L., Zapata, J., and Kellogg, D.R. (2018a). Modulation of TORC2 Signaling by a Conserved Lkb1 Signaling Axis in Budding Yeast. Genetics *210*, 155–170.

Alcaide-Gavilán, M., Lucena, R., Schubert, K., Artiles, K., Zapata, J., and Kellogg, D. (2018b). A conserved Lkb1 signaling axis modulates TORC2 signaling in budding yeast. bioRxiv 1–32.

Allard, C.A.H., Decker, F., Weiner, O.D., Toettcher, J.E., and Graziano, B.R. (2018a). A size-invariant bud-duration timer enables robustness in yeast cell size control. PLoS ONE *13*, e0209301.

Allard, C.A.H., Opalko, H.E., Liu, K.-W., Medoh, U., and Moseley, J.B. (2018b). Cell size–dependent regulation of Wee1 localization by Cdr2 cortical nodes. The Journal of Cell Biology *127*, jcb.201709171–15.

Altman, R., and Kellogg, D. (1997a). Control of mitotic events by Nap1 and the Gin4 kinase. The Journal of Cell Biology *138*, 119–130.

Altman, R., and Kellogg, D. (1997b). Control of mitotic events by Nap1 and the Gin4 kinase. The Journal of Cell Biology *138*, 119–130.

Amir (2014). Single-cell analysis of growth in budding yeast and bacteria reveals a common size regulation strategy. 1–16.

Anastasia, S.D., Nguyen, D.L., Thai, V., Meloy, M., MacDonough, T., and Kellogg, D.R. (2012a). A link between mitotic entry and membrane growth suggests a novel model for cell size control. The Journal of Cell Biology *197*, 89–104.

Anastasia, S.D., Nguyen, D.L., Thai, V., Meloy, M., MacDonough, T., and Kellogg, D.R. (2012b). A link between mitotic entry and membrane growth suggests a novel model for cell size control. The Journal of Cell Biology *197*, 89–104.

Andrews, P.D., and Stark, M.J. (2000). Dynamic, Rho1p-dependent localization of Pkc1p to sites of polarized growth. *113 (Pt 1*, 2685–2693.

Artiles, K., Anastasia, S., McCusker, D., and Kellogg, D.R. (2009). The Rts1 regulatory subunit of protein phosphatase 2A is required for control of G1 cyclin transcription and nutrient modulation of cell size. PLoS Genet *5*, e1000727–18.

Au Yong, J.Y., Wang, Y.-M., and Wang, Y. (2016). The Nim1 kinase Gin4 has distinct domains crucial for septin assembly, phospholipid binding and mitotic exit. Journal of Cell Science *129*, 2744–2756.

Banerjee, S., Lo, K., Daddysman, M.K., Selewa, A., Kuntz, T., Dinner, A.R., and Scherer, N.F. (2017). Biphasic growth dynamics control cell division in Caulobacter crescentus. Nature Microbiology *2*, 17116–17116.

Barral, Y., Parra, M., Bidlingmaier, S., and Snyder, M. (1999). Nim1-related kinases coordinate cell cycle progression with the organization of the peripheral cytoskeleton in yeast. Genes & Development *13*, 176–187.

Bean, J.M., Siggia, E.D., and Cross, F.R. (2006). Coherence and Timing of Cell Cycle Start Examined at Single-Cell Resolution. Mol. Cell *21*, 3–14.

Berchtold, D., and Walther, T.C. (2009). TORC2 plasma membrane localization is essential for cell viability and restricted to a distinct domain. Molecular Biology of the Cell *20*, 1565–1575.

Bhatia, P., Hachet, O., Hersch, M., Rincon, S.A., Berthelot-Grosjean, M., Dalessi, S., Basterra, L., Bergmann, S., Paoletti, A., and Martin, S.G. (2014). Distinct levels in Pom1 gradients limit Cdr2 activity and localization to time and position division. Cell Cycle *13*, 538–552.

Bloom, J., Cristea, I.M., Procko, A.L., Lubkov, V., Chait, B.T., Snyder, M., and Cross, F.R. (2011). Global analysis of Cdc14 phosphatase reveals diverse roles in mitotic processes. J. Biol. Chem. *286*, 5434–5445.

Breeding, C.S., Hudson, J., Balasubramanian, M.K., Hemmingsen, S.M., Young, P.G., and Gould, K.L. (1998). The cdr2(+) gene encodes a regulator of G2/M progression and cytokinesis in Schizosaccharomyces pombe. Molecular Biology of the Cell *9*, 3399–3415.

Buttery, S.M., Kono, K., Stokasimov, E., and Pellman, D. (2012a). Regulation of the formin Bnr1 by septins and a MARK/Par1-family septin-associated kinase. Molecular Biology of the Cell *23*, 4041–4053.

Buttery, S.M., Kono, K., Stokasimov, E., and Pellman, D. (2012b). Regulation of the formin Bnr1 by septins and a MARK/Par1-family septin-associated kinase. Molecular Biology of the Cell *23*, 4041–4053.

Cadart, C., Monnier, S., Grilli, J., Sáez, P.J., Srivastava, N., Attia, R., Terriac, E., Baum, B., Cosentino-Lagomarsino, M., and Piel, M. (2018a). Size control in mammalian cells involves modulation of both growth rate and cell cycle duration. Nature Communications 1–15.

Cadart, C., Monnier, S., Grilli, J., Sáez, P.J., Srivastava, N., Attia, R., Terriac, E., Baum, B., Cosentino-Lagomarsino, M., and Piel, M. (2018b). Size control in mammalian cells involves modulation of both growth rate and cell cycle duration. Nature Communications *9*, 3275.

Campos, M., Surovtsev, I.V., Kato, S., Paintdakhi, A., Beltran, B., Ebmeier, S.E., and Jacobs-Wagner, C. (2014). A constant size extension drives bacterial cell size homeostasis. Cell *159*, 1433–1446.

Carroll, C.W., Altman, R., Schieltz, D., Yates, J.R., and Kellogg, D. (1998). The septins are required for the mitosis-specific activation of the Gin4 kinase. The Journal of Cell Biology *143*, 709–717.

Carter, B.L., and Sudbery, P.E. (1980). Small-sized mutants of Saccharomyces cerevisiae. Genetics *96*, 561–566.

Chesarone, M.A., DuPage, A.G., and Goode, B.L. (2010). Unleashing formins to remodel the actin and microtubule cytoskeletons. Nature Publishing Group *11*, 62–74.

Chesarone, M., Gould, C.J., Moseley, J.B., and Goode, B.L. (2009). Displacement of Formins from Growing Barbed Ends by Bud14 Is Critical for Actin Cable Architecture and Function. Developmental Cell *16*, 292–302.

Clarke, J., Dephoure, N., Horecka, I., Gygi, S., and Kellogg, D. (2017). A conserved signaling network monitors delivery of sphingolipids to the plasma membrane in budding yeast. Molecular Biology of the Cell *28*, 2589–2599.

Coleman, T.R., Tang, Z., and Dunphy, W.G. (1993). Negative regulation of the wee1 protein kinase by direct action of the nim1/cdr1 mitotic inducer. Cell *72*, 919–929.

Cross, F.R. (1988). DAF1, a mutant gene affecting size control, pheromone arrest, and cell cycle kinetics of Saccharomyces cerevisiae. Molecular and Cellular Biology *8*, 4675–4684.

Cross, F.R. (1990). Cell cycle arrest caused by CLN gene deficiency in Saccharomyces cerevisiae resembles START-I arrest and is independent of the mating-pheromone signalling pathway. Molecular and Cellular Biology *10*, 6482–6490.

Deibler, R.W., and Kirschner, M.W. (2010). Quantitative reconstitution of mitotic CDK1 activation in somatic cell extracts. Mol. Cell *37*, 753–767.

Denis, V., and Cyert, M.S. (2005). Molecular analysis reveals localization of Saccharomyces cerevisiae protein kinase C to sites of polarized growth and Pkc1p targeting to the nucleus and mitotic spindle. Eukaryotic Cell *4*, 36–45.

Edelstein, A.D., Tsuchida, M.A., Amodaj, N., Pinkard, H., Vale, R.D., and Stuurman, N. (2014). Advanced methods of microscope control using μManager software. Journal of Biological Methods *1*, 10.

Edgar, B.A. (2006). How flies get their size: genetics meets physiology. Nature Reviews Genetics *7*, 907–916.

Ejsing, C.S., Sampaio, J.L., Surendranath, V., Duchoslav, E., Ekroos, K., Klemm, R.W., Simons, K., and Shevchenko, A. (2009). Global analysis of the yeast lipidome by quantitative shotgun mass spectrometry. Proc. Natl. Acad. Sci. U.S.a. *106*, 2136–2141.

Emptage, R.P., Lemmon, M.A., and Ferguson, K.M. (2017). Molecular determinants of KA1 domain-mediated autoinhibition and phospholipid activation of MARK1 kinase. The Biochemical Journal *474*, 385–398.

Emptage, R.P., Lemmon, M.A., Ferguson, K.M., and Marmorstein, R. (2018). Structural Basis for MARK1 Kinase Autoinhibition by Its KA1 Domain. Structure (London, England : 1993) *26*, 1137–1143.e3.

Evangelista, M., Blundell, K., Longtine, M.S., Chow, C.J., Adames, N., Pringle, J.R., Peter, M., and Boone, C. (1997). Bni1p, a yeast formin linking cdc42p and the actin cytoskeleton during polarized morphogenesis. Science *276*, 118–122.

Fairn, G.D., Hermansson, M., Somerharju, P., and Grinstein, S. (2011). Phosphatidylserine is polarized and required for proper Cdc42 localization and for development of cell polarity. Nat Cell Biol *13*, 1424–1430.

Fantes, P., and Nurse, P. (1977). Control of cell size at division in fission yeast by a growth-modulated size control over nuclear division. Experimental Cell Research *107*, 377–386.

Feng, X., and Hannun, Y.A. (1998). An essential role for autophosphorylation in the dissociation of activated protein kinase C from the plasma membrane. Journal of Biological Chemistry *273*, 26870–26874.

Ferrezuelo, F., Colomina, N., Palmisano, A., Garí, E., Gallego, C., Csikász-Nagy, A., and Aldea, M. (2012). The critical size is set at a single-cell level by growth rate to attain homeostasis and adaptation. Nature Communications *3*, 1012.

Finnigan, G.C., Sterling, S.M., Duvalyan, A., Liao, E.N., Sargsyan, A., Garcia, G., III, Nogales, E., and Thorner, J. (2016). Coordinate action of distinct sequence elements localizes checkpoint kinase Hsl1 to the septin collar at the bud neck in Saccharomyces cerevisiae. Molecular Biology of the Cell *27*, 2213–2233.

Fraschini, R., D'Ambrosio, C., Venturetti, M., Lucchini, G., and Piatti, S. (2006). Disappearance of the budding yeast Bub2-Bfa1 complex from the mother-bound spindle pole contributes to mitotic exit. The Journal of Cell Biology *172*, 335–346.

Gao, and bretscher, A. (2010). The Yeast Formin Bnr1p Has Two Localization Regions That Show Spatially and Temporally Distinct Association with Septin Structures. 1–10.

Gihana, G.M., Musser, T.R., Thompson, O., and Lacefield, S. (2018). Prolonged cyclin-dependent kinase inhibition results in septin perturbations during return to growth and mitosis. The Journal of Cell Biology *217*, 2429–2443.

Gonzalez, S., and Rallis, C. (2017). The TOR Signaling Pathway in Spatial and Temporal Control of Cell Size and Growth. Frontiers in Cell and Developmental Biology *5*, 2115–2116.

Goranov, A.I., Cook, M., Ricicova, M., Ben-Ari, G., Gonzalez, C., Hansen, C., Tyers, M., and Amon, A. (2009). The rate of cell growth is governed by cell cycle stage. Genes & Development *23*, 1408–1422.

Gould, K.L., and Nurse, P. (1989). Tyrosine phosphorylation of the fission yeast cdc2+ protein kinase regulates entry into mitosis. Nature *342*, 39–45.

Grava, S., Schaerer, F., Faty, M., Philippsen, P., and Barral, Y. (2006). Asymmetric recruitment of dynein to spindle poles and microtubules promotes proper spindle orientation in yeast. Developmental Cell *10*, 425–439.

Gray, J.V., Ogas, J.P., Kamada, Y., Stone, M., Levin, D.E., and Herskowitz, I. (1997). A role for the Pkc1 MAP kinase pathway of Saccharomyces cerevisiae in bud emergence and identification of a putative upstream regulator. The EMBO Journal *16*, 4924–4937.

Guzmán-Vendrell, M., Rincon, S.A., Dingli, F., Loew, D., and Paoletti, A. (2015). Molecular control of the Wee1 regulatory pathway by the SAD kinase Cdr2. Journal of Cell Science *128*, 2842–2853.

Hariharan, I.K. (2015). Organ Size Control: Lessons from Drosophila. Developmental Cell *34*, 255–265.

Hartmann, M. (1926). Über experimentelle Unsterblichkeit von Protozoen-Individuen. Naturwissenschaften *14*, 433–435.

Hartwell, L.H., and Unger, M.W. (1977). Unequal division in Saccharomyces cerevisiae and its implications for the control of cell division. The Journal of Cell Biology *75*, 422–435.

Harvey, S.L., and Kellogg, D.R. (2003). Conservation of mechanisms controlling entry into mitosis: budding yeast wee1 delays entry into mitosis and is required for cell size control. Curr. Biol. *13*, 264–275.

Harvey, S.L., Enciso, G., Dephoure, N., Gygi, S.P., Gunawardena, J., and Kellogg, D.R. (2011a). A phosphatase threshold sets the level of Cdk1 activity in early mitosis in budding yeast. Molecular Biology of the Cell *22*, 3595–3608.

Harvey, S.L., Harvey, S.L., Enciso, G., Enciso, G., Dephoure, N., Dephoure, N., Gygi, S.P., Gygi, S.P., Gunawardena, J., Gunawardena, J., et al. (2011b). A phosphatase threshold sets the level of Cdk1 activity in early mitosis in budding yeast. Molecular Biology of the Cell *22*, 3595–3608.

Haupt, A., and Minc, N. (2017). Gradients of phosphatidylserine contribute to plasma membrane charge localization and cell polarity in fission yeast. Molecular Biology of the Cell *28*, 210–220.

Hikiji, T., Miura, K., Kiyono, K., Shibuya, I., and Ohta, A. (1988). Disruption of the CHO1 gene encoding phosphatidylserine synthase in Saccharomyces cerevisiae. Journal of Biochemistry *104*, 894–900.

Horton, R.M., Cai, Z.L., Ho, S.N., and Pease, L.R. (1990). Gene splicing by overlap extension: tailor-made genes using the polymerase chain reaction. BioTechniques *8*, 528–535.

Huang, H.-L., Wang, S., Yin, M.-X., Dong, L., Wang, C., Wu, W., Lu, Y., Feng, M., Dai, C., Guo, X., et al. (2013). Par-1 Regulates Tissue Growth by Influencing Hippo Phosphorylation Status and Hippo-Salvador Association. PLoS Biol *11*, e1001620–15.

Inagaki, M., Schmelzle, T., Yamaguchi, K., Irie, K., Hall, M.N., and Matsumoto, K. (1999). PDK1 homologs activate the Pkc1-mitogen-activated protein kinase pathway in yeast.

Jaspersen, S.L., Charles, J.F., Tinker-Kulberg, R.L., and Morgan, D.O. (1998). A late mitotic regulatory network controlling cyclin destruction in Saccharomyces cerevisiae. Molecular Biology of the Cell *9*, 2803–2817.

Jiang, T., and Harris, T.J.C. (2019). Par-1 controls the composition and growth of cortical actin caps during Drosophila embryo cleavage. The Journal of Cell Biology *127*, jcb.201903152.

Johnston, G.C., Ehrhardt, C.W., Lorincz, A., and Carter, B.L. (1979). Regulation of cell size in the yeast Saccharomyces cerevisiae. Journal of Bacteriology *137*, 1–5.

Johnston, G.C., Pringle, J.R., and Hartwell, L.H. (1977a). Coordination of growth with cell division in the yeast Saccharomyces cerevisiae. Experimental Cell Research *105*, 79–98.

Johnston, G.C., Pringle, J.R., and Hartwell, L.H. (1977b). Coordination of growth with cell division in the yeast Saccharomyces cerevisiae. Experimental Cell Research *105*, 79–98.

Jonasson, E.M., Abe, M., Ohya, Y., Rossio, V., Hatakeyama, R., and Yoshida, S. (2016). Zds1/Zds2–PP2A Cdc55complex specifies signaling output from Rho1 GTPase. The Journal of Cell Biology *212*, 51–61.

Jorgensen, P., and Tyers, M. (2004). A dynamic transcriptional network communicates growth potential to ribosome synthesis and critical cell size. Genes & Development *18*, 2491–2505.

Jorgensen, P., Nishikawa, J.L., Breitkreutz, B.-J., and Tyers, M. (2002). Systematic identification of pathways that couple cell growth and division in yeast. Science *297*, 395–400.

Jun, S., and Taheri-Araghi, S. (2014). Cell-size maintenance: universal strategy revealed. Trends in Microbiology 1–3.

Kabeche, R., Madrid, M., Cansado, J., and Moseley, J.B. (2015). Eisosomes Regulate Phosphatidylinositol 4,5-Bisphosphate (PI(4,5)P2) Cortical Clusters and Mitogen-activated Protein (MAP) Kinase Signaling upon Osmotic Stress. J. Biol. Chem. *290*, 25960–25973.

Kamada, Y., Qadota, H., Python, C.P., Anraku, Y., Ohya, Y., and Levin, D.E. (1996). Activation of yeast protein kinase C by Rho1 GTPase. J. Biol. Chem. *271*, 9193–9196.

Kanoh, J., and Russell, P. (1998). The protein kinase Cdr2, related to Nim1/Cdr1 mitotic inducer, regulates the onset of mitosis in fission yeast. Molecular Biology of the Cell *9*, 3321–3334.

Kellogg, D.R., and Murray, A.W. (1995). NAP1 acts with Clb2 to perform mitotic functions and to suppress polar bud growth in budding yeast. The Journal of Cell Biology *130*, 675–685.

Klose, C., Surma, M.A., Gerl, M.J., Meyenhofer, F., Shevchenko, A., and Simons, K. (2012). Flexibility of a eukaryotic lipidome--insights from yeast lipidomics. PLoS ONE *7*, e35063.

Klug, L., and Daum, G. (2014). Yeast lipid metabolism at a glance. FEMS Yeast Research *14*, 369–388.

Knapp, B.D., Odermatt, P., Rojas, E.R., Cheng, W., He, X., Huang, K.C., and Chang, F. (2019). Decoupling of Rates of Protein Synthesis from Cell Expansion Leads to Supergrowth. Cell Systems.

Kono, K., Saeki, Y., Yoshida, S., Tanaka, K., and Pellman, D. (2012). Proteasomal Degradation Resolves Competition between Cell Polarization and Cellular Wound Healing. Cell *150*, 151–164.

Kumagai, A., and Dunphy, W.G. (1991). The cdc25 protein controls tyrosine dephosphorylation of the cdc2 protein in a cell-free system. Cell *64*, 903–914.

Lecuit, T., and Wieschaus, E. (2000). Polarized insertion of new membrane from a cytoplasmic reservoir during cleavage of the Drosophila embryo. The Journal of Cell Biology *150*, 849–860.

Lee, S., Lim, W.A., and Thorn, K.S. (2013a). Improved Blue, Green, and Red Fluorescent Protein Tagging Vectors for S. cerevisiae. PLoS ONE *8*, e67902.

Lee, S., Lim, W.A., and Thorn, K.S. (2013b). Improved blue, green, and red fluorescent protein tagging vectors for S. cerevisiae. PLoS ONE *8*, e67902–e67911.

Leitao, R.M., and Kellogg, D.R. (2017a). The duration of mitosis and daughter cell size are modulated by nutrients in budding yeast. The Journal of Cell Biology *216*, 3463–3470.

Leitao, R.M., and Kellogg, D.R. (2017b). The duration of mitosis and daughter cell size are modulated by nutrients in budding yeast. The Journal of Cell Biology *216*, 3463–3470.

Leitao, R.M., Jasani, A., Talavara, R.A., Pham, A., Okobi, Q.J., and Kellogg, D.R. (2019a). A Conserved PP2A Regulatory Subunit Enforces Proportional Relationships Between Cell Size and Growth Rate. Genetics *213*, 517–528.

Leitao, R.M., Jasani, A., Talavera, R.A., Pham, A., Okobi, Q.J., and Kellogg, D.R. (2019b). A Conserved PP2A Regulatory Subunit Enforces Proportional Relationships Between Cell Size and Growth Rate. Genetics *213*, 517–528.

Leskoske, K.L., Roelants, F.M., Emmerstorfer-Augustin, A., Augustin, C.M., Si, E.P., Hill, J.M., and Thorner, J. (2018). Phosphorylation by the stress-activated MAPK Slt2 down-regulates the yeast TOR complex 2. Genes & Development 1–16.

Levin, D.E., and Bartlett-Heubusch, E. (1992). Mutants in the S. cerevisiae PKC1 gene display a cell cycle-specific osmotic stability defect. The Journal of Cell Biology *116*, 1221–1229.

Lew, D.J., and Reed, S.I. (1993). Morphogenesis in the yeast cell cycle: regulation by Cdc28 and cyclins. The Journal of Cell Biology *120*, 1305–1320.

Li, C.-R., Au Yong, J.Y., Wang, Y.-M., and Wang, Y. (2012). CDK regulates septin organization through cell-cycle-dependent phosphorylation of the Nim1-related kinase Gin4. Journal of Cell Science *125*, 2533–2543.

Li, Y., Moir, R.D., Sethy-Coraci, I.K., Warner, J.R., and Willis, I.M. (2000). Repression of Ribosome and tRNA Synthesis in Secretion-Defective Cells Is Signaled by a Novel Branch of the Cell Integrity Pathway. Molecular and Cellular Biology *20*, 3843–3851.

Lianga, N., Williams, E.C., Kennedy, E.K., Doré, C., Pilon, S., Girard, S.L., Deneault, J.-S., and Rudner, A.D. (2013). A Wee1 checkpoint inhibits anaphase onset. The Journal of Cell Biology *201*, 843–862.

Longtine, M.S., Fares, H., and Pringle, J.R. (1998a). Role of the yeast Gin4p protein kinase in septin assembly and the relationship between septin assembly and septin function. The Journal of Cell Biology *143*, 719–736.

Longtine, M.S., McKenzie, A., DeMarini, D.J., Shah, N.G., Wach, A., Brachat, A., Philippsen, P., and Pringle, J.R. (1998b). Additional modules for versatile and economical PCR-based gene deletion and modification in Saccharomyces cerevisiae. Yeast *14*, 953–961.

Longtine, M.S., Theesfeld, C.L., McMillan, J.N., Weaver, E., Pringle, J.R., and Lew, D.J. (2000). Septin-Dependent Assembly of a Cell Cycle-Regulatory Module in Saccharomyces cerevisiae. Molecular and Cellular Biology *20*, 4049–4061.

Lucena, R., Alcaide-Gavilán, M., Anastasia, S.D., and Kellogg, D.R. (2017a). Wee1 and Cdc25 are controlled by conserved PP2A-dependent mechanisms in fission yeast. Cell Cycle *16*, 428–435.

Lucena, R., Alcaide-Gavilán, M., Schubert, K., He, M., Domnauer, M., Marquer, C., and Kellogg, D. (2017b). Cell size and growth rate are modulated by TORC2-dependent signals. bioRxiv 1–41.

Ma, X.J., Lu, Q., and Grunstein, M. (1996). A search for proteins that interact genetically with histone H3 and H4 amino termini uncovers novel regulators of the Swe1 kinase in Saccharomyces cerevisiae. Genes & Development *10*, 1327–1340.

Martin, S.G., and Berthelot-Grosjean, M. (2009). Polar gradients of the DYRK-family kinase Pom1 couple cell length with the cell cycle. Nature *459*, 852–856.

Matsuo, Y., Fisher, E., Patton-Vogt, J., and Marcus, S. (2007). Functional Characterization of the Fission Yeast Phosphatidylserine Synthase Gene, pps1, Reveals Novel Cellular Functions for Phosphatidylserine. Eukaryotic Cell *6*, 2092–2101.

McCusker, D., Denison, C., Anderson, S., Egelhofer, T.A., Yates, J.R., Gygi, S.P., and Kellogg, D.R. (2007). Cdk1 coordinates cell-surface growth with the cell cycle. Nat Cell Biol *9*, 506–515.

McCusker, D., Royou, A., Velours, C., and Kellogg, D. (2012). Cdk1-dependent control of membrane-trafficking dynamics. Molecular Biology of the Cell *23*, 3336–3347.

McMillan, J.N., and Lew, D.J. (1999). The Morphogenesis Checkpoint in *Saccharomyces cerevisiae*: Cell Cycle Control of Swe1p Degradation by Hsl1p and Hsl7p. 1–12.

Meca, J., Massoni Laporte, A., Martinez, D., Sartorel, E., Loquet, A., Habenstein, B., and McCusker, D. (2019). Avidity-driven polarity establishment via multivalent lipid–GTPase module interactions. The EMBO Journal *38*, e99652–19.

Mitchison, J.M. (1958). The growth of single cells. II. Saccharomyces cerevisiae. Experimental Cell Research *15*, 214–221.

Mizuta, K., and Warner, J.R. (1994). Continued functioning of the secretory pathway is essential for ribosome synthesis. Molecular and Cellular Biology *14*, 2493–2502.

Moffat, J., and Andrews, B. (2004). Late-G1 cyclin-CDK activity is essential for control of cell morphogenesis in budding yeast. Nat Cell Biol *6*, 59–66.

Moravcevic, K., Mendrola, J.M., Schmitz, K.R., Wang, Y.H., Slochower, D., Janmey, P.A., and Lemmon, M.A. (2010). Kinase associated-1 domains drive MARK/PAR1 kinases to membrane targets by binding acidic phospholipids. Cell *143*, 966–977.

Mortensen, E.M., McDonald, H., Yates, J., and Kellogg, D.R. (2002). Cell cycle-dependent assembly of a Gin4-septin complex. Molecular Biology of the Cell *13*, 2091–2105.

Nepper-Christensen, L., Lønborg, J., Ahtarovski, K.A., Høfsten, D.E., Kyhl, K., Ghotbi, A.A., Schoos, M.M., Göransson, C., Bertelsen, L., Køber, L., et al. (2017). Left Ventricular Hypertrophy Is Associated With Increased Infarct Size and Decreased Myocardial Salvage in Patients With ST-Segment Elevation Myocardial Infarction Undergoing Primary Percutaneous Coronary Intervention. J Am Heart Assoc *6*, 613.

Nishimura, K., Fukagawa, T., Takisawa, H., Kakimoto, T., and Kanemaki, M. (2009). An auxin-based degron system for the rapid depletion of proteins in nonplant cells. Nature Methods *6*, 917–922.

Nomura, W., and Inoue, Y. (2015). Methylglyoxal Activates the Target of Rapamycin Complex 2-Protein Kinase C Signaling Pathway in Saccharomyces cerevisiae. Molecular and Cellular Biology *35*, 1269–1280.

Nomura, W., and Inoue, Y. (2017). Contribution of phosphatidylserine to Rho1- and Pkc1-related repolarization of the actin cytoskeleton under stressed conditions in Saccharomyces cerevisiae. Small GTPases *0*, 1–7.

Nomura, W., Ito, Y., and Inoue, Y. (2017). Role of phosphatidylserine in the activation of Rho1-related Pkc1 signaling in Saccharomyces cerevisiae. Cellular Signalling *31*, 146–153.

Novick, P., TerBush, D.R., Maurice, T., and Roth, D. (1996). The Exocyst is a multiprotein complex required for exocytosis in Saccharomyces cerevisiae.

Nurse, P. (1975). Genetic control of cell size at cell division in yeast. , Published Online: 14 August 1975; | Doi:10.1038/256547a0 *256*, 547–551.

Okuzaki, D., Tanaka, S., Kanazawa, H., and Nojima, H. (1997). Gin4 of S. cerevisiae is a bud neck protein that interacts with the Cdc28 complex. Genes to Cells : Devoted to Molecular & Cellular Mechanisms *2*, 753–770.

Opalko, H.E., Nasa, I., Kettenbach, A.N., and Moseley, J.B. (2019). A mechanism for how Cdr1/Nim1 kinase promotes mitotic entry by inhibiting Wee1. Molecular Biology of the Cell mbcE19080430.

Ozaki-Kuroda, K., Yamamoto, Y., Nohara, H., Kinoshita, M., Fujiwara, T., Irie, K., and Takai, Y. (2001). Dynamic localization and function of Bni1p at the sites of directed growth in Saccharomyces cerevisiae. Molecular and Cellular Biology *21*, 827–839.

Pal, G., Paraz, M.T.Z., and Kellogg, D.R. (2008). Regulation of Mih1/Cdc25 by protein phosphatase 2A and casein kinase 1. The Journal of Cell Biology *180*, 931–945.

Pan, K.Z., Saunders, T.E., Flor-Parra, I., Howard, M., and Chang, F. (2014). Cortical regulation of cell size by a sizer cdr2p. eLife *3*, e02040–24.

Parker, P.J., Mellor, H., Parker, P.J., and Parker, P.J. (1998). The extended protein kinase C superfamily. *332 (Pt 2*, 281–292.

Pomorski, T., Lombardi, R., Riezman, H., Devaux, P.F., van Meer, G., and Holthuis, J.C.M. (2003). Drs2p-related P-type ATPases Dnf1p and Dnf2p are required for phospholipid translocation across the yeast plasma membrane and serve a role in endocytosis. Molecular Biology of the Cell *14*, 1240–1254.

Prescott, D.M. (1956). Relation between cell growth and cell division III. Changes in nuclear volume and growth rate and prevention of cell division in Amoeba proteus resulting from cytoplasmic amputations. Experimental Cell Research *11*, 94–98.

Pruyne, D., Gao, L., Bi, E., and Bretscher, A. (2004a). Stable and dynamic axes of polarity use distinct formin isoforms in budding yeast. Molecular Biology of the Cell *15*, 4971–4989.

Pruyne, D., Gao, L., Bi, E., and Bretscher, A. (2004b). Stable and dynamic axes of polarity use distinct formin isoforms in budding yeast. Molecular Biology of the Cell *15*, 4971–4989.

Qadota, H., Kamada, Y., Python, C.P., Anraku, Y., Ohya, Y., and Levin, D.E. (1996). Activation of yeast protein kinase C by Rho1 GTPase. Journal of Biological Chemistry *271*, 9193–9196.

Raspelli, E., Cassani, C., Lucchini, G., and Fraschini, R. (2011). Budding yeast Dma1 and Dma2 participate in regulation of Swe1 levels and localization. Molecular Biology of the Cell *22*, 2185–2197.

Raspelli, E., Cassani, C., Chiroli, E., and Fraschini, R. (2015). Budding yeast Swe1 is involved in the control of mitotic spindle elongation and is regulated by Cdc14 phosphatase during mitosis. J. Biol. Chem. *290*, 6006–6006.

Richardson, H.E., Wittenberg, C., Cross, F., and Reed, S.I. (1989). An essential G1 function for cyclin-like proteins in yeast. Cell *59*, 1127–1133.

Roelants, F.M., Su, B.M., Wulffen, von, J., Ramachandran, S., Sartorel, E., Trott, A.E., and Thorner, J. (2015). Protein kinase Gin4 negatively regulates flippase function and controls plasma membrane asymmetry. The Journal of Cell Biology *208*, 299–311.

Rossio, V., and Yoshida, S. (2011a). Spatial regulation of Cdc55-PP2A by Zds1/Zds2 controls mitotic entry and mitotic exit in budding yeast. The Journal of Cell Biology *193*, 445–454.

Rossio, V., and Yoshida, S. (2011b). Spatial regulation of Cdc55-PP2A by Zds1/Zds2 controls mitotic entry and mitotic exit in budding yeast. The Journal of Cell Biology *193*, 445–454.

Rossio, V., Kazatskaya, A., Hirabayashi, M., and Yoshida, S. (2014). Comparative genetic analysis of PP2A-Cdc55 regulators in budding yeast. Cell Cycle *13*, 2073–2083.

Sagot, I., Klee, S.K., and Pellman, D. (2002). Yeast formins regulate cell polarity by controlling the assembly of actin cables. Nat Cell Biol *4*, 42–50.

Schindelin, J., Arganda-Carreras, I., Frise, E., Kaynig, V., Longair, M., Pietzsch, T., Preibisch, S., Rueden, C., Saalfeld, S., Schmid, B., et al. (2012). Fiji: an open-source platform for biological-image analysis. Nature Methods *9*, 676–682.

Schmitz, H.-P., Lorberg, A., and Heinisch, J.J. (2002). Regulation of yeast protein kinase C activity by interaction with the small GTPase Rho1p through its amino-terminal HR1 domain. Molecular Microbiology *44*, 829–840.

Schmoller, K.M., Turner, J.J., Kõivomägi, M., and Skotheim, J.M. (2015). Dilution of the cell cycle inhibitor Whi5 controls budding-yeast cell size. Nature *526*, 268–272.

Shao, C., Novakovic, V.A., Head, J.F., Seaton, B.A., and Gilbert, G.E. (2008). Crystal structure of lactadherin C2 domain at 1.7A resolution with mutational and

computational analyses of its membrane-binding motif. Journal of Biological Chemistry *283*, 7230–7241.

Shulewitz, M.J., Inouye, C.J., and Thorner, J. (1999). Hsl7 localizes to a septin ring and serves as an adapter in a regulatory pathway that relieves tyrosine phosphorylation of Cdc28 protein kinase in Saccharomyces cerevisiae. Molecular and Cellular Biology *19*, 7123–7137.

Sia, R.A.R., Bardes, E.S.E., and Lew, D.J.D. (1998). Control of Swe1p degradation by the morphogenesis checkpoint. The EMBO Journal *17*, 6678–6688.

Sokoloff, B. (1922). The nucleo-cytoplasmic ratio and cancer. The Journal of Cancer Research *7*, 395–415.

Sreenivasan, A., and Kellogg, D. (1999). The elm1 kinase functions in a mitotic signaling network in budding yeast. Molecular and Cellular Biology *19*, 7983–7994.

Sreenivasan, A., Bishop, A.C., Shokat, K.M., and Kellogg, D.R. (2003). Specific inhibition of Elm1 kinase activity reveals functions required for early G1 events. Molecular and Cellular Biology *23*, 6327–6337.

Tabler, J.M., Yamanaka, H., and Green, J.B.A. (2010). PAR-1 promotes primary neurogenesis and asymmetric cell divisions via control of spindle orientation. Development *137*, 2501–2505.

Takeda, M., Yamagami, K., and Tanaka, K. (2014). Role of phosphatidylserine in phospholipid flippase-mediated vesicle transport in Saccharomyces cerevisiae. Eukaryotic Cell *13*, 363–375.

Tang, X., Punch, J.J., and Lee, W.-L. (2014). A CAAX motif can compensate for the PH domain of Num1 for cortical dynein attachment. Cell Cycle *8*, 3182–3190.

Thai, V., Dephoure, N., Weiss, A., Ferguson, J., Leitao, R., Gygi, S.P., and Kellogg, D.R. (2017). Protein Kinase C Controls Binding of Igo/ENSA Proteins to Protein Phosphatase 2A in Budding Yeast. J. Biol. Chem. *292*, 4925–4941.

Thornton, B.R., and Toczyski, D.P. (2003). Securin and B-cyclin/CDK are the only essential targets of the APC. Nat Cell Biol *5*, 1090–1094.

Tkacz, J.S., and Lampen, J.O. (1972). Wall replication in saccharomyces species: use of fluorescein-conjugated concanavalin A to reveal the site of mannan insertion. Journal of General Microbiology *72*, 243–247.

Vallen, E.A., Caviston, J., and Bi, E. (2000). Roles of Hof1p, Bni1p, Bnr1p, and myo1p in cytokinesis in Saccharomyces cerevisiae. Molecular Biology of the Cell *11*, 593–611.

van Meer, G., Voelker, D.R., and Feigenson, G.W. (2008). Membrane lipids: where they are and how they behave. Nat Rev Mol Cell Biol *9*, 112–124.

Varsano, G., Wang, Y., and Wu, M. (2017). Probing Mammalian Cell Size Homeostasis by Channel-Assisted Cell Reshaping. CellReports *20*, 397–410.

Visintin, R., Craig, K., Hwang, E.S., Prinz, S., Tyers, M., and Amon, A. (1998). The phosphatase Cdc14 triggers mitotic exit by reversal of Cdk-dependent phosphorylation. Mol. Cell *2*, 709–718.

Wicky, S., Tjandra, H., Schieltz, D., Yates, J., and Kellogg, D.R. (2011). The Zds proteins control entry into mitosis and target protein phosphatase 2A to the Cdc25 phosphatase. Molecular Biology of the Cell *22*, 20–32.

Wu, J.-X., Cheng, Y.-S., Wang, J., Chen, L., Ding, M., and Wu, J.-W. (2015). Structural insight into the mechanism of synergistic autoinhibition of SAD kinases. Nature Communications *6*, 1–12.

Xie, X., and Guan, K.-L. (2011). The Ribosome and TORC2: Collaborators for Cell Growth. Cell *144*, 640–642.

Yamane-Sando, Y., Shimobayashi, E., Shimobayashi, M., Kozutsumi, Y., Oka, S., and Takematsu, H. (2014). Fpk1/2 kinases regulate cellular sphingoid long-chain base abundance and alter cellular resistance to LCB elevation or depletion. MicrobiologyOpen *3*, 196–212.

Yasutis, K.M., and Kozminski, K.G. (2013). Cell cycle checkpoint regulators reach a zillion. Cell Cycle *12*, 1501–1509.

Yeung, T., Gilbert, G.E., Shi, J., Silvius, J., Kapus, A., and Grinstein, S. (2008). Membrane phosphatidylserine regulates surface charge and protein localization. Science *319*, 210–213.

Young, P.G., and Fantes, P.A. (1987). Schizosaccharomyces pombe mutants affected in their division response to starvation. Journal of Cell Science *88 (Pt 3)*, 295–304.

Zapata, J., Dephoure, N., MacDonough, T., Yu, Y., Parnell, E.J., Mooring, M., Gygi, S.P., Stillman, D.J., and Kellogg, D.R. (2014). PP2A Rts1is a master regulator of pathways that control cell size. The Journal of Cell Biology *204*, 359–376.

Zeng, Q., and Hong, W. (2008). The emerging role of the hippo pathway in cell contact inhibition, organ size control, and cancer development in mammals. Cancer Cell *13*, 188–192.